GDAŃSK UNIVERSITY OF TECHNOLOGY

Faculty of Civil and Environmental Engineering

Wojciech MIGDA

Study on deformed steel columns subjected to impact load due to soft-storey failure in buildings during earthquakes

DOCTORAL DISSERTATION

DOCTORAL SUPERVISOR: dr hab. inż. Robert JANKOWSKI, prof. PG

DEPARTMENT OF METAL STRUCTURES

AND CONSTRUCTION MANAGEMENT

GDAŃSK 2013

Tobie Mamo.

CONTENTS

SUMMARY

The so called soft-storey failure is one of the most typical types of damage induced in buildings as the result of earthquake excitation. It has been observed during ground motions that the failure of an upper soft storey of a structure results in large vertical impact load acting on the lower floors. If the resistance of the structural members of the lower storeys is not sufficient it may further lead to progressive collapse of the whole building substantially intensifying material damages as well as human loses.

The main aim of the dissertation is to study the behaviour of steel columns that experience horizontal deformations due to earthquake forces and are additionally subjected to vertical impact load (the effect of the soft-storey failure during ground motion). Furthermore, the response of a multi-storey steel frame building that suffers from a soft-storey failure under real earthquake excitation is also investigated in details.

First, the horizontal stiffness degradation of deformed building steel columns subjected to vertical impact has been investigated. The results of the study indicate that the degradation of horizontal stiffness of the columns may have a considerable influence on the structural response under earthquake excitation. Moreover, the results show that the time of impact plays a substantial role in the overall behaviour of a building indicating that the structural response may be increased significantly if impact takes place when the structure is in the range of its peak deformations during the ground motion.

Then, the experimental investigation focused on the behaviour of models of deformed steel columns that are additionally subjected to vertical impact load, by

dropping the steel sphere from different heights onto the top of the models, has been carried out. The results of the experiments show that, with the increase in the pre-deformation of a column, the value of the peak force acting on its top initially decreases and then shows a considerable increase trend. Moreover, the experimental results indicate that, with the increase in the pre-deformation, the peak horizontal displacement of the middle part of column substantially increases for all drop height values considered.

The detailed numerical investigation concerning the behaviour of a model of deformed steel column that is additionally subjected to vertical impact load has been studied in the next part of this dissertation. The geometric nonlinearity (large strain analysis) as well as the elasto-plastic material behaviour with the strain rate effect have been considered in the analysis. The accuracy of the numerical model of the specimen has been confirmed by comparing the results of the numerical analysis with the experimental results. The first stage of the numerical study show that with the increase in the static pre-deformation of the column the peak mean normal stress values induced at the bottom of the specimen as well as the peak horizontal displacement at the middle of the column show a substantial increase trend for all height drop values considered. The results of the second stage of the study show that vertical impact may substantially influence the response of the column, which is dynamically excited in its horizontal direction, indicating that the response may be increased significantly if impact is initiated when the specimen is in the range of its peak horizontal deformation.

Finally, the detailed, nonlinear, three-dimensional numerical analysis using FEM, focused on the behaviour of multi-storey steel frame building that suffers from

a soft-storey failure under ground motion excitation, has been conducted. The geometric nonlinearity due to impact and the second order effects as well as the elasto-plastic material behaviour with the strain rate effect have been considered in the numerical analysis. The results of the study confirm conclusions obtained in the previous chapters of the dissertation in which simplified numerical models have been used. They show that not only the value of the impact force is crucial but also the moment when impact occurs. It has been confirmed, based on the results obtained, that the most critical moment for the structure for being subjected to a vertical impact, due to the soft-storey failure, is when its horizontal deformation is close to its peak. Moreover, the results clearly indicate that the incorporation of the strain rate effect in the impact-involved numerical analysis is really important in order to increase its accuracy.

STRESZCZENIE

Podczas trzęsień ziemi wielokrotnie obserwowano występowanie tzw. awarii słabego piętra w budynkach polegającej na zniszczeniu elementów nośnych danej kondygnacji. Tego typu awaria, jeżeli dotyczy wyższych pięter, powoduje znaczące pionowe obciążenie uderzeniowe działające na elementy nośne w kondygnacjach znajdujących się poniżej. Przy braku dostatecznego zapasu nośności tych elementów konstrukcji może to spowodować postępujące zniszczenie całego budynku, a co za tym idzie znaczne straty materialne oraz ofiary śmiertelne.

Niniejsza rozprawa poświęcona jest analizie zachowania się stalowych słupów poddanych deformacji poprzecznej, spowodowanej siłami poziomymi będącymi skutkiem trzęsienia ziemi, oraz dodatkowo pionowym obciążeniom uderzeniowym spowodowanym awarią słabego piętra budynku. W pracy szczegółowo przeanalizowano również zachowanie się wielopiętrowego budynku o konstrukcji szkieletowej stalowej, w którym wystąpiła awaria słabego piętra podczas rzeczywistego obciążenia sejsmicznego.

Pierwsza część pracy dotyczy problemu degradacji sztywności poprzecznej stalowych słupów poddanych deformacji oraz pionowemu obciążeniu uderzeniowemu. Wyniki analizy wskazują, iż degradacja sztywności słupów może mieć znaczny wpływ na odpowiedź budynku poddanego obciążeniu dynamicznemu w postaci trzęsienia ziemi. Analiza wykazała ponadto, że moment wystąpienia obciążenia uderzeniowego odgrywa istotną rolę. Uzyskane wyniki pokazują, iż sytuacja, w której moment wystąpienia obciążenia uderzeniowego zbiega się z maksymalną poziomą deformacją budynku powoduje największy wzrost w odpowiedzi konstrukcji podczas trzęsienia ziemi.

W kolejnym etapie przeprowadzono badania doświadczalne, w których to wstępnie zdeformowane modele stalowych słupów poddano uderzeniowym obciążeniom pionowym poprzez zrzucanie na górną podporę słupa stalowej kuli spuszczanej z różnych wysokości. Wyniki tych badań wskazują, iż wraz ze wzrostem wstępnej deformacji poziomej, maksymalna wartość siły działającej na górę słupa początkowo maleje, a następnie wzrasta w sposób istotny. Dodatkowo potwierdzono, iż wraz ze wzrostem wstępnej deformacji następuje znaczny wzrost wartości ekstremalnego przemieszczenia poziomego środka słupa dla wszystkich analizowanych wysokości zrzutu kuli.

Szczegółowym badaniom numerycznym dotyczącym modelu zdeformowanego słupa stalowego poddanego pionowemu obciążeniu uderzeniowemu poświęcono następny rozdział rozprawy. Analiza obejmowała nieliniowość geometryczną (duże odkształcenia) oraz nieliniowość materiałową poprzez zastosowanie modelu elastyczno-plastycznego z uwzględnieniem efektu prędkości odkształcenia. Dokładność modelu numerycznego badanego elementu potwierdzono poprzez porównanie wyników analiz numerycznych z wynikami badań eksperymentalnych. Rezultaty pierwszej części badań numerycznych pokazują, że wzrost wstępnej deformacji prowadzi do wzrostu ekstremalnych naprężeń normalnych u podstawy słupa oraz ekstremalnych wartości przemieszczenia poziomego środka słupa. Wyniki drugiej części badań numerycznych wskazują, iż obciążenie uderzeniowe ma istotny wpływ na odpowiedź słupa, który jest poddany poziomemu wymuszeniu dynamicznemu. Zaobserwowano, iż największy wzrost odpowiedzi dynamicznej ma miejsce w sytuacji, gdy obciążenie uderzeniowe występuje w chwili ekstremalnej deformacji słupa.

W końcowej części dysertacji przeprowadzono dokładną, nieliniową, trójwymiarową analizę numeryczną z wykorzystaniem MES, dotyczącą zachowania się budynku wielokondygnacyjnego o konstrukcji stalowej szkieletowej poddanego obciążeniu sejsmicznemu, w którym wystąpiła awaria słabego pietra. Analiza obejmowała nieliniowość geometryczną (zderzenia i efekty drugiego rzędu) oraz nieliniowość materiałową poprzez zastosowanie modelu elastyczno-plastycznego stali z uwzględnieniem efektu prędkości odkształcenia. Wyniki analizy potwierdzają wnioski otrzymane podczas wcześniejszych badań przy zastosowaniu prostszych modeli numerycznych. Wyniki te wskazują, iż nie tylko wartość obciążenia uderzeniowego, ale również moment jego wystąpienia ma istotny wpływ na zachowanie się konstrukcji. Potwierdzono, iż najbardziej krytyczną chwilą w trakcie trzęsienia ziemi dla budynku poddanemu dodatkowo obciążeniu uderzeniowemu, na skutek awarii słabego piętra, jest moment, gdy pozioma deformacja konstrukcji jest bliska wartości ekstremalnej. Zaobserwowano również, iż uwzględnienie efektu prędkości odkształcenia stali w analizie numerycznej uwzględniającej zderzenia ma istotny wpływ na dokładność uzyskiwanych wyników.

LIST OF SYMBOLS

$a(t)$ - parameter

a_0 - mass matrix multiplier

a_1 - stiffness matrix multiplier

$a_{platform}$ - peak acceleration of the top supporting platform

a_{sphere} - peak acceleration of the sphere

$b(t)$ - parameter

$\bar{c}(t)$ - impact element's damping

$\bar{d}(t)$ - stiffness degradation parameter

e - coefficient of restitution

f_i - frequency for *i*-th vibration mode

g - gravity acceleration

h - thickness

$k(t)$ - parameter

l - storey height

$m_{platform}$ - mass of the top supporting platform

m_{sphere} - mass of the steel sphere

t - time

$u(t)$ - displacement

$u(x,t)$ - horizontal displacement

$\dot{u}(t)$ - velocity

$\ddot{u}(t)$ - acceleration

x - distance from the middle of the column

A - cross section area

C_i - damping coefficient for the *i*-th storey

$\mathbf{C}$ - damping matrix

D - pre-deformation

E - Young's modulus

LIST OF SYMBOLS

$F(t)$ - vertical force

$F_{cr}(t)$ - vertical critical dynamic force

F_{peak} - peak impact force acting on top of the specimen

H - drop height

I - moment of inertia of cross section

K_i - stiffness coefficient for the *i*-th storey

$\overline{K}(t)$ - nonlinear stiffness coefficient

$\mathbf{K}$ - stiffness matrix

M_i - mass of the *i*-th storey

$\mathbf{M}$ - mass matrix

NV - number of values in the time history

$P(t)$ - horizontal inertial force

P_{cr} - vertical critical static force

$U_i(t)$ - displacement of the *i*-th storey

$\mathbf{U}(t)$ - displacement matrix

$\dot{U}_i(t)$ - velocity of the *i*-th storey

$\dot{\mathbf{U}}(t)$ - velocity matrix

$\ddot{U}_g(t)$ - ground motion acceleration

$\ddot{U}_i(t)$ - acceleration of the *i*-th storey

$\ddot{\mathbf{U}}(t)$ - acceleration matrix

V_i - value from the time history obtained from the experiment

$\bar{V}_i$ - value from the time history obtained from the numerical analysis

$W_H(t)$ - resultant horizontal displacement

$W_X(t)$ - horizontal displacement in X direction

$W_Y(t)$ - horizontal displacement in Y direction

β_N - parameter of the Newmark method

$\bar{\beta}$ - impact stiffness parameter

γ_N - parameter of the Newmark method

$\delta(t)$ - relative deformation

Δt - time step

ε - strain

$\dot{\varepsilon}$ - strain rate

ν - Poisson's ratio

ξ - damping ratio

$\bar{\xi}$ - impact damping ratio

ρ - mass density

σ - stress

σ_y - yield strength

σ_u - ultimate tensile strength

ω_i - circular frequency for *i*-th vibration mode

WYKAZ OZNACZEŃ

$a(t)$ - parametr

a_0 - mnożnik macierzy mas

a_1 - mnożnik macierzy sztywności

$a_{platform}$ - ekstremalne przyspieszenie górnej platformy nośnej

a_{sphere} - ekstremalne przyspieszenie kuli

$b(t)$ - parametr

$\bar{c}(t)$ - tłumienie w modelu zderzenia

$\bar{d}(t)$ - parametr degradacji sztywności

e - współczynnik odbicia

f_i - częstotliwość dla *i*-tej postaci drgań własnych

g - przyspieszenie ziemskie

h - grubość

$k(t)$ - parametr

l - wysokość kondygnacji

$m_{platform}$ - masa górnej platformy nośnej

m_{sphere} - masa stalowej kuli

t - czas

$u(t)$ - przemieszczenie

$u(x,t)$ - przemieszczenie poziome

$\dot{u}(t)$ - prędkość

$\ddot{u}(t)$ - przyspieszenie

x - odległość od środka słupa

A - pole przekroju poprzecznego

C_i - współczynnik tłumienia dla *i*-tej kondygnacji

$\mathbf{C}$ - macierz tłumienia

D - deformacja wstępna

E - moduł Young’a

$F(t)$ - siła pionowa

$F_{cr}(t)$ - dopuszczalna pionowa siła dynamiczna

F_{peak} - ekstremalna siła uderzeniowa działająca na górę elementu

H - wysokość zrzutu

I - moment bezwładności przekroju

K_i - współczynnik tłumienia dla *i*-tej kondygnacji

$\overline{K}(t)$ - nieliniowy współczynnik tłumienia

$\mathbf{K}$ - macierz sztywności

M_i - masa *i*-tej kondygnacji

$\mathbf{M}$ - macierz mas

NV - liczba wartości w przebiegu czasowym

$P(t)$ - pozioma siła bezwładności

P_{cr} - pionowa statyczna siła wyboczeniowa

$U_i(t)$ - przemieszczenie *i*-tej kondygnacji

$\mathbf{U}(t)$ - macierz przemieszczeń

$\dot{U}_i(t)$ - prędkość *i*-tej kondygnacji

$\dot{\mathbf{U}}(t)$ - macierz prędkości

$\ddot{U}_g(t)$ - przyspieszenie ziemi podczas wstrząsu sejsmicznego

$\ddot{U}_i(t)$ - przyspieszenie *i*-tej kondygnacji

$\ddot{\mathbf{U}}(t)$ - macierz przyspieszeń

V_i - wartość z przebiegu czasowego uzyskanego z eksperymentu

$\bar{V}_i$ - wartość z przebiegu czasowego uzyskanego z analizy numerycznej

$W_H(t)$ - wypadkowe przemieszczenie poziome

$W_X(t)$ - przemieszczenie poziome w kierunku X

$W_Y(t)$ - przemieszczenie poziome w kierunku Y

β_N - parametr metody Newmark’a

$\bar{\beta}$ - parametr sztywności w modelu zderzenia

γ_N - parametr metody Newmark’a

$\delta(t)$ - deformacja względna

Δt - krok czasowy

ε - odkształcenie

$\dot{\varepsilon}$ - prędkość odkszatłcenia

ν - współczynnik Poisson’a

ξ - liczba tłumienia

$\bar{\xi}$ - liczba tłumienia w modelu zderzenia

ρ - gęstość

σ - naprężenie

σ_y - granica plastyczności

σ_u - wytrzymałość na rozciąganie

ω_i - częstość kołowa dla *i*-tej postaci drgań własnych

LIST OF FIGURES

SPIS RYSUNKÓW

LIST OF TABLES

SPIS TABEL

Chapter 1.

INTRODUCTION

1.1 Preface

Civil and structural engineering has experienced a vast improving, unifying and standardising process over the past thirty years. Also, the accessibility of fast computers and sophisticated computer software integrates this achievement into advanced tools for engineers. Nowadays, as an outcome of this development, engineers can create designs that have not been possible two or three decades ago with the certainty of complete calculations based on standards that have been created, developed and confirmed by scientists and engineers worldwide. But one of the most critical aspects in structural engineering are the design loads applied. Among them, earthquake excitations are considered to be the most dangerous and, at the same time, the most unpredictable dynamic loads acting on civil engineering structures (see Ciesielski and Kawecki 1978-2009, El Kafrawy and Bagchi 2007, Amiri *et al.* 2008, Davoodi *et al.* 2009, Naeini and Zarincheh 2010, Paulay and Priestley 1992, Sasan and Mohammadsadegh 2011, Zembaty 1987, 2007).

1.2 The phenomenon and problem

The so called soft-storey failure is one of the most typical types of damage observed in buildings during earthquakes. In the 1989 Loma Prieta earthquake, for

example, many wood-frame buildings in the Marina District experienced permanent offsets of their soft storeys (Maison *et al*. 2011). During the Boumerdès earthquake of 2003, substantial number of buildings were subjected to the soft-storey failure at the ground level of the structure (see Figure 1.1). As the result of the Hyougoken-Nanbu (Kobe) earthquake of 1995, a large number of the damaged steel and reinforced concrete buildings suffered from failure of the first or intermediate storey (see Figure 1.2) due to lack of lateral strength as well as ductility of columns (Elkholy and Meguro 2004, Watanabe 1997). The soft-storey failure was very common during the 2004 Asia earthquake resulting in major damage in downtown of Banda Aceh (Ghobarah *et al*. 2006). Destruction of one particular storey in buildings was also observed during other ground motions, including the collapses of the top storeys of structures – see Figure 1.3.

Fig. 1.1: Soft-storey failure of the first storey of building (Boumerdès earthquake, 2003)

It has been observed during earthquakes that the failure of an upper soft storey of a structure results in large impact load acting on the lower floors. If the resistance of the structural members of the lower storeys is not sufficient it may further lead to progressive collapse of the whole building (see Figure 1.4) substantially intensifying material damages as well as human loses (see, for example, Talaat and Mosalam, 2009).

Fig. 1.2: Soft-storey failure of the intermediate storey of building (Kobe earthquake, 1995)

1.3 Previous studies on earthquake-induced impacts in buildings

The investigation on earthquake-induced impacts in buildings has been conducted in earthquake engineering for more than two decades now. However, all of the previous studies were only focused on horizontal structural interactions observed during earthquakes as the result of the difference in dynamic properties of

neighbouring buildings. This phenomenon, known as the earthquake-induced structural pounding, may lead to substantial damage or even collapse of colliding structures.

Fig. 1.3: Soft-storey failure of the top storey of building (Haiti earthquake, 2010)

The basic investigation on pounding between insufficiently separated buildings in series, modelled as single degree-of-freedom systems, was carried out by Anagnostopoulos (1988). Davis (1992) used this simple structural model to study pounding of a building against a rigid adjacent structure. Single-degree-of-freedom models were also employed by other researchers (see, for example, Chau and Wei 2001, Ruangrassamee and Kawashima 2001, Mahmoud *et al.* 2008, Jankowski 2010).

Fig. 1.4: Progressive collapse of building (Kocaeli earthquake, 1999)

More detailed analyses were carried out using discrete multi degree-of-freedom structural models, in which mass of each storey was lumped at each floor level. Maison and Kasai (1992) employed such models to study the response of a light high-rise structure colliding against a massive low building. The lumped mass models of 5-storey and 10-storey buildings were used by Anagnostopoulos and Spiliopoulos (1992). Further investigation concerned nonlinear analysis of pounding between two neighbouring 3-storey and 4-storey buildings with substantially different dynamic properties (Jankowski 2008, Mahmoud and Jankowski 2009). A study on multi-degree-of-freedom models of colliding structures of unequal storey heights was also carried out by Karayannis and Favvata (2005).

The research on earthquake-induced pounding was also conducted using the Finite Element Method (FEM). The method was employed in the study conducted by Papadrakakis *et al.* (1996), in which floors of colliding buildings were modelled as single four-node plane stress elements and walls as four linear beam-column elements. More accurate, three-dimensional, nonlinear analyses of pounding between two insufficiently separated buildings using FEM have been recently carried out by Jankowski (2009, 2012).

1.4 Aim and scope of the dissertation

On the contrary to the earthquake-induced horizontal collisions in buildings, impact between the damaged upper part of the building falling onto the lower storeys after the soft-storey failure has not been investigated so far. Therefore, the main aim of the present work is to study the behaviour of the steel columns that experience horizontal deformations due to earthquake forces and are additionally subjected to vertical impact load (the effect of the soft-storey failure). Furthermore, the response of a multi-storey steel frame building that suffers from a soft-storey failure under real earthquake excitation is also investigated in details.

This PhD dissertation consists of the following chapters:

Chapter 1 introduces the problem of a soft-storey failure in buildings during earthquakes and describes previous research on earthquake-induced impacts in structures. The aim and scope of the work are also presented.

The preliminary problems related to the subject of the dissertation are described in **Chapter 2**. The chapter includes such topics as: soft-storey failure mechanism, impact loads acting on steel columns/bars and strain rate effect in steel.

The influence of the horizontally deformed steel columns that are additionally subjected to vertical impact load (the effect of the soft-storey failure during earthquakes) on the response of the building is considered in **Chapter 3**. Basic results are obtained based on the theoretical approach as well as on the simplified numerical analysis using the lumped mass model of the building. Special attention is paid to investigate the influence of the horizontal stiffness degradation of columns on the overall structural response during the ground motion.

Chapter 4 is focused on the experimental investigation concerning the behaviour of models of horizontally deformed steel columns that are additionally subjected to vertical impact load. In the experiment, impact load has been generated by a steel sphere dropped onto a pad of technical clay, so as to simulate nearly plastic impact observed in the reality during earthquakes.

The detailed numerical analysis concerning the behaviour of the model of horizontally deformed steel column under impact load is described in **Chapter 5**. In the first stage of the study, different static pre-deformations of the column as well as various impact load time histories have been considered. Then, the detailed nonlinear analysis has been conducted by exciting dynamically the base of the specimen as well as by applying impact vertical load at different times of the harmonic ground motion excitation.

Chapter 6 deals with the detailed, nonlinear, three-dimensional numerical analysis concerning the behaviour of a multi-storey steel frame building that suffers from a soft-storey failure under real earthquake excitation. A model of the structure has been exposed to an impact that would have been generated after a soft-storey failure due to falling of the upper floors. The geometric nonlinearity due to impact and the second order effects as well as the elasto-plastic material behaviour with the

strain rate effect have been considered. During the analysis, different moments have been chosen for the impact so as to estimate the most critical moment for the building.

Final conclusions and general remarks of the study are presented in **Chapter 7**.

Chapter 2.

PRELIMINARY PROBLEMS

2.1 Soft-storey failure and its reasons

The presence of a soft-storey in a building is strictly related to the weakness of structural elements, which can be verified by comparing the lateral stiffness of adjacent storeys. According to ASCE (2006), we usually deal with a soft-storey if the lateral stiffness of particular storey is less than 70% of the stiffness of the storey above or less than 80% of the average stiffness of the three storeys above. It should be underlined, however, that in some cases, a soft-storey failure might take place even if the above criteria are not satisfied (ASCE 2006). It is due to the fact that the soft-storey failure is also much dependant on the nature of the earthquake, which is a random phenomenon with its unpredictable properties such as direction of seismic wave, peak ground acceleration, frequency contents and duration (Chen and Scawthorn 2003, Green 1981, Wiegel 1970).

The mechanism that leads to a soft-storey failure in a steel frame building under earthquake excitation is schematically shown in Figure 2.1. It starts with seismic induced horizontal ground motion that generates a horizontal excitation of the foundation. This excitation results in horizontal movement of the whole building (swaying of the structure) and the structural response increases during the time of the earthquake due to inertial forces (see stage 1 of Figure 2.1). The increased vibrations

may cause significant increase in the internal forces, especially bending moments and shearing forces at the connections between horizontal elements (slabs and beams) and vertical members (columns) of the structure (Yoshimura 1997, Plumier *et al.* 2005). This increase may remarkably exceed the yield strength of steel leading to damage of connections (see Figure 2.2 and Figure 2.3) or damage of columns in the vicinity of connections (see Figures 2.4-2.6). This may further results in forming the plastic hinges (stage 2 of Figure 2.1) and a failure of the particular structural element or the collapse of the whole storey, as has been schematically shown at the stage 3 of Figure 2.1 (Yoshimura 1997, Plumier *et al.* 2005).

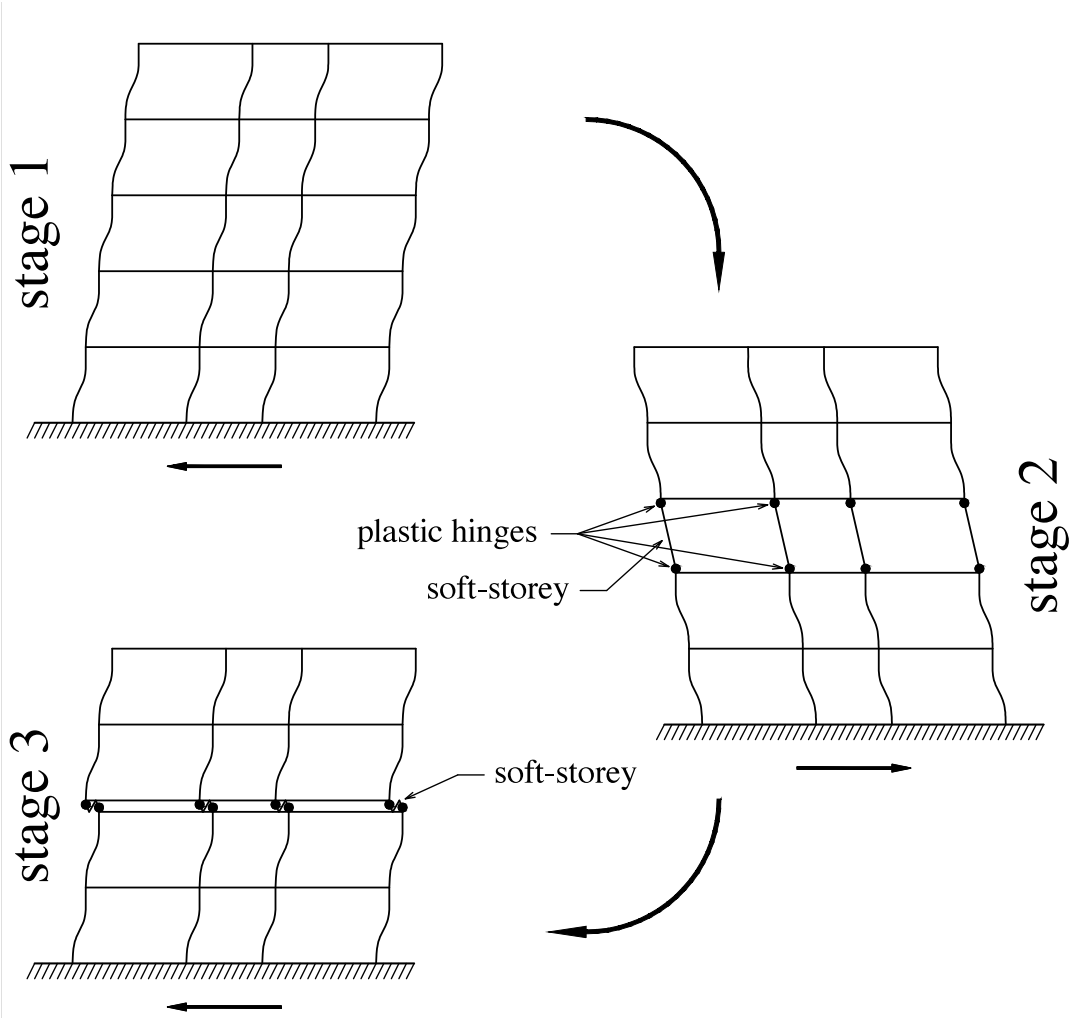

Fig. 2.1: Schematic illustration of the stages of a soft-storey mechanism in building under earthquake excitation

The lateral stiffness of particular storeys of the building as well as the nature of the ground motion excitation determine the location of the storey, which exhibits failure. It is usually the first storey of a structure, which is in the largest danger of being damaged. However, in the case of multi-storey buildings, damage is quite often concentrated at the intermediate or top storey level. It is due to the fact that it is a common practice in multi-storey buildings to reduce the cross section of the load carrying elements (i.e. columns) at particular level in order to minimize the dead load of the upper storeys of the structure as well as the construction costs. Such a reduction in the cross section, and therefore the reduction in the lateral stiffness, may cause the concentrations of high values of stresses at this particular storey leading to its failure. Moreover, as it can be seen form Figure 1.3, the same structural elements, in this case reinforced concrete columns, may suffer from damage at different heights due to different support conditions or due to the presence of adjacent secondary elements. It is also possible that the soft-storey failure is initiated at the particular level of the structure due to failure of some secondary elements, such as bracings (see Figure 2.7).

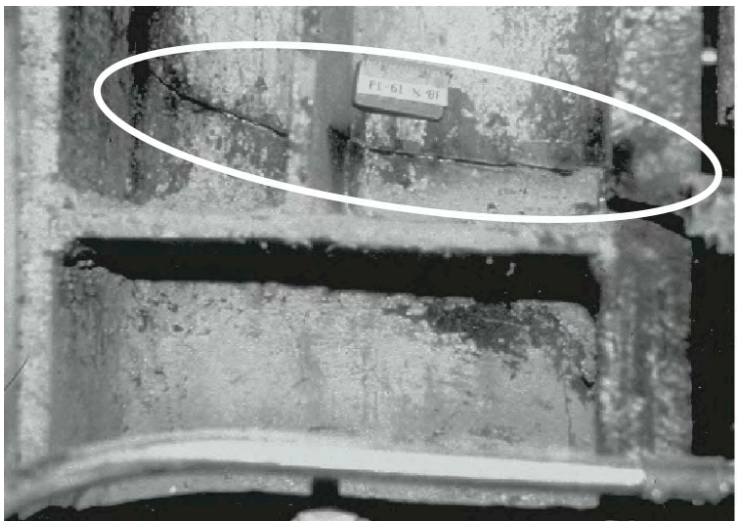

Fig. 2.2: Damage to beam-to-column connection – crack in a web of I cross section (Naeim 2001)

Fig. 2.3: Damage to beam-to-column connection – crack in a flange of I cross section (Naeim 2001)

Fig. 2.4: Buckling of the top of column as the result of the 1964 Alaska earthquake (Elnashai and Di Sarno 2008)

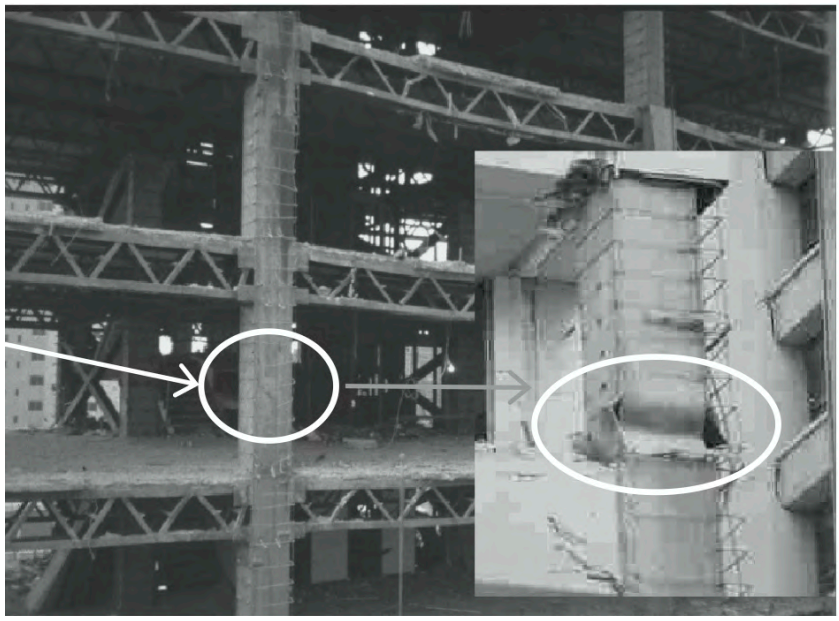

Fig. 2.5: Damage at the bottom of the box column as the result of the 1985 Michoacan (Mexico City) earthquake (Elnashai and Di Sarno 2008)

Fig. 2.6: Damage at the top of the I column as the result of the 1964 Alaska earthquake (Elnashai and Di Sarno 2008)

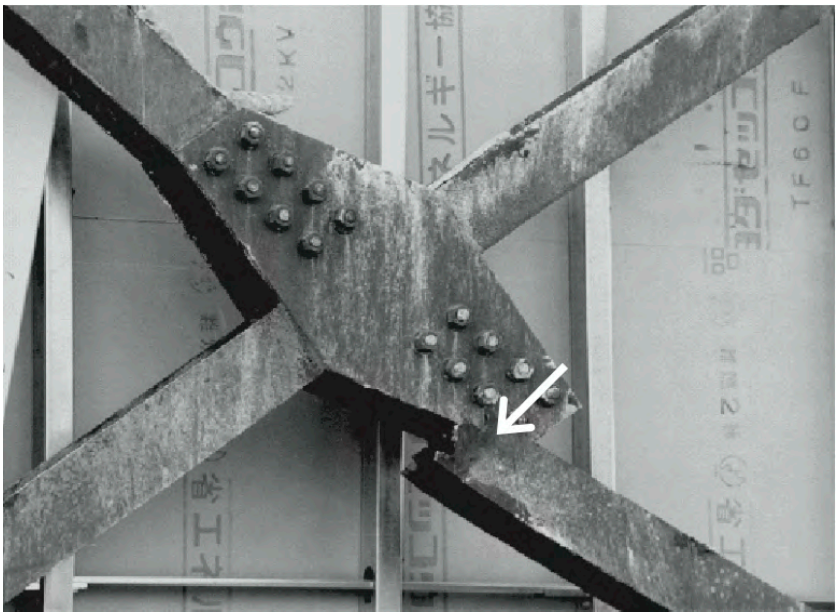

Fig. 2.7: Fracture in a brace connection as the result of the 1995 Kobe earthquake (Elnashai and Di Sarno 2008)

A number of studies were conducted in the past so as to verify the reasons of a soft-storey failure in steel as well as in reinforced concrete buildings and investigate the problem in more details (see, for example, Sezen *et al.* 2002, Plumier *et al.* 2005, Arslan and Korkmaz 2007, Inel *et al.* 2007, Wibowo *et al.* 2010, Ju *et al.* 2012). A detailed experimental investigation was carried out on a part of existing building by Wibowo *et al.* (2010) by conducting a push-over test (see also Krawinkler and Seneviratna 1998). The preparation of a part of the structure for the test is presented in Figure 2.8; whereas Figure 2.9 shows the setup of the push-over test. The results of the study have confirmed that the failure of connections between vertical and horizontal structural elements are the major reasons initiating the soft-storey failure. Other studies were focused on the failure behaviour of beam-column connections caused by inappropriate stiffness relation between beams and columns (strong beam - weak column failure as well as weak beam - strong column failure – see Figure 2.10), insufficient reinforcement ratio, poorly designed building geometry

or wrong material combinations (see Sezen *et al.* 2002, Plumier *et al.* 2005, Arslan and Korkmaz 2007, Inel *et al.* 2007, Ju *et al.* 2012, Zhoudao *et al.* 2011).

Fig. 2.8: Preparation of a part of existing building for a push-over test (Wibowo *et al.* 2010)

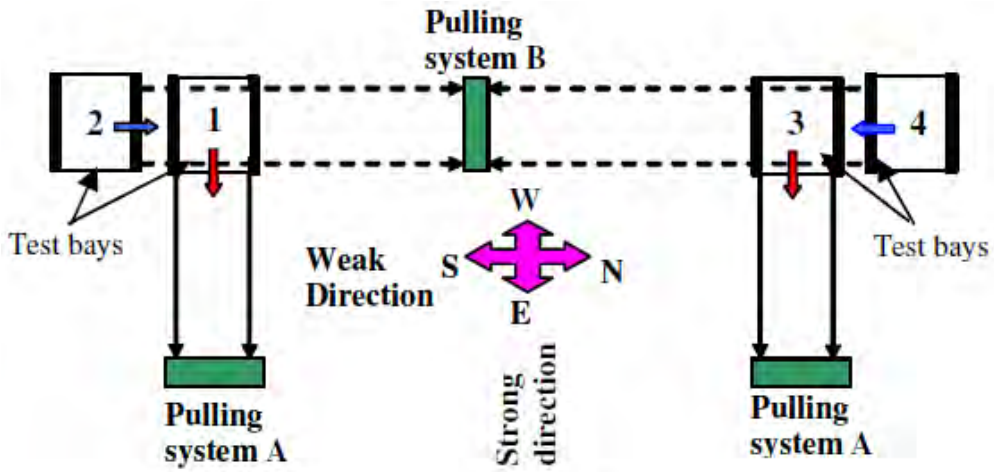

Fig. 2.9: The setup of a push-over test on a part of existing building (Wibowo *et al.* 2010)

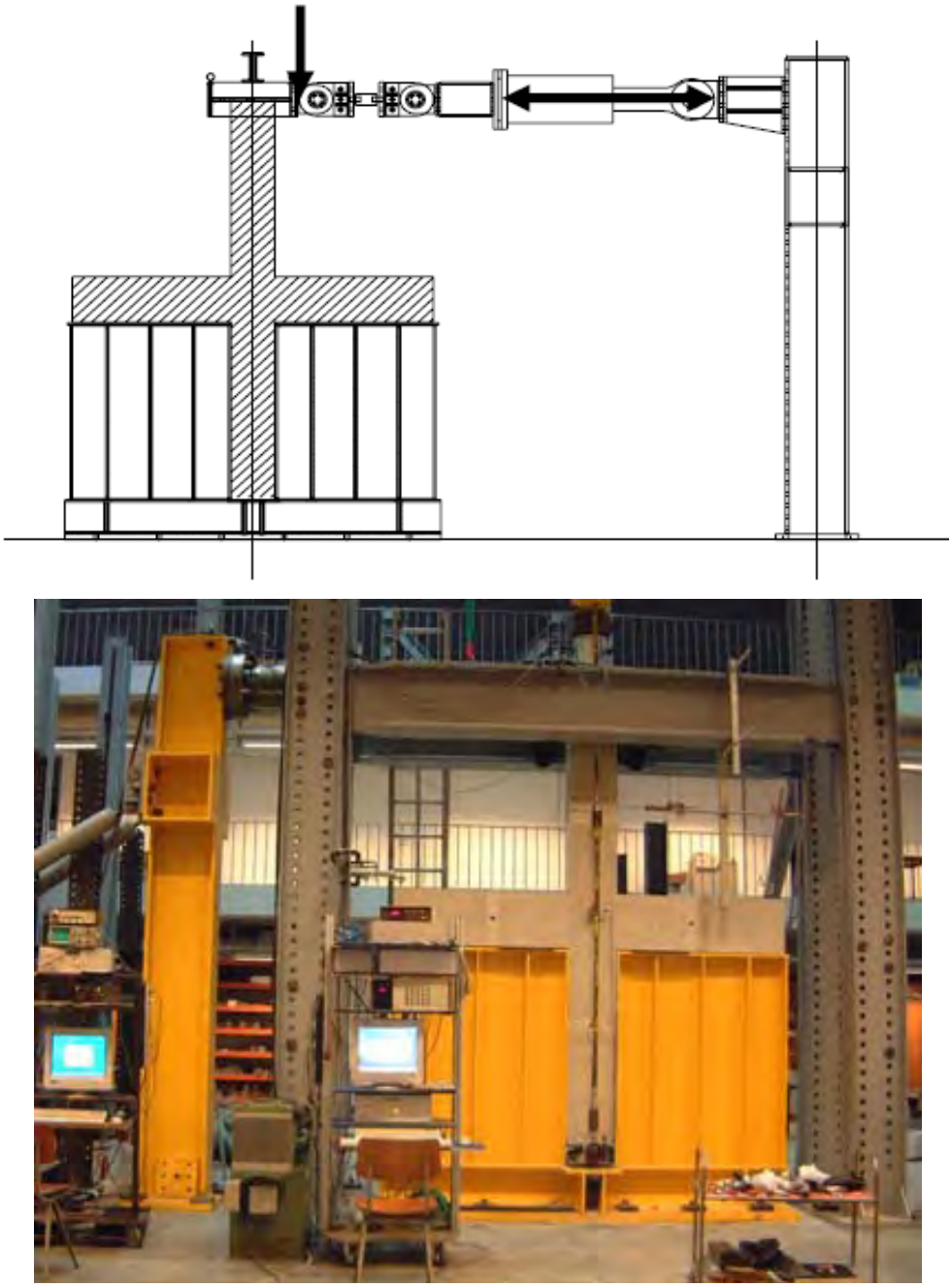

Fig. 2.10: The test setup reproducing a ‘weak beam - strong column’ configuration (Plumier *et al.* 2005)

There have also been some ideas to use the first soft-storey as a kind of a base-isolation system for buildings in order to reduce damage generated by an earthquake at the levels of the upper storeys (see Mo and Chang 1993). It should be underlined, however, that such kind of solutions allow for major damage at the ground level of the structure what can be dangerous for inhabitants and what leads to

the necessity of demolishing the building after the earthquake, so it cannot be considered as the effective seismic isolation technique (Naeim and Kelly 1999). Because of the above, it is rather a common practice to consider a soft-storey failure as not desired under any circumstances due to possible human as well as material losses.

2.2 Impact loads acting on steel columns and bars

The failure of the intermediate or top storey of a building during earthquake results in large vertical impact load acting on the top of columns of the lower storey due to the fall of the upper floors. The earthquake-induced horizontal impacts between insufficiently separated buildings have also been recorded, as described in Introduction. Besides cases observed during ground motions, other situations may also induce impact loads acting on buildings, in particular on columns of structures. One of the most common reason of such a situation is related to the impact of a vehicle or forklift, in which impact force is exerted on the column perpendicularly to its axis (see Figure 2.11). The studies on such types of impacts have recently been much advanced. Hilpert and Willnow (1999) studied the load bearing behaviour of thin-walled columns subjected to impact loads from any direction. A study concerning a collapse of a column by vehicle impact was also conducted by Tsang and Lam (2008). Więch and Jankowski (2012) analysed impacts at steel I-columns of the building investigating the influence of support conditions of the column and place of force application. The problem of transverse impact on columns was also analysed by other researchers (see, for example, Adachi *et al.* 2004, Sastranegara *et al.* 2005, 2006).

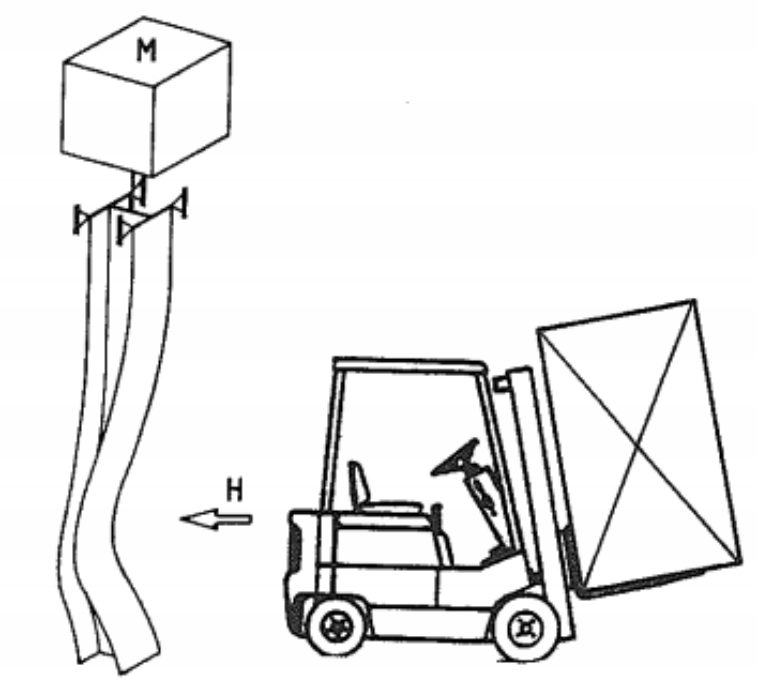

Fig. 2.11: Impact load on a steel column by a forklift (Hilpert and Willnow 1999)

There have also been a number of studies related to axial impact loading acting on steel columns and bars, which are observed in the mechanical systems. The studies have concerned perfectly straight elements as well as elements with some initial imperfections in the form of a bow, under the assumption that both ends of the column/bar are not displaced (see Figure 2.12). Very extensive theoretical fundamentals for analyses concerning such problems were given by Gryboś (1980). Some aspects of dynamic buckling of axially loaded steel columns were also considered by Langer (1980). More recently, Cui *et al.* (1999) analysed a fluid-solid impact of columns that were mounted in a frame which was dropped into water. Another example was considered by Kenny *et al.* (2000), where a dynamic elastic buckling of a slender beam with geometric imperfections was investigated after being subjected to an axial impulse. Wu and Zhong, 2000 analysed the computation efficiency of the lower bound dynamic buckling loads of imperfect bars under impact loading. Dynamic buckling of columns with initial imperfections under intermediate

velocity impact was considered by Hao *et al.* 2000. The problem of axial loading acting on columns and bars was also studied by other researchers (see, for example, Cui *et al.* 2001, 2002, Gur and Elishakoff 1997, Karagiozova and Jones 1996, Zhang and Taheri 2002).

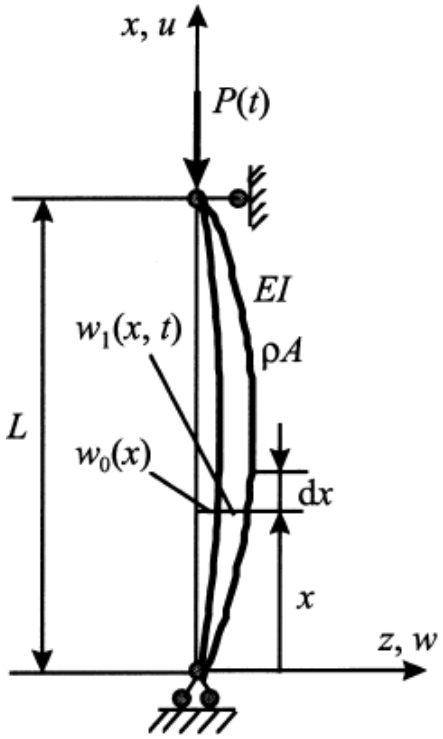

Fig. 2.12: Axial impact loading acting on a column with initial imperfection in the form of a bow (Hao *et al.* 2000)

2.3 Strain rate effect in steel

Impact loads acting on structural elements induce usually high values of strain rates. Experimental studies have shown that some materials are sensitive to the speed of load applied and their properties may differ for different strain rates (see Mania 2010). This phenomenon, known as the strain rate effect, concerns particularly structural elements made of steel, for which, with rising strain rate, the yield strength and the ultimate strength also gain. The strain rate effect is traditionally tested using the Hopkinson bar or the Kolsky bar (see Figure 2.13).

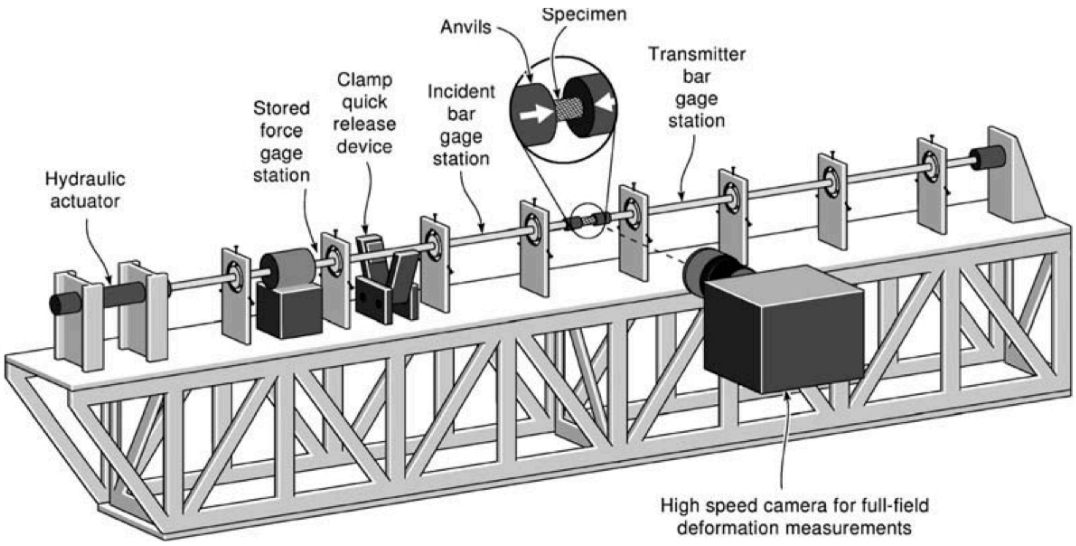

Fig. 2.13: Schematics of Kolsky bar setup (Vaynman *et al.* 2006)

The general principle of operation of the apparatus is as follows. A sample of the material is placed between two straight bars (incident and transmitter bar), that are mounted in bearings allowing for only axial motion. An impact (generated, for example, by a pressure gun) is applied onto the incident bar and transferred through the specimen into the transmitter bar. The pulse is reflected and comes back. Both the transmitted and reflected pulses are measured by strain gauge station and based on those records the strain rate can be obtained. A camera can be used to obtain additional information about the deformation of the specimen.

Since steel is a material commonly used in a variety of technical applications, including military, car or aircraft industry where impact loads are considered in the design process, the influence of the strain rate effect in steel has been studied quite extensively. In the case of the above technical applications, the strain rate during impact may attain very high values from circa 300 s^{-1} up to even 10000 s^{-1} (see, for example, Shah 2006). The analyses have been conducted for different types and grades of steel for various strain rates. The examples of the results, obtained from the

experimental tests carried out for different types of steel (their chemical composition is summarized in Table 2.1), are shown in Figure 2.14 (Ansell 2006).

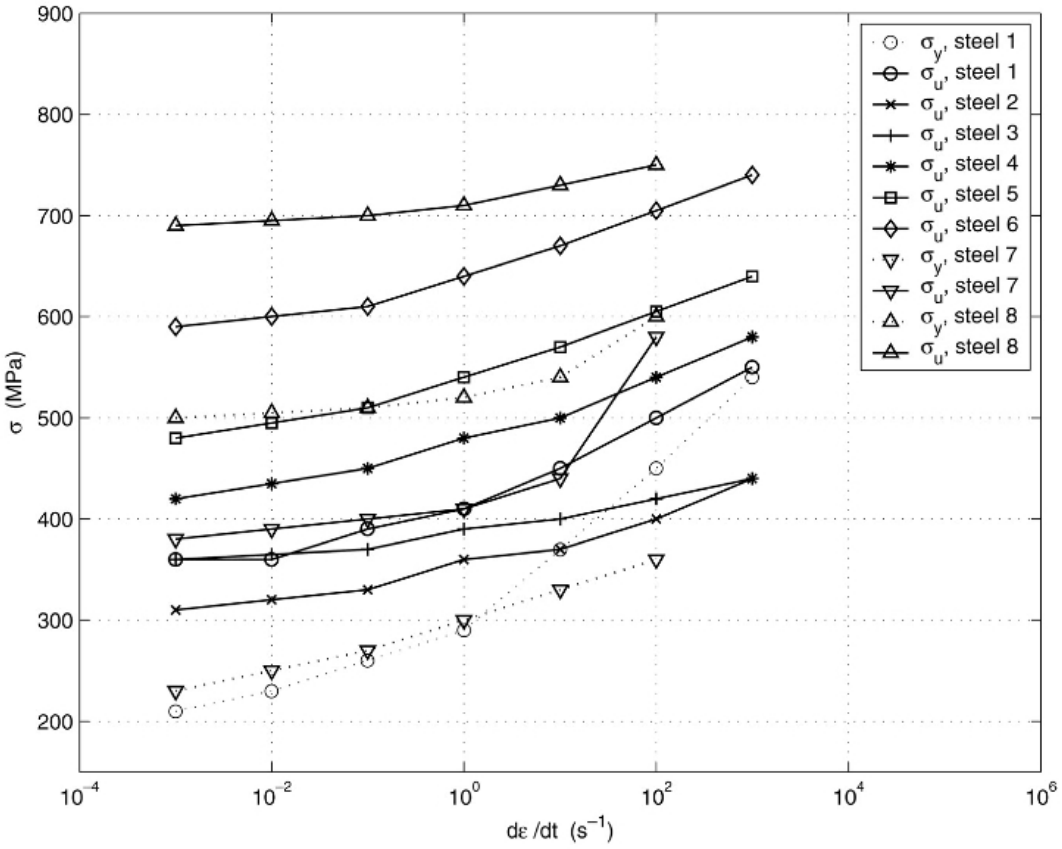

Fig. 2.14: Yield strength, σ_y, and ultimate tensile strength, σ_u, vs. strain rate for different types of steel summarized in Tab. 2.1 (Ansell 2006)

Steel		C (%)	Si (%)	Mn (%)
1	Mild steel[a]	Unknown	Unknown	Unknown
2	Annealed 1010[b]	0.10	Unknown	0.50
3	Hot-rolled 0.10C[b]	0.10	Unknown	0.50
4	Hot-rolled 0.19C[b]	0.19	Unknown	0.75
5	Hot-rolled 0.32C[b]	0.32	Unknown	0.75
6	Hot-rolled 0.47C[b]	0.47	Unknown	0.74
7	Mild steel C10[c]	0.12	0.15	0.27
8	High strength StE47[c]	0.16	0.30	1.36

Tab. 2.1: Chemical composition of different types of steel considered in Fig. 2.14: a - from Manjoine 1944; b - from Davies and Magee 1976; c - from Krabiell and Dahl 1981 (Ansell 2006)

As it can be seen from Figure 2.14, with the increase in the strain rate, the increase in the yield strength as well as the ultimate strength can be substantial. Moreover, the figure indicates that the level of the increase depends on the type of steel showing higher increase for low strength steels and lower increase for high strength steels. In the case of a mild steel (steel 7), for example, the values of the yield strength and the ultimate strength for the strain rate of 100 s^{-1} are as much as 50% larger comparing to the corresponding values when the strain rate is equal to 0.001 s^{-1} (quasi-static conditions). On the other hand, it can be seen from Figure 2.14 that, for the high strength steels, the increase in the yield strength and the ultimate strength values is not so significant. In the case of steel 8, the difference between corresponding values for various strain rates is within the range of 8% (Ansell 2006).

A number of other studies have concerned the strain rate effect in steel under different temperatures. Malinowski *et al.* (2007), for example, studied the influence of the strain rate on the properties of material exposed to heat treatment, which results in releasing the residual stress coming from the production process. The stress-strain curves for different strain rates, as obtained for steel 18G2 (S355 according to the actual Eurocode standards) at the stage of delivery are shown in Figure 2.15. Additionally, the detailed comparison between the results obtained for the strain rate of 0.001 s^{-1} (quasi-static conditions) and 5 s^{-1} is presented in Figure 2.16. On the other hand, the stress-strain curves for different strain rates for steel 18G2 after heat treatment are shown in Figure 2.17.

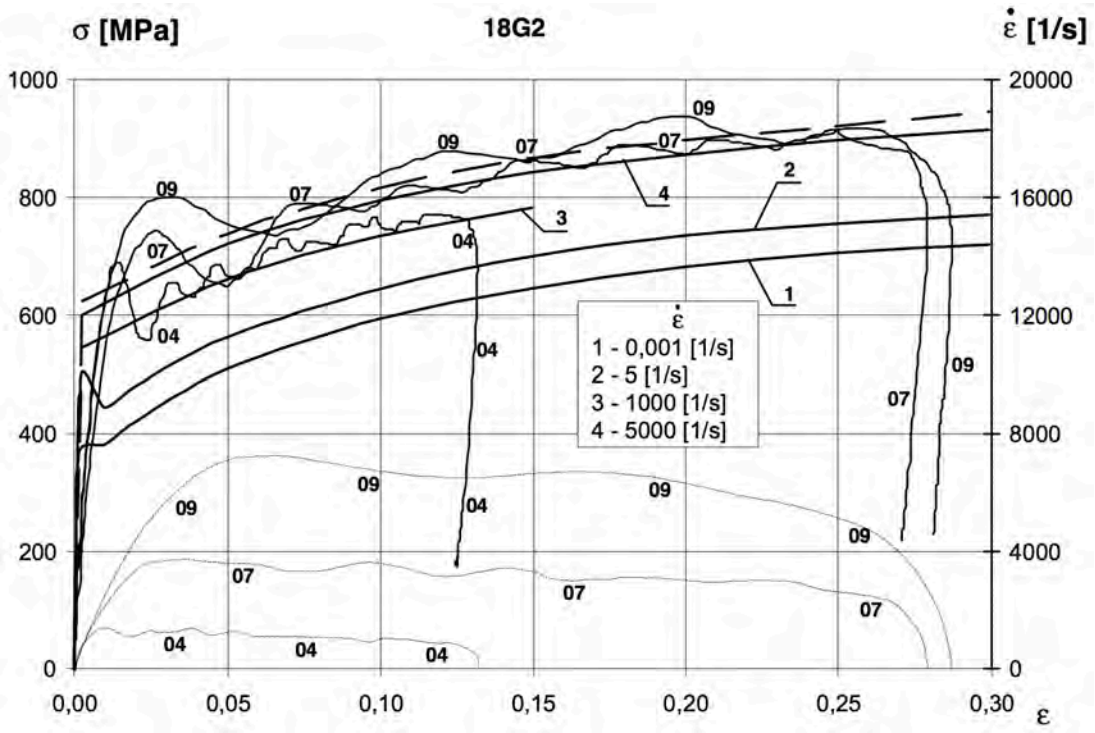

Fig. 2.15: Stress-strain curves for different strain rates test for 18G2 steel at delivery state (numbers at curves refer to tests as described by the authors, Malinowski *et al.* 2007)

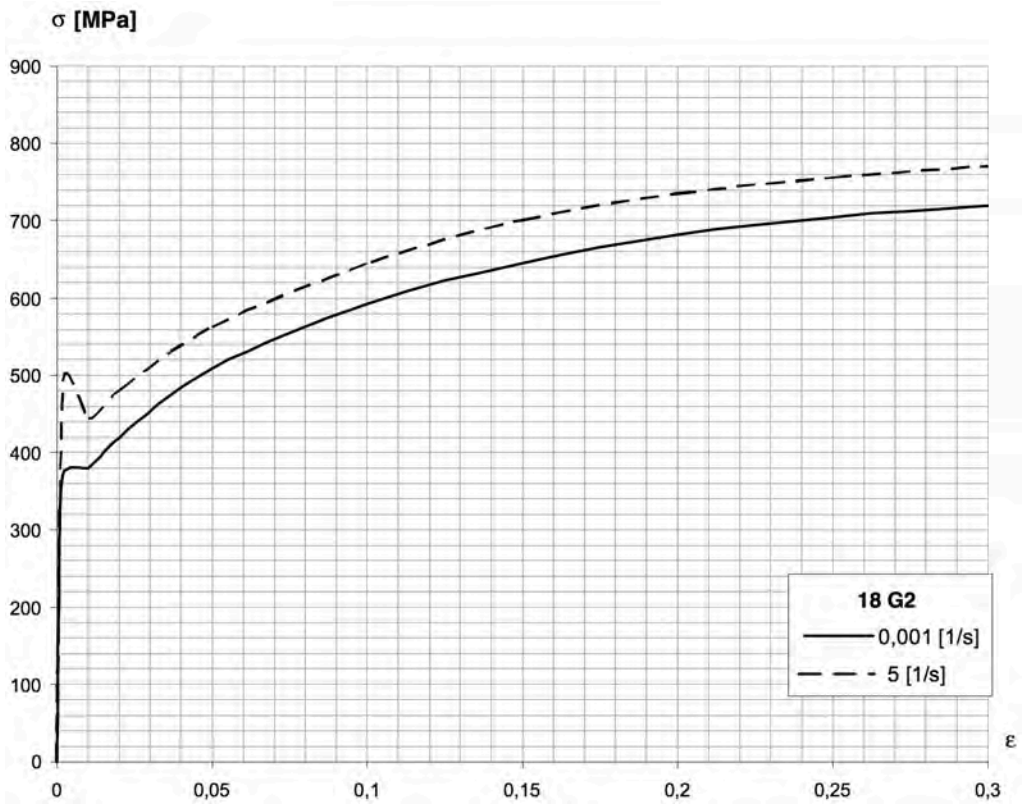

Fig. 2.16: Detailed comparison between stress-strain curves for strain rate of 0.001 s^{-1} and 5 s^{-1} for 18G2 steel (Malinowski *et al.* 2007)

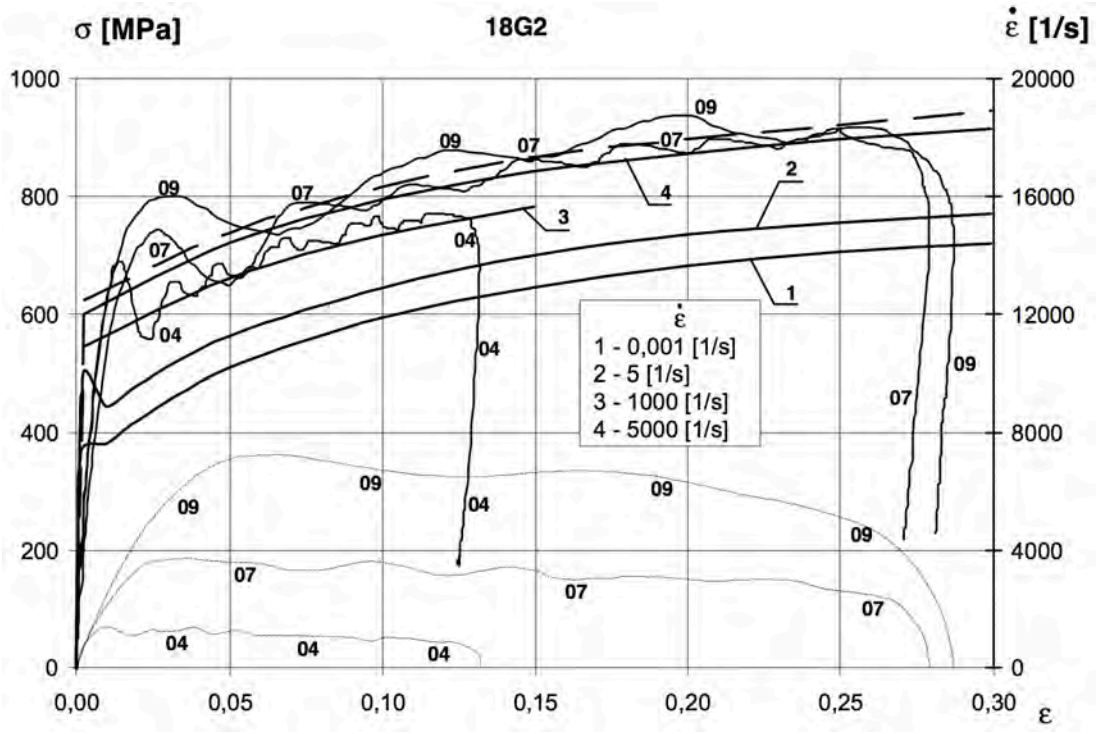

Fig. 2.17: Stress-strain curves for different strain rates test for 18G2 steel after heat treatment (numbers at curves refer to tests as described by the authors, Malinowski *et al.* 2007)

The results shown Figures 2.15-2.17 indicate that the heat treatment has negligible influence on the yield strength and the ultimate strength of steel. It has been therefore concluded that welding steel, which generates residual stress through locally induced high temperature, does not really influence the material properties related to the strain rate effect (Malinowski *et al.* 2007). The results of the study presented in Figure 2.16 also indicate that the strain rate may considerably influence the material properties, even if the strain rate is relatively low. It can be seen comparing the stress-strain curves that the increase in the strain rate from 0.001 s^{-1} (quasi-static conditions) to 5 s^{-1} leads to the increase in the yield strength and the ultimate strength of tested steel by about 16% (Malinowski *et al.* 2007).

The strain rate effect in steel under different temperatures was also studied by Vaynman *et al.* (2006). The examples of the results of the study are presented in

Figure 2.18 and Figure 2.19. In particular, Figure 2.18 shows the relation between the strain rate and the flow stress at 5% at the temperature of 25°C for HSLA-65 and AlNiCu-150 steels (their chemical composition is summarized in Table 2.2), whereas the effect of strain rate and temperature on flow stress at 0.05 true strain for AlNiCu-150 steel is presented in Figure 2.19. It can be seen from the figures that, in the case of the temperature range that building structures might be exposed to (in this study from -40°C to 25°C), the influence of temperature on the strain rate effect for two types of steel considered in the study is very low.

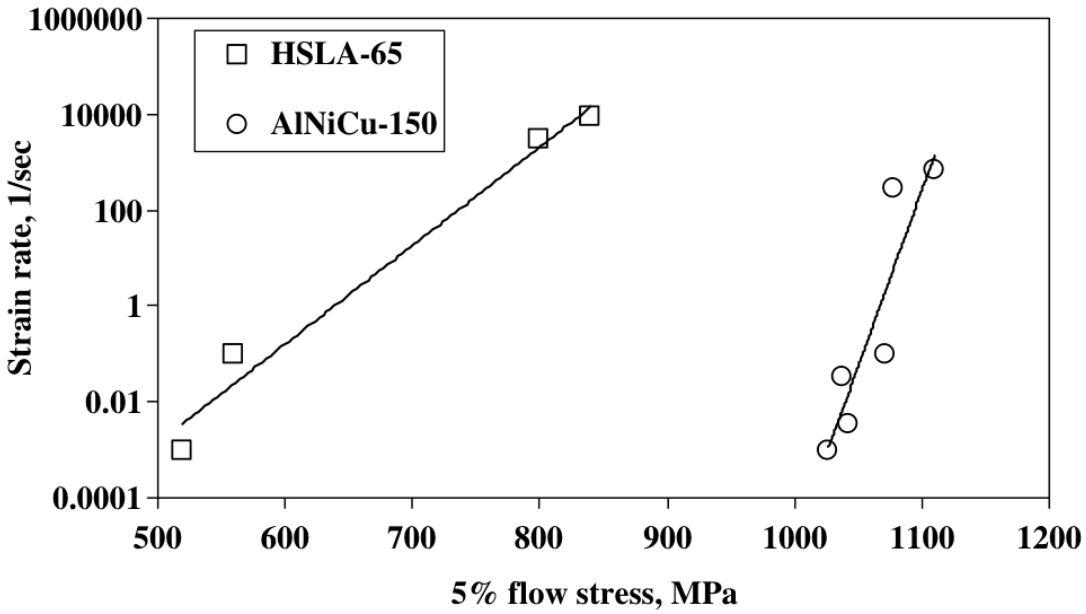

Fig. 2.18: Relation between strain rate and flow stress at 5% at 25°C (Vaynman *et al.* 2006)

	C	Mn	P	S	Si	Cu	Ni	Al	Nb
AlNiCu 150	0.05	0.47	0.005	0.001	0.46	1.34	2.71	0.60	0.07
HSLA 65	0.08	1.40	0.005	0.005	0.24	<0.01	<0.01	0.03	0.04

Tab. 2.1: Chemical composition of steel considered in Fig. 2.18 and 2.19 (Vaynman *et al.* 2006)

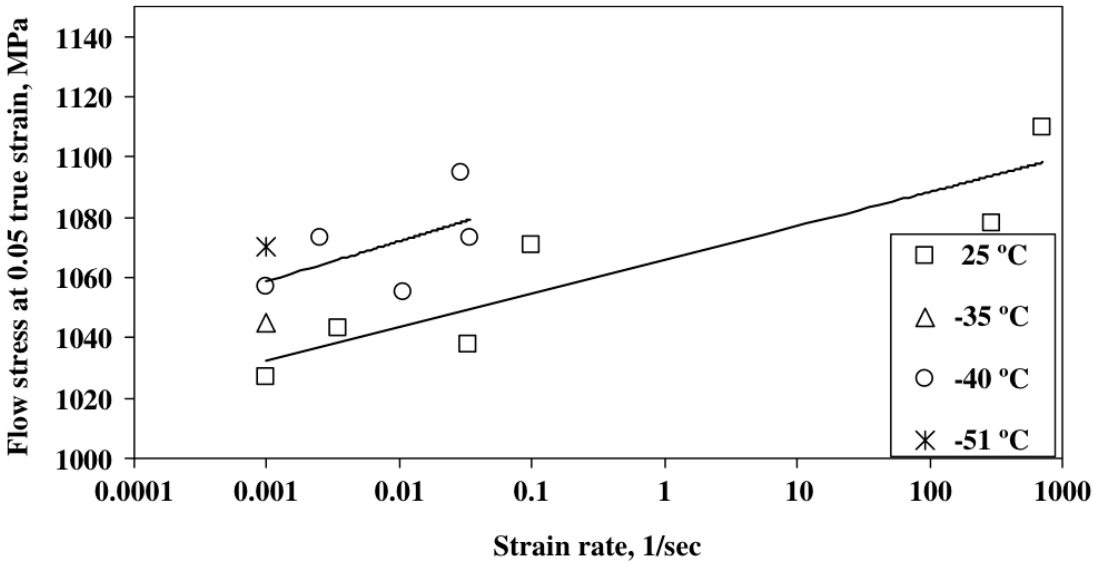

Fig. 2.19: Effect of strain rate and temperature on flow stress at 0.05 true strain for AlNiCu-150 steel (Vaynman *et al.* 2006)

Chapter 3.

STIFFNESS DEGRADATION OF DEFORMED COLUMNS UNDER IMPACT LOAD

3.1 Introduction

The influence of the horizontally deformed steel columns that are additionally subjected to vertical impact load, on the response of the building, based on the theoretical approach as well as on the simplified numerical analysis using the lumped mass model of the structure, is considered in this chapter. Special attention is paid to investigate the influence of the horizontal stiffness degradation of columns on the overall structural response during earthquake. The derivation of the formula for the degradation of the column's stiffness as the result of dynamic vertical load is shown.

3.2 Theoretical approach

As a response to the horizontal component of earthquake excitation, a building will also displace laterally in the horizontal direction. The action of vertical gravity loads, due to the weight of the storeys, on the displaced configuration of the structure leads to the increased translation. This phenomenon is known as the P-delta or the second order effect (see, for example, Juhasova 1991, Chopra 1995).

Let us consider a column of a building with both ends fixed to the floor slabs, which is exposed to bending (as the result of horizontal earthquake loading) and

simultaneously to vertical load acting on its top (see Figure 3.1). The case of the vertical load which results only from the weight of the storeys has been intensively studied by a number of earthquake engineers. A simplified approach to the problem assumes that the deflected shape of the column is a straight line and the horizontal stiffness degradation (allowing for the increased displacement) can be obtained by the use of additional fictitious column with the specified negative stiffness properties (see, for example, Rutenberg 1981, 1982, Wilson 2002). More accurate methods take into account the details of the deflected shape of the building column due to its bending. Such an approach to the case of the vertical load, which results only from the weight of the floor slab (static load) was studied by Juhasova (1991). In this chapter let us consider a more general case, in which the vertical load results also from impact of the upper storeys falling onto the top of a column after the soft-storey failure (dynamic load).

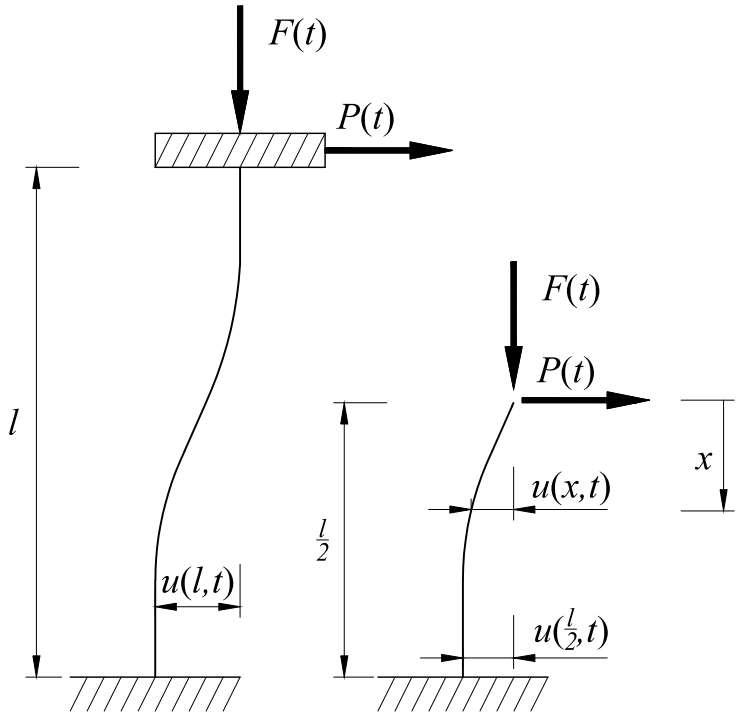

Fig. 3.1: Deformed column exposed to bending (as the result of horizontal earthquake loading) and simultaneously to vertical load acting on its top

Taking into account the theory of the second order (see, for example, Timoshenko and Gere 1961), the differential equation describing the deformation of the column at a given time, t, of the ground motion can be written as:

$$EI\frac{\partial^2 u(x,t)}{\partial x^2} + P(t)x + F(t)u(x,t) = 0 \qquad (3.1)$$

where E is the Young's modulus of elasticity, I is the moment of inertia of the cross section, $u(x,t)$ denotes the horizontal displacement at the distance x from the middle of the column (see Figure 3.1), $P(t)$ is the horizontal inertial force due to earthquake loading and $F(t)$ stands for the vertical force, which consists of the weight of the floor slab as well as the load due to impact of the upper storeys falling onto the top of the column after the soft-storey failure. The general solution of equation (3.1) can be expressed as (compare Juhasova 1991):

$$u(x,t) = a(t)\sin(k(t)x) + b(t)\cos(k(t)x) - \frac{P(t)x}{EIk^2(t)} \qquad (3.2)$$

where

$$k^2(t) = \frac{F(t)}{EI},\ k(t) \geq 0 \qquad (3.3)$$

Considering the boundary conditions (see direction of x at Figure 3.1), parameters $a(t)$ and $b(t)$ can be calculated as equal to:

a) from the condition: $u(0,t) = 0$ we have: $u(0,t) = b(t)\cos 0 = 0$,

   so: $b(t) = 0$,

b) from the condition: $u'\left(\frac{l}{2},t\right) = 0$ we have:

   $u'\left(\frac{l}{2},t\right) = a(t)k(t)\cos\left(k(t)\frac{l}{2}\right) - \frac{P(t)}{EIk^2(t)} = 0$, so:

   $a(t) = \frac{P(t)}{EIk^3(t)\cos\left(k(t)\frac{l}{2}\right)}$.

Substituting the derived values of $a(t)$ and $b(t)$ into equation (3.2) leads to:

$$u(x,t) = \frac{P(t)}{EIk^3(t)\cos\left(k(t)\frac{l}{2}\right)}\sin(k(t)x) - \frac{P(t)x}{EIk^2(t)} \tag{3.4}$$

$$u(x,t) = \frac{P(t)}{EIk^2(t)}\left(\frac{\sin(k(t)x)}{\mathrm{k}(t)\cos\left(k(t)\frac{l}{2}\right)} - x\right) \tag{3.5}$$

For $x = \frac{l}{2}$ we obtain:

$$u\left(\frac{l}{2},t\right) = \frac{P(t)}{EIk^2(t)}\left(\frac{\tan\left(k(t)\frac{l}{2}\right)}{\mathrm{k}(t)} - \frac{l}{2}\right) \tag{3.6}$$

The total horizontal displacement of the upper support $u(l,t)$ can be obtained from the following formula:

$$u(l,t) = 2u\left(\frac{l}{2},t\right) \tag{3.7}$$

Substituting equation (3.6) into equation (3.7) yields:

$$u(l,t) = \frac{2P(t)}{EIk^2(t)}\left(\frac{\tan\left(k(t)\frac{l}{2}\right)}{\mathrm{k}(t)} - \frac{l}{2}\right) \tag{3.8}$$

Neglecting the influence of horizontal damping at this stage of considerations (such an assumption is reasonable in the case of steel structures, which are usually characterized by the damping ratio of less than 1% or 2%), the horizontal stiffness of the column, $\overline{K}(t)$, can be obtained from the following formula:

$$\overline{K}(t) = \frac{P(t)}{u(l,t)} \tag{3.9}$$

Substituting equation (3.8) into equation (3.9) leads to:

$$\overline{K}(t) = \frac{EIk^2(t)}{2}\frac{2k(t)}{2\tan\left(k(t)\frac{l}{2}\right) - \mathrm{k}(t)l} \tag{3.10}$$

$$\overline{K}(t) = \frac{EIk^3(t)}{2\tan\left(k(t)\frac{l}{2}\right) - \mathrm{k}(t)l} \tag{3.11}$$

The above relation can also be expressed in the form:

$$\overline{K}(t) = \frac{12EI}{l^3}\frac{k^3(t)l^3}{24\tan\left(k(t)\frac{l}{2}\right) - 12\mathrm{k}(t)l} = K\bar{d}(t) \tag{3.12}$$

where:

$$K = \frac{12EI}{l^3} \tag{3.13}$$

is the horizontal stiffness of the column fixed at both ends (see Timoshenko and Gere 1961) and

$$\bar{d}(t) = \frac{k^3(t)l^3}{24\tan\left(k(t)\frac{l}{2}\right) - 12\mathrm{k}(t)l} \tag{3.14}$$

is a parameter describing the degradation of the horizontal stiffness as the result of dynamic vertical load and is valued within the interval $(0,1)$ for $0 < k(t)l < \pi$. The relation between $\bar{d}(t)$ and $k(t)l$ is shown at Figure 3.2. It can be seen from the figure that the value of $\bar{d}(t)$ is nearly equal to 1 for small values of $k(t)l\epsilon(0,0.2)$ indicating that, in this range, the influence of vertical dynamic load on the horizontal stiffness can be neglected. On the other hand, for higher values of $k(t)l$ the value of $\bar{d}(t)$ substantially decreases and for $k(t)l \to \pi$ the degradation parameter, $\bar{d}(t)$, tends to be equal to zero.

Considering equation (3.12), the dynamic equation of motion in the horizontal direction for a structure modelled as an inelastic single degree-of-freedom system (see Figure 3.3) under earthquake excitation can be written as (compare Chmielewski and Zembaty 1998, Chopra 1995):

$$M\ddot{U}(t) + C\dot{U}(t) + \bar{K}(t)U(t) = -M\ddot{U}_g(t) \tag{3.15}$$

where $\ddot{U}(t)$, $\dot{U}(t)$, $U(t)$ is the horizontal acceleration, velocity and displacement of the structure with relation to the ground; M, C, $\bar{K}(t)$ is the mass, damping coefficient and nonlinear stiffness coefficient, respectively; and $\ddot{U}_g(t)$ denotes the ground motion acceleration.

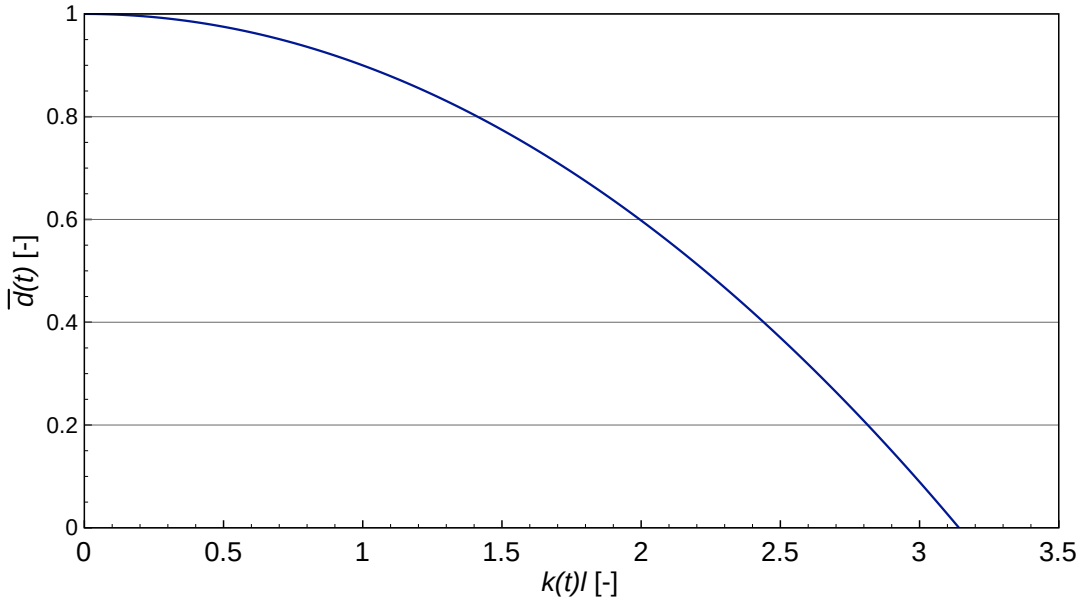

Fig. 3.2: Relation between the degradation parameter, $\bar{d}(t)$, and $k(t)l$

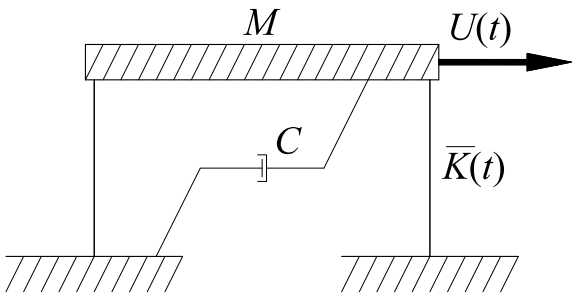

Fig. 3.3: Inelastic single degree-of-freedom system

3.3 Numerical model

In order to investigate the influence of stiffness degradation of columns on the structural behaviour under seismic excitation, a number of numerical simulations have been conducted. The study has been focused on the response of a three-storey building, in which failure of the second and the third storey takes place at a given time of the earthquake and those upper storeys fall onto the top slab of the first

storey. The analysis has been conducted for the following three phases (changes between particular phases make the analysis nonlinear).

3.3.1 Response of building before impact

In the first phase of analysis (before impact), the building has been modelled as an elastic three degree-of-freedom system (see Figure 3.4).

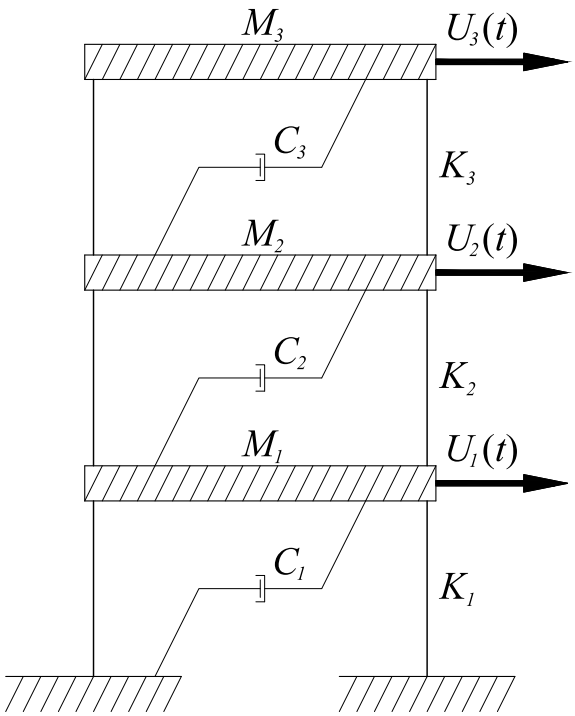

Fig. 3.4: Elastic three degree-of-freedom system

The dynamic equation of motion for such a structural model under earthquake excitation can be formulated as (Chmielewski and Zembaty 1998, Chopra 1995):

$$\mathbf{M}\ddot{\mathbf{U}}(t) + \mathbf{C}\dot{\mathbf{U}}(t) + \mathbf{K}\mathbf{U}(t) = -\mathbf{M}\mathbf{1}\ddot{U}_g(t) \tag{3.16a}$$

$$\mathbf{M} = \begin{bmatrix} M_1 & 0 & 0 \\ 0 & M_2 & 0 \\ 0 & 0 & M_3 \end{bmatrix} \tag{3.16b}$$

$$\ddot{\mathbf{U}}(t) = \begin{bmatrix} \ddot{U}_1(t) \\ \ddot{U}_2(t) \\ \ddot{U}_3(t) \end{bmatrix} \tag{3.16c}$$

$$\dot{\mathbf{U}}(t) = \begin{bmatrix} \dot{U}_1(t) \\ \dot{U}_2(t) \\ \dot{U}_3(t) \end{bmatrix} \tag{3.16d}$$

$$\mathbf{U}(t) = \begin{bmatrix} U_1(t) \\ U_2(t) \\ U_3(t) \end{bmatrix} \tag{3.16e}$$

$$\mathbf{C} = \begin{bmatrix} C_1 + C_2 & -C_2 & 0 \\ -C_2 & C_2 + C_3 & -C_3 \\ 0 & -C_3 & C_3 \end{bmatrix} \tag{3.16f}$$

$$\mathbf{K} = \begin{bmatrix} K_1 + K_2 & -K_2 & 0 \\ -K_2 & K_2 + K_3 & -K_3 \\ 0 & -K_3 & K_3 \end{bmatrix} \tag{3.16g}$$

where: $\ddot{U}_i(t)$, $\dot{U}_i(t)$, $U_i(t)$, K_i, C_i (i=1,2,3) is the horizontal acceleration, velocity, displacement, damping coefficient and elastic stiffness coefficient for a storey with mass M_i, respectively.

3.3.2 Response of building during impact

After the failure of the second and the third storey, the behaviour of the remaining first storey of the building has been modelled as an inelastic single degree-of-freedom system (see Figure 3.3). The dynamic equation of motion formulated in equation (3.15) has been employed taking $M = M_1$, $C = C_1$ and $\overline{K}(t)$ determined according to equation (3.12). The displacement, velocity and acceleration of the first storey, as obtained at the end of the previous phase for the three degree-of-freedom system, have been taken as the initial values. In this phase of the analysis, the vertical force, $F(t)$ (see Figure 3.1), due to impact of the upper storeys falling onto the top of

the first storey, has been calculated at each time step using the nonlinear viscoelastic model of impact force expressed by the formula (Jankowski 2005):

$$F(t) = \bar{\beta}\delta^{\frac{3}{2}}(t) + \bar{c}(t)\dot{\delta}(t) \quad \text{for } \dot{\delta}(t) > 0 \text{ (approach period of impact)}$$

$$F(t) = \bar{\beta}\delta^{\frac{3}{2}}(t) \quad \text{for } \dot{\delta}(t) \leq 0 \text{ (restitution period of impact)} \tag{3.17}$$

where $\bar{\beta}$ is the impact stiffness parameter, $\delta(t)$ describes the relative deformation of colliding structural members and $\bar{c}(t)$ is the impact element's damping which, for the free fall of the second and the third storey onto the top of the first storey, can be obtained from the formula (compare Jankowski 2005):

$$\bar{c}(t) = 2\bar{\xi}\sqrt{\bar{\beta}\sqrt{\delta(t)}\frac{M_1(M_2+M_3)}{M_1+M_2+M_3}} \tag{3.18}$$

where $\bar{\xi}$ denotes the impact damping ratio related to a coefficient of restitution, *e*. The approximate relation between $\bar{\xi}$ and *e* in the nonlinear viscoelastic model can be expressed by the formula (Jankowski 2006):

$$\bar{\xi} = \frac{9\sqrt{5}}{2}\frac{1-e^2}{e(e(9\pi-16)+16)} \tag{3.19}$$

3.3.3 Response of building after impact

It has been assumed in the analysis that after impact the weight of the second and the third storey stays at the top of the remaining first storey and the building has also been modelled as an inelastic single degree-of-freedom system (see Figure 3.3). The dynamic equation of motion formulated in equation (3.15) has been used taking $M = M_1 + M_2 + M_3$, $C = C_1$ and $\overline{K}(t)$ determined according to equation (3.12). In this phase of the analysis, the constant value of the vertical force, $F(t) = (M_1 +$

$M_2 + M_3)g$ (g is the gravity acceleration), which results only from the weight of all floor slabs, has been applied.

3.4 Results of the numerical simulations

The numerical simulations have been focused on the behaviour of a three-storey building, in which failure of the second and the third storey is assumed to take place at a given time of the earthquake and those upper storeys fall onto the top slab of the first storey (see also Migda and Jankowski 2012c, 2013b). The following values describing the structural properties of the intact building have been used in the analysis (see Jankowski 2008):

$$M_1 = M_2 = M_3 = 25{\times}10^3 \text{ kg},$$

$$K_1 = K_2 = K_3 = 3.460{\times}10^6 \text{ N/m},$$

$$C_1 = C_2 = C_3 = 6.609{\times}10^4 \text{ kg/s},$$

$$l = 3.5 \text{ m}.$$

The values of the nonlinear viscoelastic impact force model's parameters have been applied as equal to: $\bar{\beta} = 2.75{\times}10^9 \text{ N/m}^{3/2}$, $\bar{\xi} = 0.35$ $(e = 0.65)$ (see Jankowski 2005, 2008). In order to solve the equations of motion (3.15) and (3.16) numerically, the time-stepping Newmark method (Newmark 1959), with the standard parameters: $\gamma_N = 0.5$, $\beta_N = 0.25$ (see Chopra 1995) and constant time step $\Delta t = 0.0002$ s, has been used. The numerical procedure has been programmed using MATLAB software. The NS component of the El Centro earthquake (18.05.1940) has been applied in the analysis (see the acceleration time history in Figure 3.5).

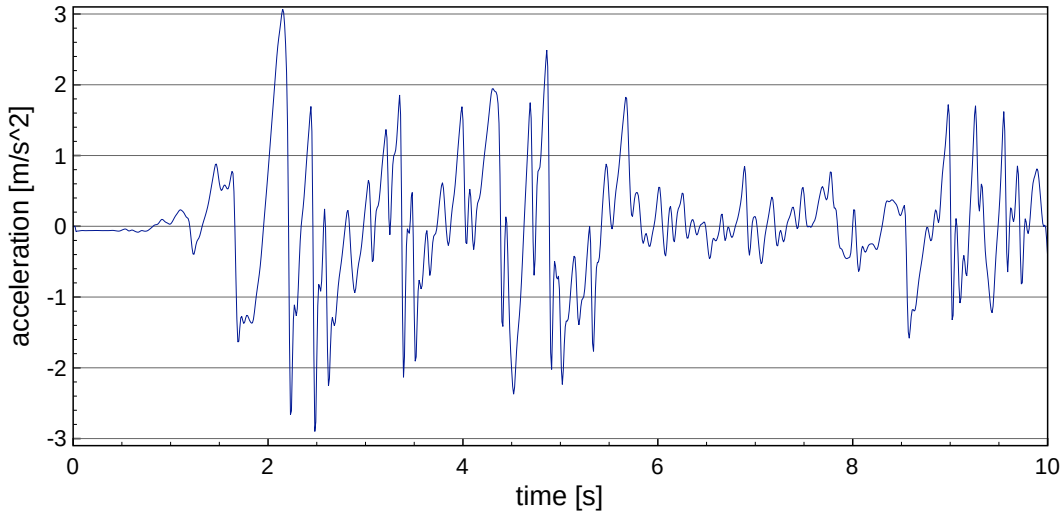

Fig. 3.5: Acceleration time history of the NS component of the El Centro earthquake (18.05.1940)

The analysis has been conducted for two cases. First, the response of the building has been determined taking into account the degradation of horizontal stiffness of columns under seismic excitation and vertical load. Then, a similar analysis has been carried out without considering the effect of stiffness degradation. It has been assumed in the analysis that impact (due to the fall of the upper storeys onto the top of the first storey) takes place at different times of the earthquake. The examples of the results, for impact at $t = 1$ s, $t = 2$ s, $t = 3$ s, $t = 4$ s, $t = 5$ s, $t = 6$ s, $t = 7$ s, $t = 8$ s and $t = 9$ s of the El Centro earthquake, are shown in Figures 3.6-3.14. The peak displacement response values for different cases of impact times are denoted in the figures by arrows and also summarized in Table 3.1. Additionally, Figure 3.15 presents the time histories of impact force, $F(t)$, relative vertical deformation of colliding structural members, $\delta(t)$, and the impact element's damping during impact, $\bar{c}(t)$, which gives some insight into the model of impact force defined in equations (3.17)-(3.19).

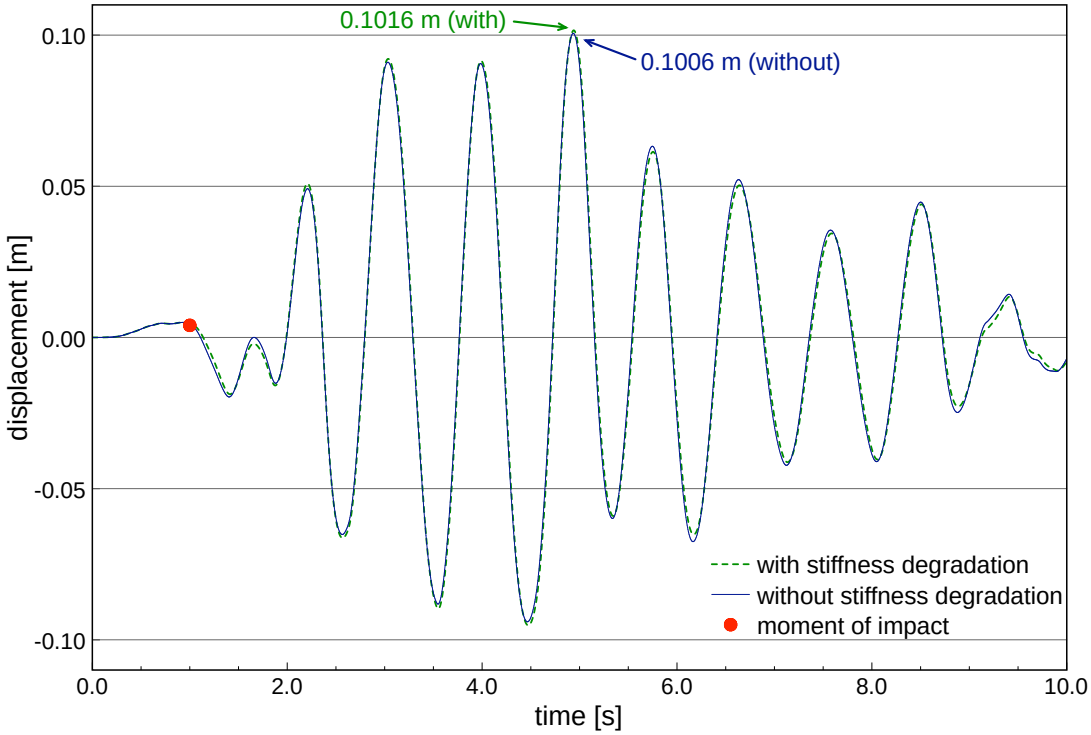

Fig. 3.6: Displacement history of the first storey of building under the El Centro earthquake with and without considering the degradation of horizontal stiffness for impact at t=1 s

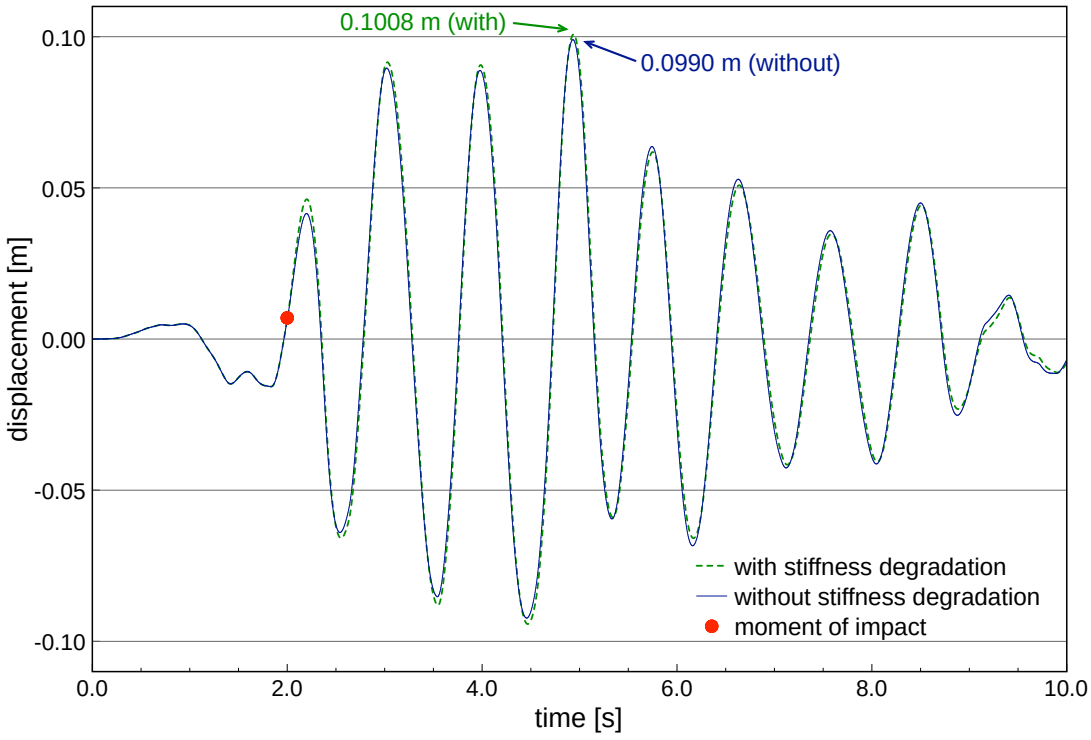

Fig. 3.7: Displacement history of the first storey of building under the El Centro earthquake with and without considering the degradation of horizontal stiffness for impact at t=2 s

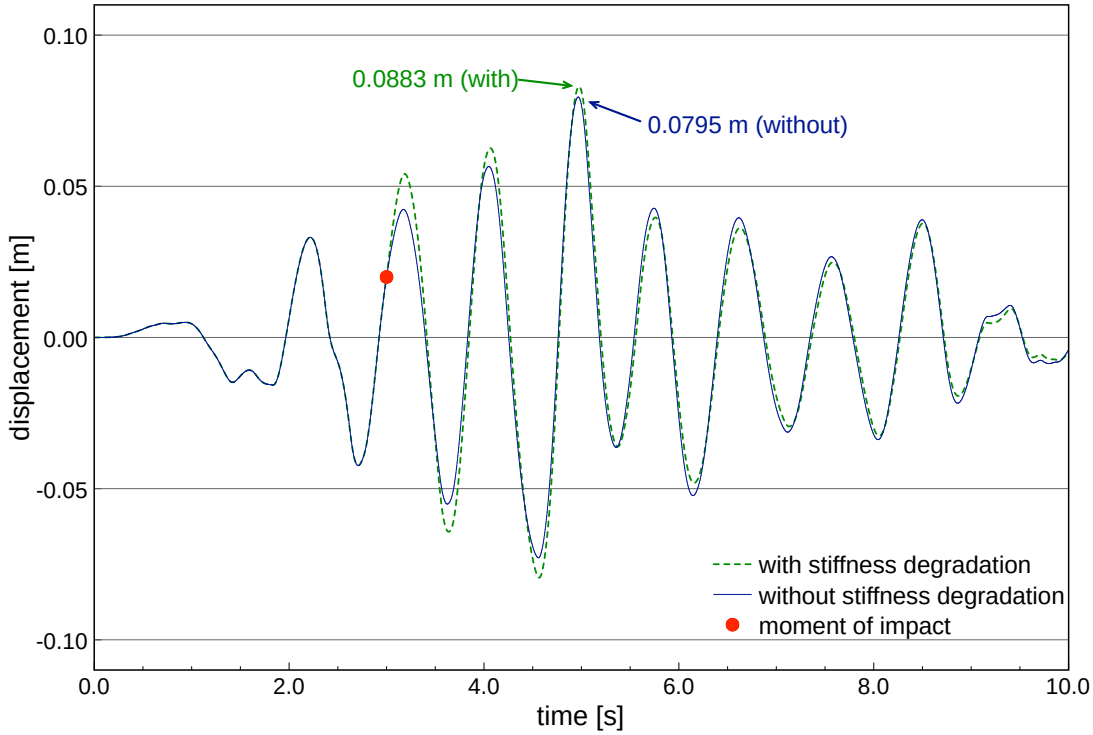

Fig. 3.8: Displacement time of the first storey of building under the El Centro earthquake with and without considering the degradation of horizontal stiffness for impact at t=3 s

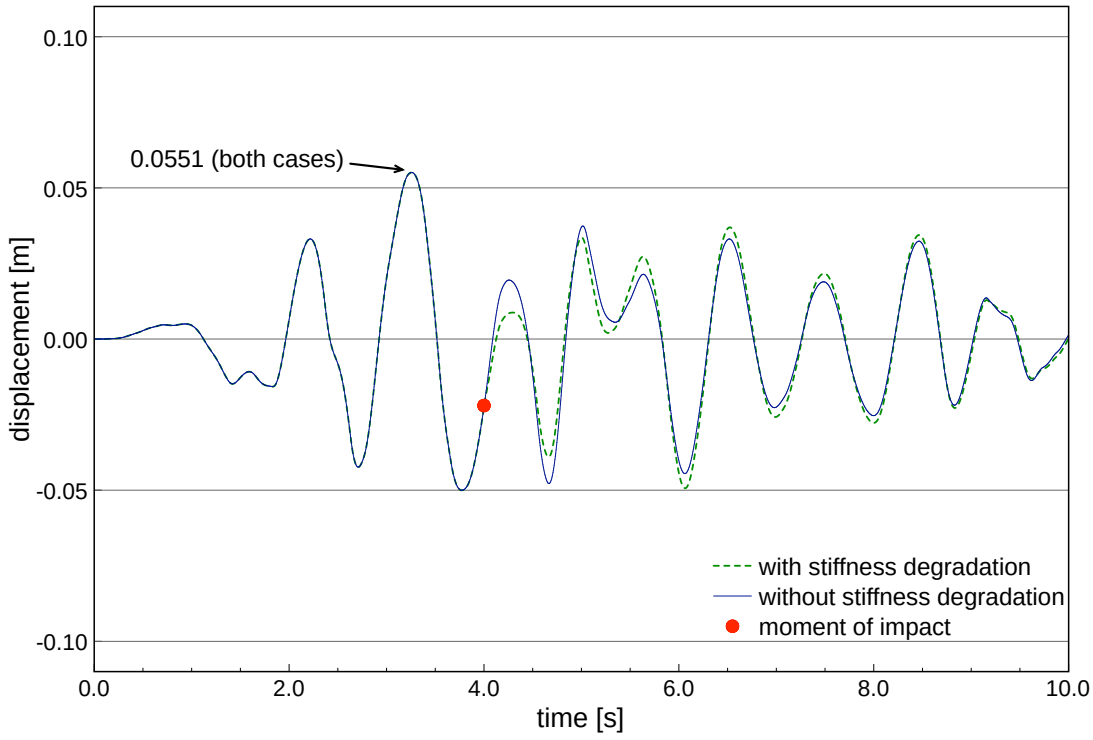

Fig. 3.9: Displacement history of the first storey of building under the El Centro earthquake with and without considering the degradation of horizontal stiffness for impact at t=4 s

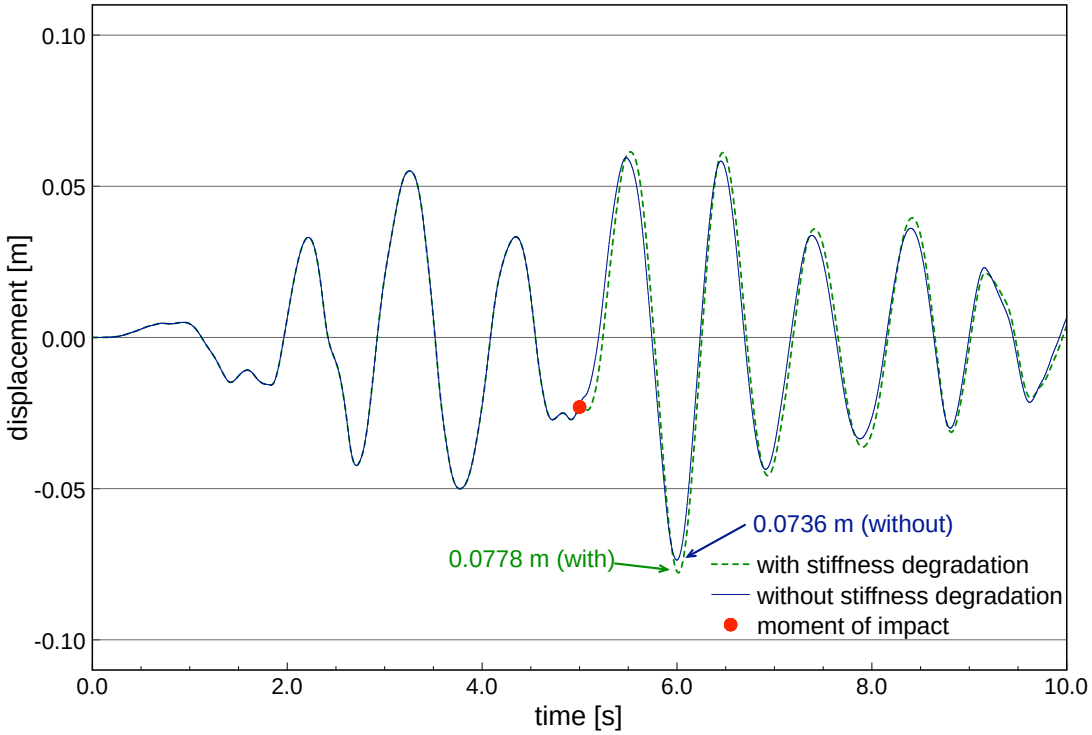

Fig. 3.10: Displacement history of the first storey of building under the El Centro earthquake with and without considering the degradation of horizontal stiffness for impact at t=5 s

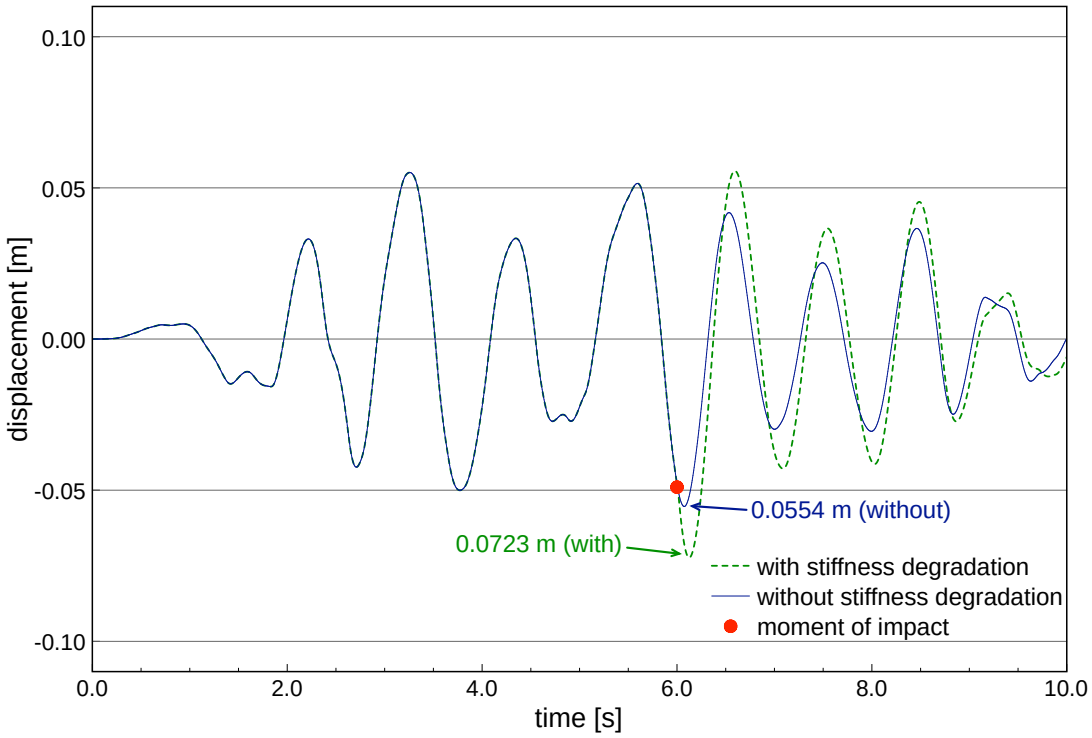

Fig. 3.11: Displacement history of the first storey of building under the El Centro earthquake with and without considering the degradation of horizontal stiffness for impact at t=6 s

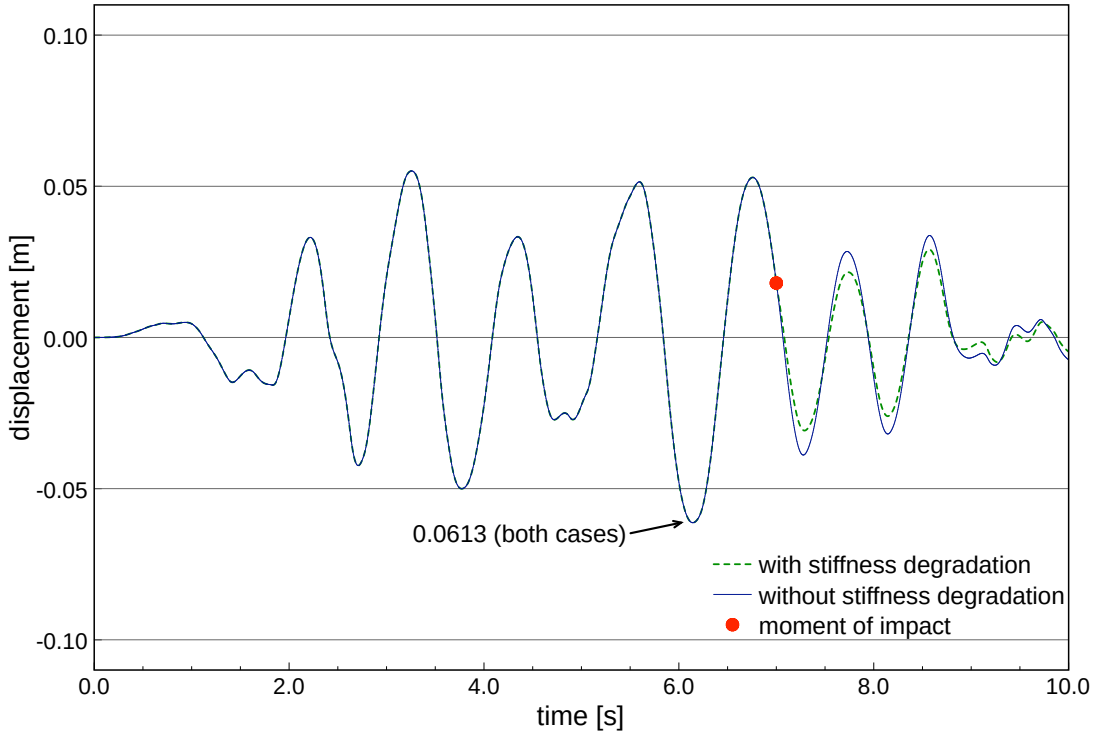

Fig. 3.12: Displacement history of the first storey of building under the El Centro earthquake with and without considering the degradation of horizontal stiffness for impact at t=7 s

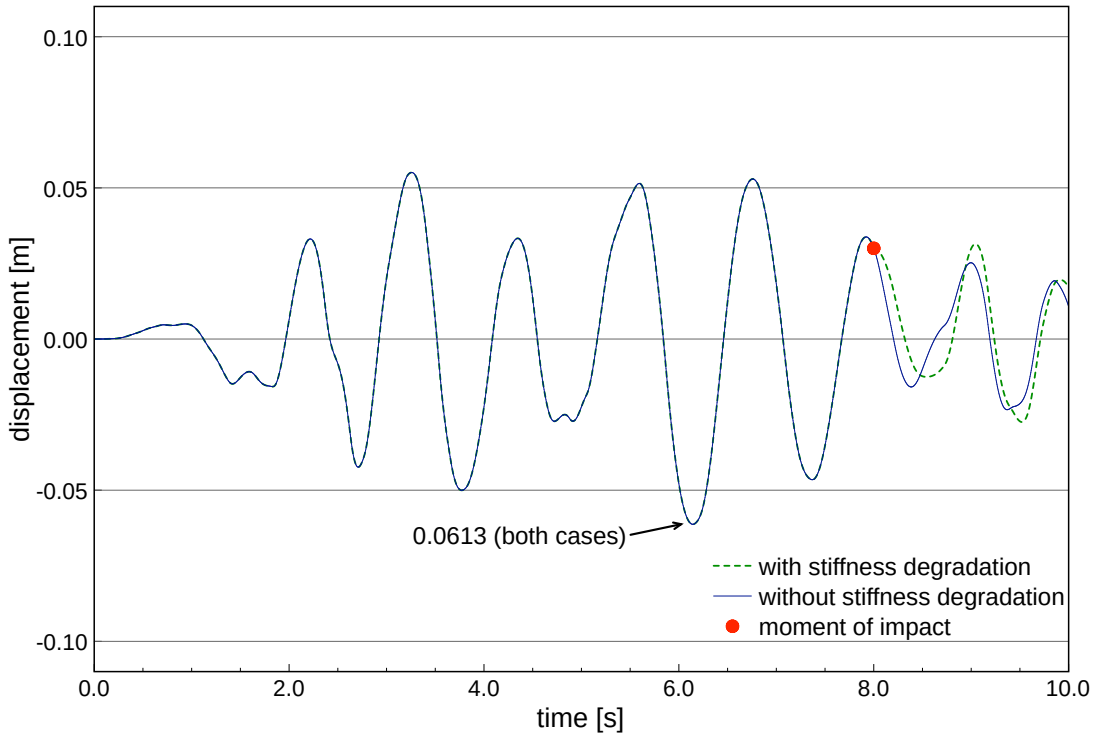

Fig. 3.13: Displacement history of the first storey of building under the El Centro earthquake with and without considering the degradation of horizontal stiffness for impact at t=8 s

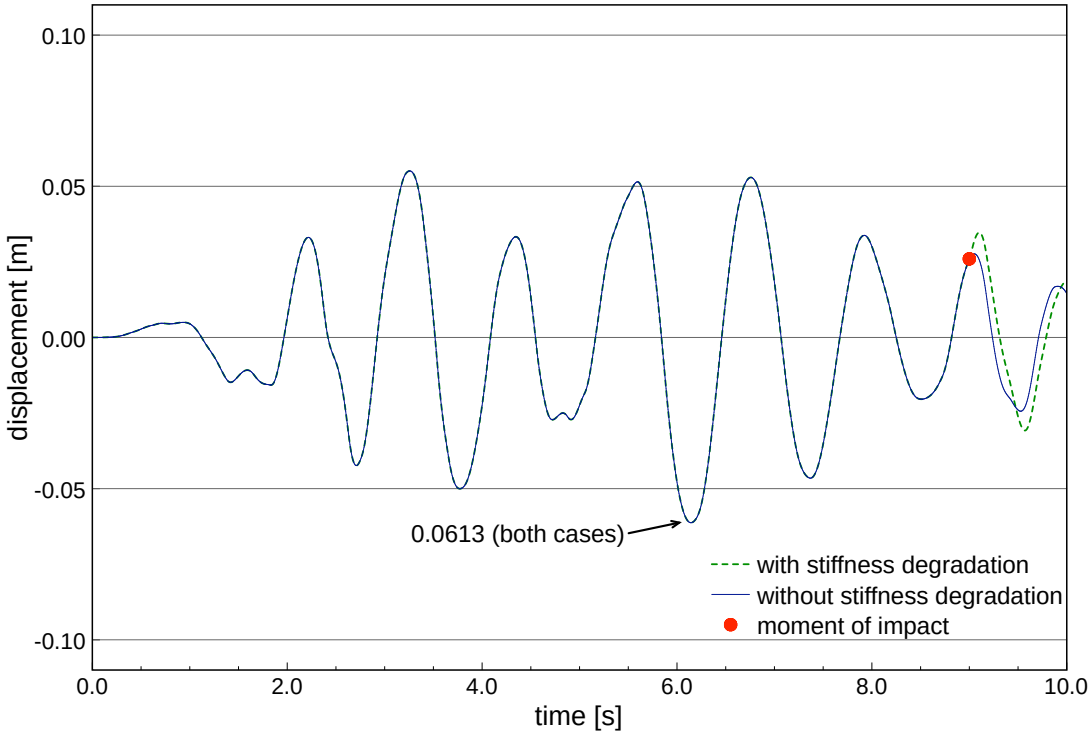

Fig. 3.14: Displacement history of the first storey of building under the El Centro earthquake with and without considering the degradation of horizontal stiffness for impact at t=9 s

Time of impact	Peak displacement		Increase
[s]	[m]		%
	with stiffness degradation	without stiffness degradation	
1	0.1016	0.1006	0.99
2	0.1008	0.0990	1.82
3	0.0883	0.0795	11.1
4	0.0551	0.0551	-
5	0.0778	0.0736	5.71
6	0.0723	0.0554	30.5
7	0.0613	0.0613	-
8	0.0613	0.0613	-
9	0.0613	0.0613	-

Tab. 3.1: Peak displacement values under the El Centro earthquake for different cases of impact times

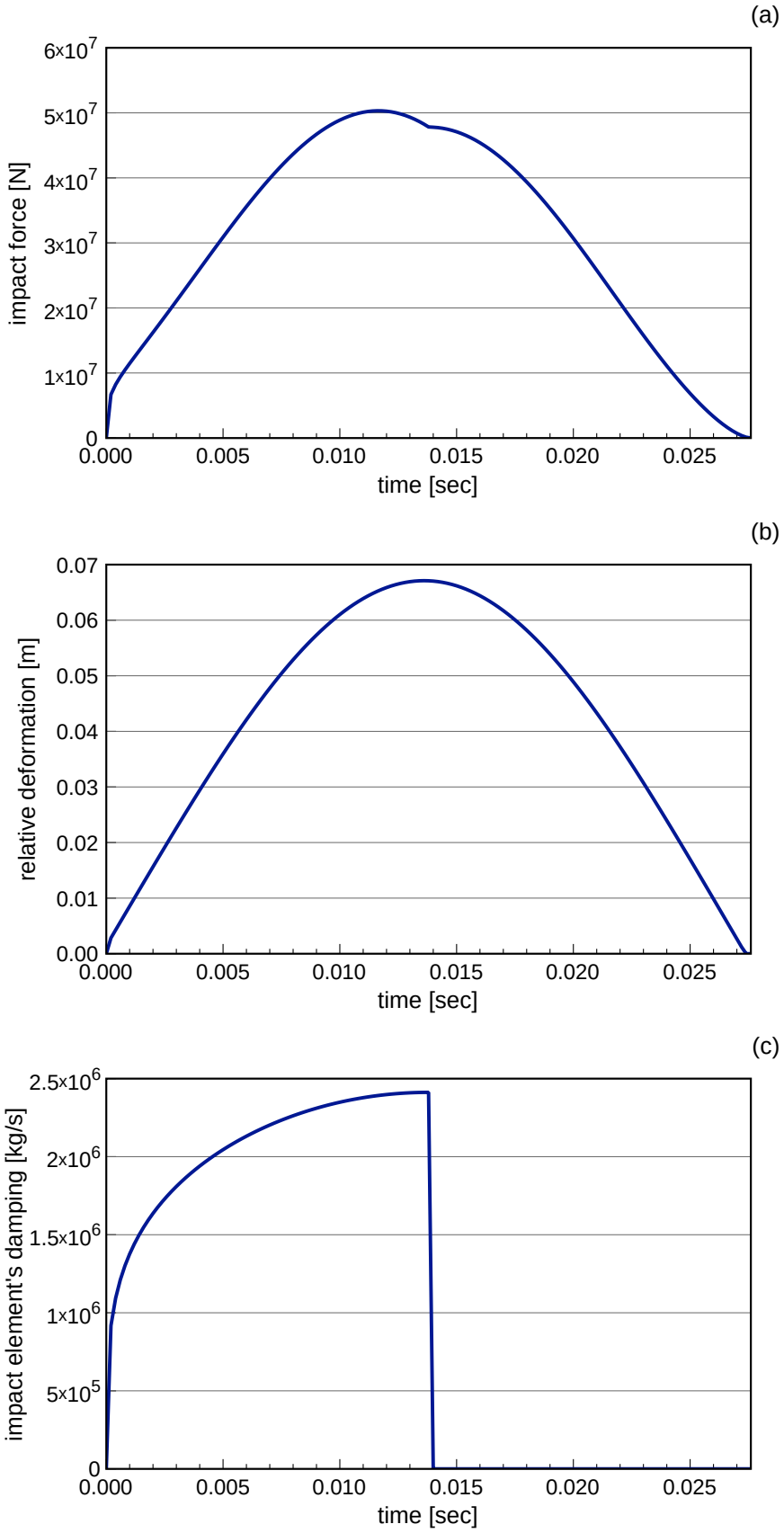

Fig. 3.15: Time histories during impact: a) impact force; b) relative vertical deformation of colliding structural members; c) impact element's damping

It can be seen from Figures 3.6-3.14 that incorporation in the numerical analysis the degradation of horizontal stiffness has a considerable influence on the structural behaviour under earthquake excitation. In nearly all of the cases, the stiffness degradation leads to the increase in the response of the first storey of building (the only exception is the reduced response shown in Figure 3.12 for impact at $t = 7$ s). Moreover, the curves shown in Figures 3.6-3.14 indicate that the time of impact plays a substantial role in the overall behaviour of the structure. It can be seen from Figure 3.8, Figure 3.11 and Figure 3.14 that, for the case when impact takes place when the structure is in the range of its peak deformations during the earthquake, the increase in the structural response can be really substantial (especially in the case when the structure is just approaching its extreme position). In the case of impact at $t = 6$ s (see Figure 3.11), for example, the increase in the peak displacement due to the degradation of horizontal stiffness is as high as 30.5%. Relatively high increase in the peak displacement value (by 11.1%) can also be observed in Figure 3.8 obtained for impact at $t = 3$ s. On the other hand, when impact takes place when the displacement of the building is relatively small (see Figure 3.6, Figure 3.7, Figure 3.9, Figure 3.12), the incorporation of the stiffness degradation on the structural response is less important, even that some increase in the peak displacement (on the order of 1-2%) due to the degradation of horizontal stiffness has also been recorded (see Table 3.1).

3.5 Conclusions

The horizontal stiffness degradation of building columns, subjected to impact load after soft-storey failure due to ground motion excitation, has been investigated in this chapter. First, the theoretical approach to the problem of the column's

deformation has been presented. Then, the numerical analysis concerning the behaviour of a three-storey building suffering from the earthquake-induced soft-storey failure has been described.

The results of the study show that the degradation of horizontal stiffness of building columns, due to impact caused by the fall of the upper storeys onto the lower one, may have a considerable influence on the structural response. Moreover, the results clearly indicate that the time of impact plays a substantial role in the overall behaviour of a building under earthquake excitation. It has been shown that the structural response may be increased significantly if impact takes place when the structure is in the range of its peak deformations during the ground motion, especially when the structure is just approaching the extreme position. On the other hand, when impact takes place when the actual displacement of the building during earthquake is relatively small, the influence of the stiffness degradation on the structural response is less significant.

Chapter 4.

EXPERIMENTAL STUDY ON MODELS OF DEFORMED STEEL COLUMNS

4.1 Introduction

The basic numerical analysis described in Chapter 3 has indicated that the structural response may be increased significantly if vertical impact takes place when the structure is in the range of its peak deformations during earthquake, i.e. when the horizontal deformation of columns is the largest. In order to investigate this effect in more details, the experimental study concerning the behaviour of models of horizontally deformed steel columns that are additionally subjected to vertical impact load (see Figure 4.1), has been conducted and described in this chapter. Models of steel columns with high slenderness ratio have been considered in the study. The investigation has been conducted for different values of the initial relative horizontal displacement between the base and the top of the columns. In the experiment, impact load has been generated by a steel sphere dropped onto a pad of technical clay, so as to simulate nearly plastic impact observed in the reality during earthquakes.

4.2 Setup of the experiment

The experimental study was conducted using the stand structure shown in Figure 4.2. It consisted of a thick steel plate at the bottom, to which four steel rods

(precision shafts) were mounted. The top ends of the rods were connected using a steel diaphragm. Another diaphragm was located in the lower part of the stand in order to increase the overall rigidness. Along the steel rods, a moving platform with the mass of 6 kg, acting as a top support for the investigated specimens, was installed (see Figure 4.3). The platform was equipped with four industrial linear bearings, so that only a free vertical movement of the platform was allowed. The bottom support plate was equipped with a mechanism (see Figure 4.4) that allowed us to introduce a horizontal displacement of the bottom end of the specimen, making it possible to simulate impact load on a pre-deformed column (compare Migda and Jankowski 2009, 2010).

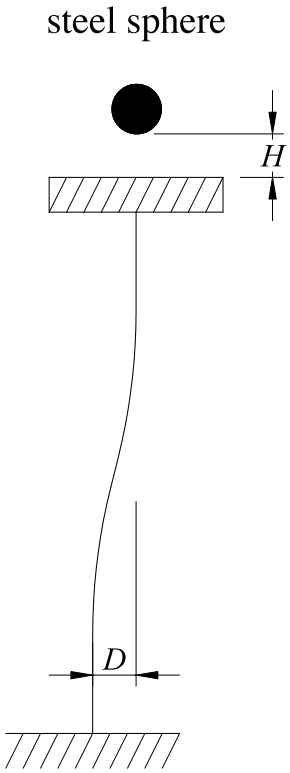

Fig. 4.1: Schematic diagram of a steel sphere dropped onto the top of a deformed column

During the experiment, a steel sphere with a mass of 2.1 kg was dropped from a pre-defined height onto the platform, where a pad of technical clay was placed with a diameter of approximately 100 mm and a thickness of 20 mm. The use of this pad

allowed the impact between the sphere and the platform to be nearly plastic, which is observed in the reality during earthquakes. It also prevented the sphere from bouncing of the platform and kept it in place after impact (see also Migda 2007).

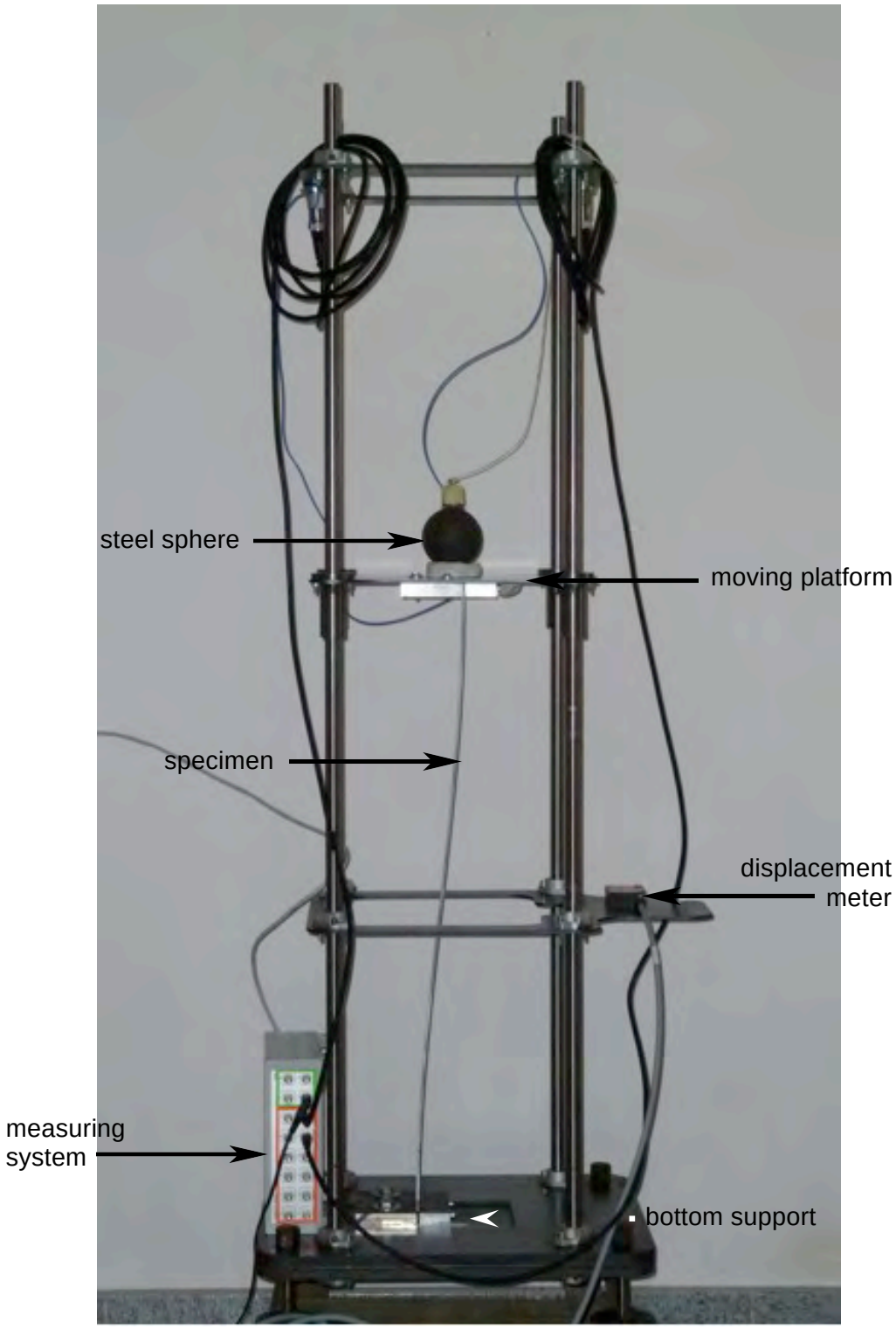

Fig. 4.2: Experimental setup (general view)

Acceleration of the sphere (accelerometer shown in Figure 4.3) as well as acceleration of the platform (accelerometer shown in Figure 4.5) were recorded during the experiment. Furthermore, the horizontal displacement of the specimen was measured at its mid-height using the laser displacement meter (see Figure 4.2).

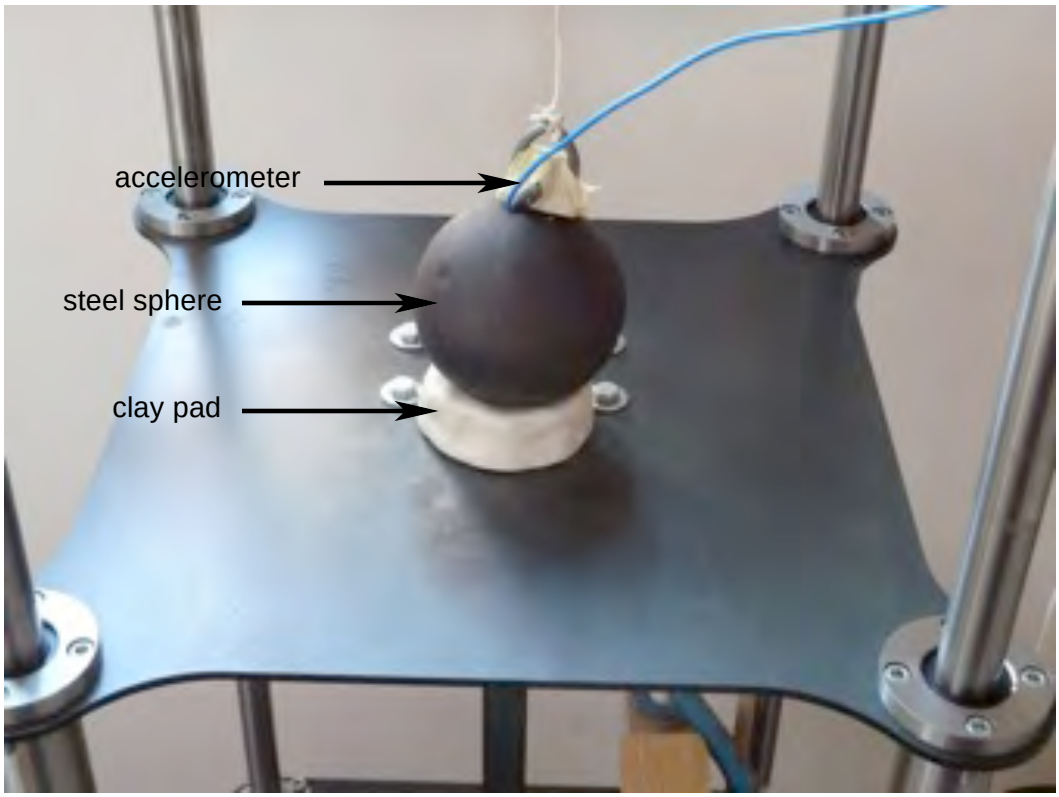

Fig. 4.3: Moving platform with the steel sphere and clay pad

A number of steel columns, with the length of 800 mm and cross section of 3×20 mm, have been prepared to be tested experimentally. Each column specimen was mounted in fixed supports located at the bottom and at the moving platform (see Figure 4.4 and Figure 4.5). The critical static load of the specimen has been analytically calculated as equal to 395.2 N. The initial pre-deformation of the column, *D*, i.e. the horizontal displacement between the theoretical axis of the top and the bottom support was increased from 0 mm by 10 mm up to 60 mm. The drop height, *H*, was increased from 50 mm up to 350 mm with a step of 50 mm. The

above conditions allowed the steel columns to remain in the elastic range as well as to prevent from dynamic stability loss during all experimental tests.

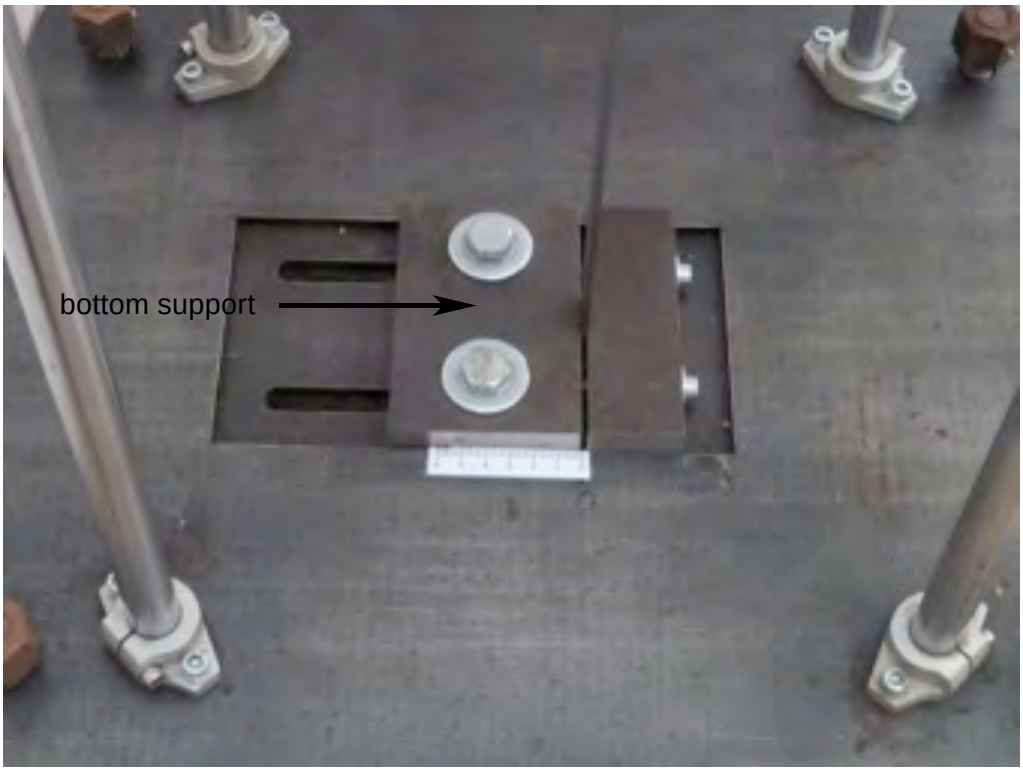

Fig. 4.4: Bottom support with the mechanism of column pre-deformation

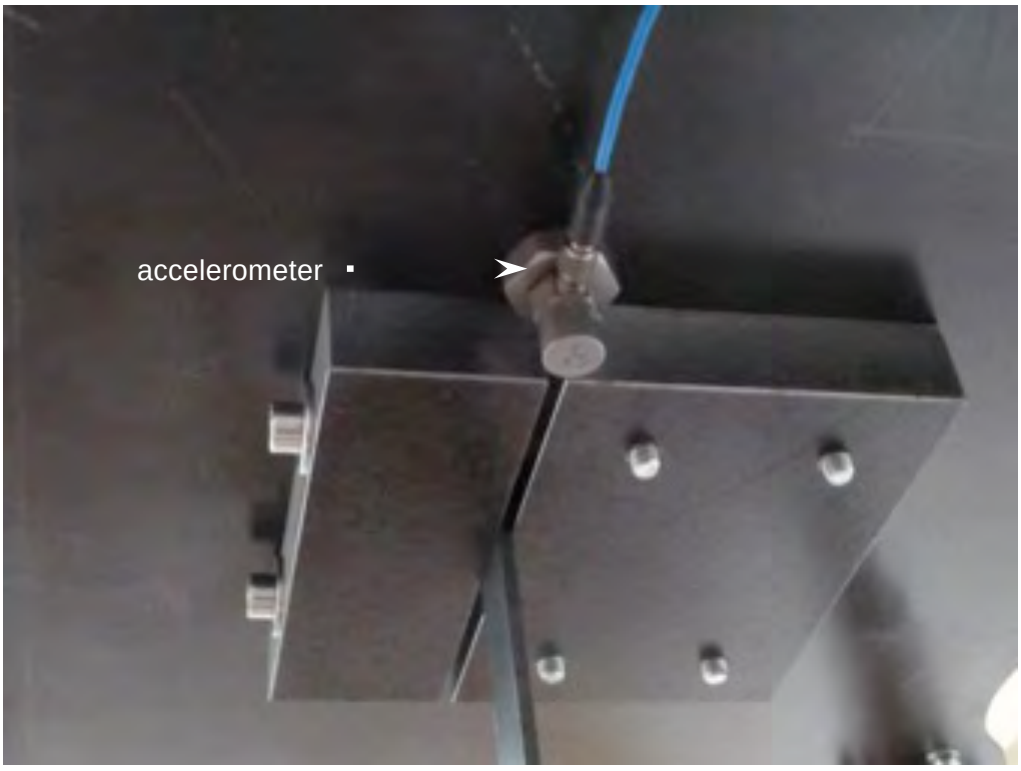

Fig. 4.5: Bottom part of the moving platform with top support of column and accelerometer

4.3 Experimental results

The experimental study has been conducted for all combinations of pre-deformations of columns, *D*, and drop heights, *H* (see also Migda and Jankowski 2011, 2012a). The examples of the results for a drop height of 200 mm are shown in Figures 4.6-4.11. They illustrate the directly recorded values of acceleration of the sphere (Figure 4.6 and Figure 4.9), acceleration of the platform (Figure 4.7 and Figure 4.10) and the horizontal displacement of the column at its mid-height (Figure 4.8 and Figure 4.11) for the case without pre-deformation (straight column) and for *D*=60 mm, respectively. Additionally, the peak accelerations of the sphere and the platform during impact, for different drop heights, *H*, and pre-deformations, *D*, are also summarized in Table 4.1 and Table 4.2, respectively.

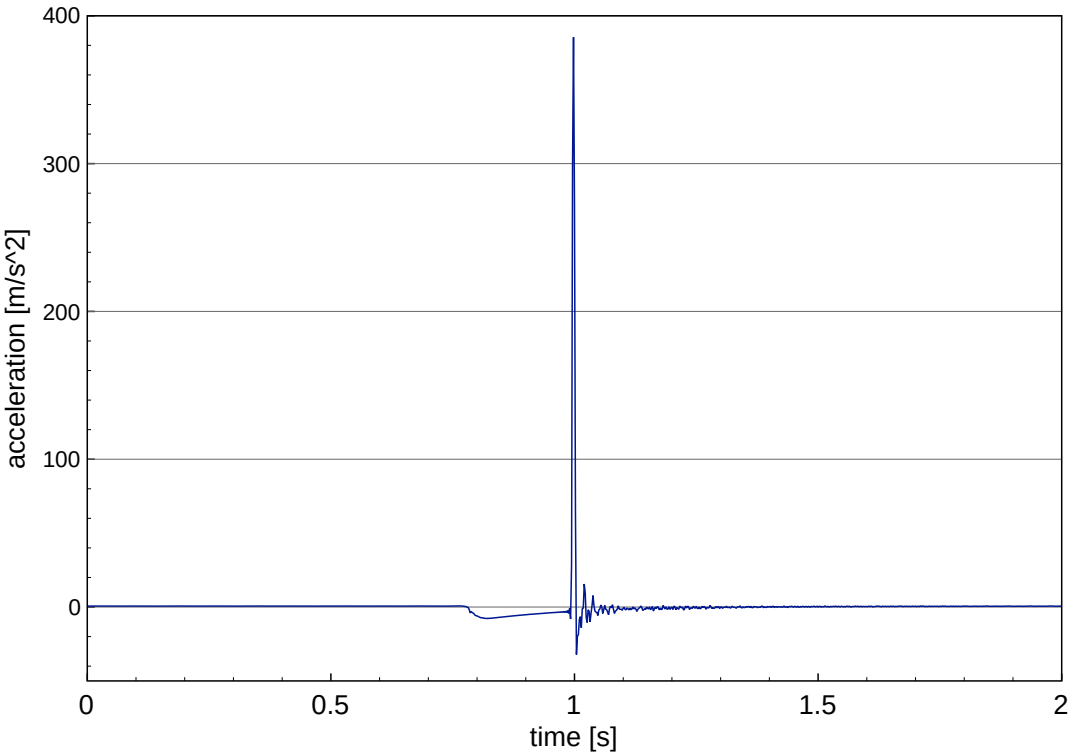

Fig. 4.6: Acceleration of the sphere during impact without pre-deformation for a drop height of 200 mm

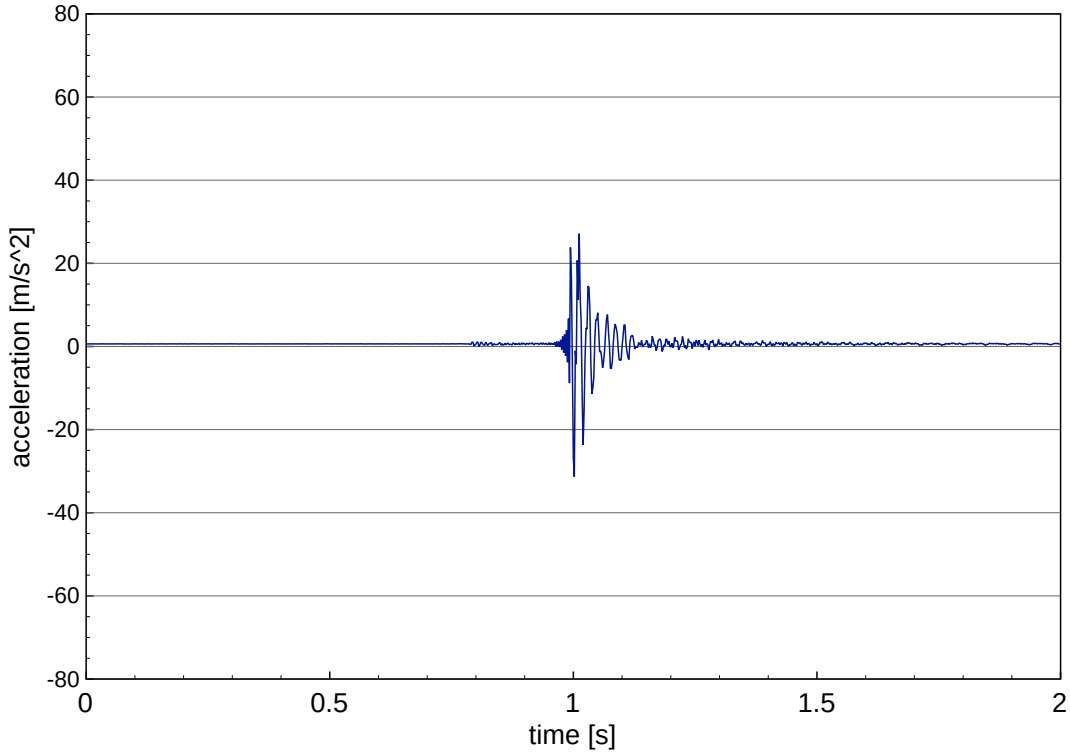

Fig. 4.7: Acceleration of the platform during impact without pre-deformation for a drop height of 200 mm

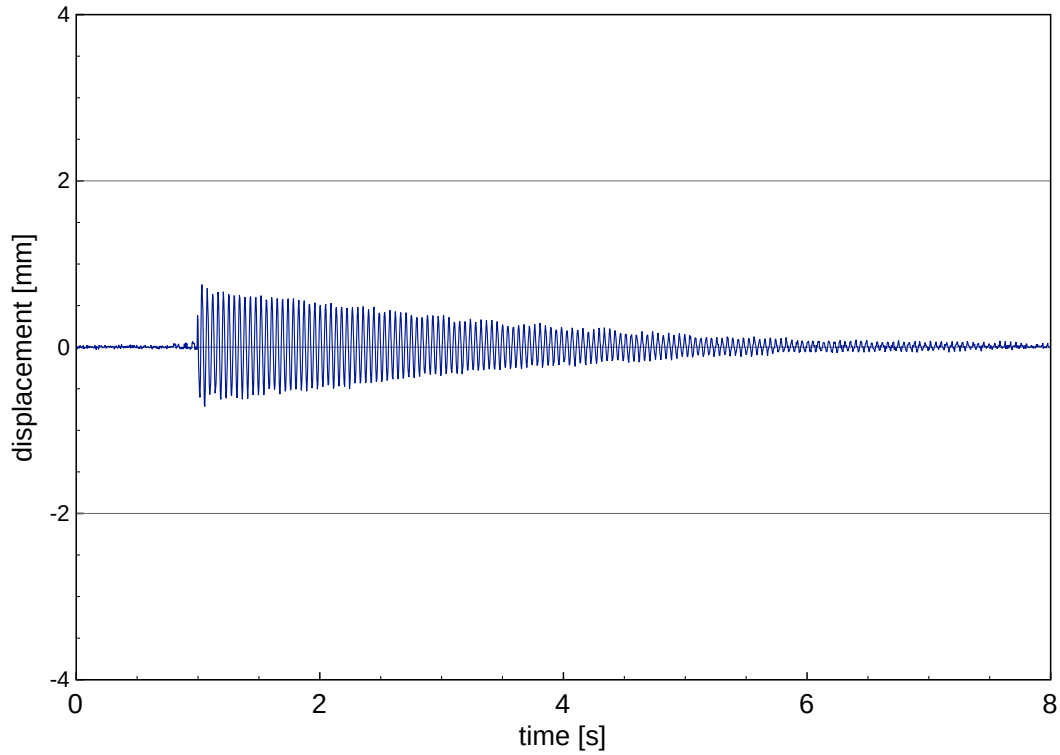

Fig. 4.8: Horizontal displacement recorded in the mid-height of the column during impact without pre-deformation for a drop height of 200 mm

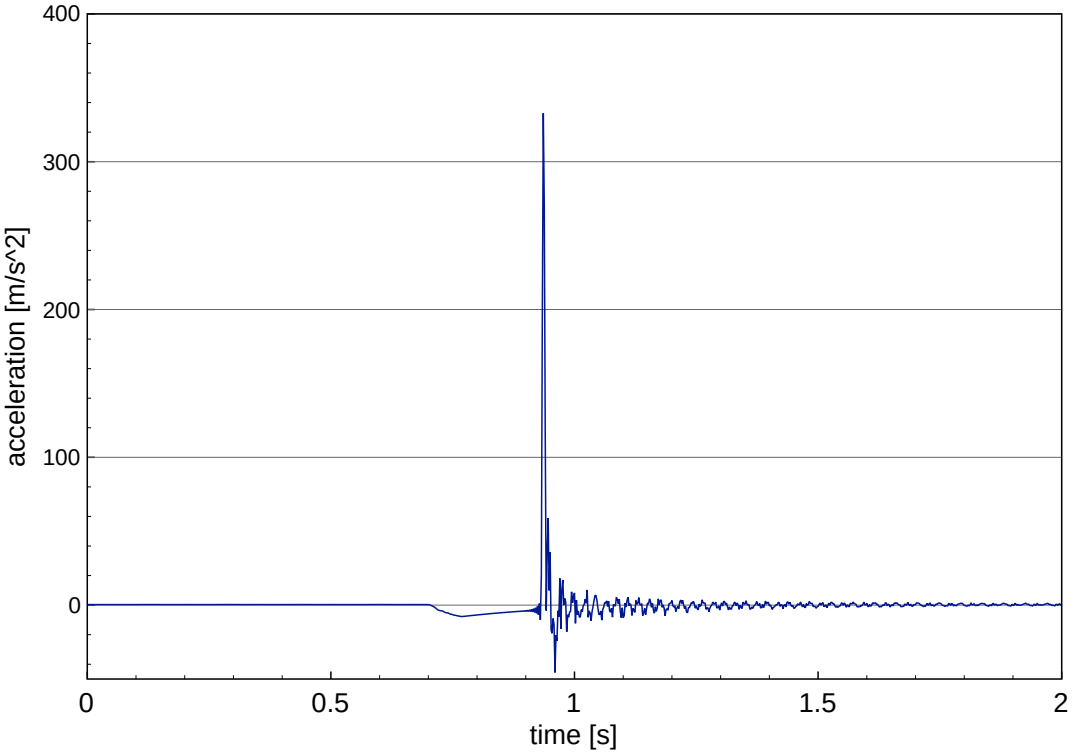

Fig. 4.9: Acceleration of the sphere during impact for a pre-deformation of 60 mm and a drop height of 200 mm

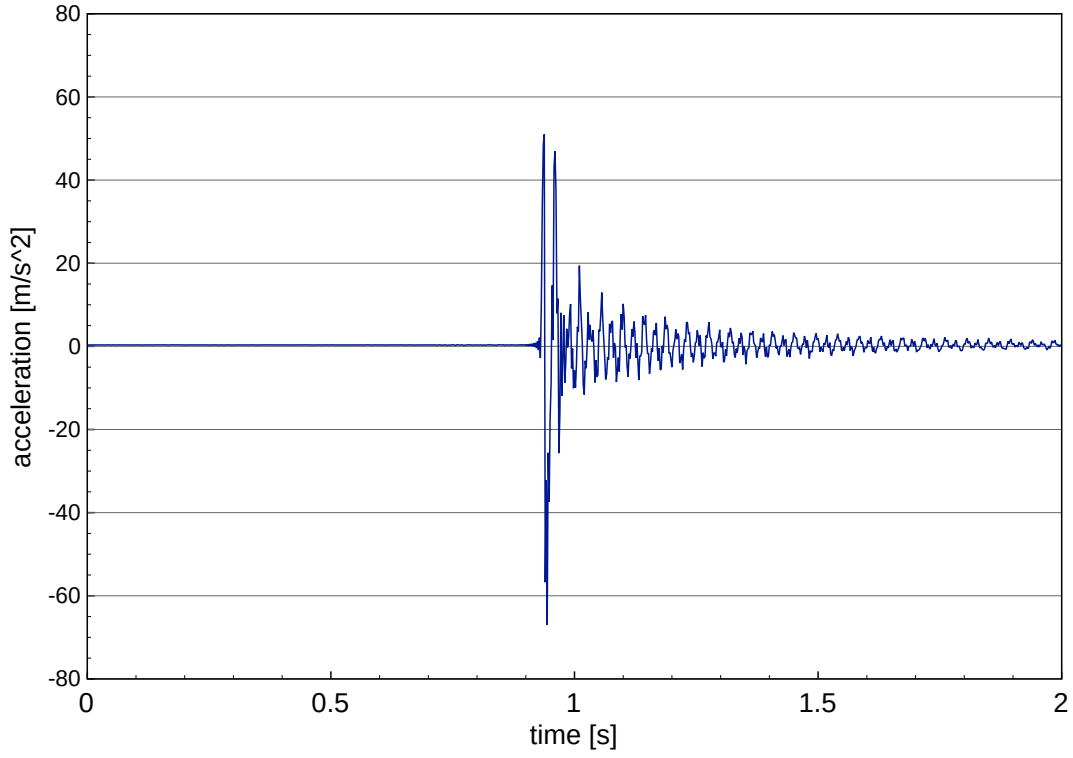

Fig. 4.10: Acceleration of the platform during impact for a pre-deformation of 60 mm and a drop height of 200 mm

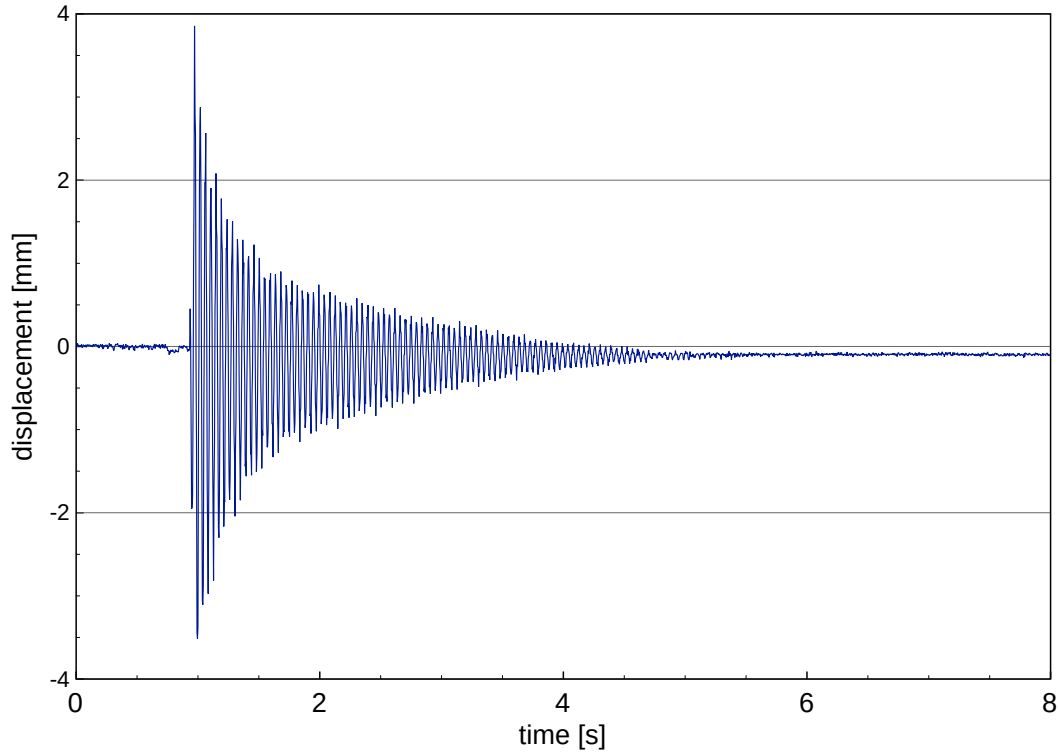

Fig. 4.11: Displacement recorded in the mid-height of the column during impact for a pre-deformation of 60 mm and a drop height of 200 mm

a_{sphere} [m/s^2]	H [mm]						
D [mm]	50	100	150	200	250	300	350
0	246.46	322.06	383.75	423.85	475.07	466.47	478.52
10	212.44	288.30	328.52	374.25	428.18	470.35	479.91
20	215.70	244.87	321.92	319.17	395.22	407.44	458.64
30	221.75	239.88	292.77	349.37	383.76	437.21	468.66
40	250.47	261.07	311.78	345.34	421.52	428.22	446.18
50	145.98	299.18	364.29	410.65	434.29	479.93	480.71
60	196.55	246.11	280.06	337.46	476.20	470.60	480.70

Tab. 4.1: Peak accelerations of the sphere during impact for different drop heights, *H*, and pre-deformations, *D*

$a_{platform}$ [m/s^2]	H [mm]						
D [mm]	50	100	150	200	250	300	350
0	26.11	32.29	33.48	37.19	40.78	46.22	52.55
10	18.89	21.43	27.35	29.14	37.44	39.99	43.57
20	20.41	27.77	37.39	39.96	43.97	47.71	47.64
30	26.93	37.63	45.52	53.37	61.00	63.14	70.56
40	39.35	42.29	49.61	51.76	59.20	66.54	71.50
50	32.97	46.62	58.22	64.33	73.59	73.13	79.37
60	40.98	45.67	55.41	67.43	88.23	90.12	90.44

Tab. 4.2: Peak accelerations of the platform during impact for different drop heights, *H*, and pre-deformations, *D*

It can be seen comparing Figure 4.6 with Figure 4.9 that the difference between the peak acceleration values of the sphere for two different pre-deformation cases is equal 13.7%, which is not really much. On the other hand, the results shown in Figures 4.7-4.8 and Figure 4.10-4.11 indicate that the pre-deformation has a substantial influence on the acceleration of the platform as well as on the horizontal displacement of the column. The increase in the peak measured values is as large as 88.0% in the case of platform acceleration and 413.3% in the case of column displacement.

In order to determine the peak force acting during impact on the top of the column, the following formula has been used (see Dorf 2005, Goldsmith 1960, Jankowski 2010, Leyko 1997, Zhang and Scharf 2009, 2011):

$$F_{peak} = a_{platform}\left(m_{sphere} + m_{platform}\right) \tag{4.1}$$

where:

$a_{platform}$ – peak acceleration of the platform,

m_{sphere} – mass of the sphere (2.1 kg),

$m_{platform}$ – mass of the platform (6.0 kg).

The peak force acting on the top of the column gives us an insight into the actual impact load to which the column is exposed to. The values of the peak forces acting on specimens for different drop heights and pre-deformations are summarised in Table 4.3. The graphical representation of these results is also shown in Figure 4.12. It can be observed from the figure that the value of the peak force generally increases starting from the first pre-deformation increment of 10 mm, after a little decrease between a non pre-deformed state and the first deformation. It is believed that this decline is the result of higher vertical stiffness of undeformed column, as compared to the case of pre-deformation equal to 10 mm. In addition, it can be noticed, that the dynamic peak force exceeds the theoretical critical static force by more than 85.4% for *H*=350 mm and *D*=60 mm, while still the plastic yield and the stability loss have not been reached.

F_{peak} [N]	*H* [mm]						
D [mm]	50	100	150	200	250	300	350
0	211.50	261.56	271.19	301.21	330.35	374.39	425.66
10	152.98	173.55	221.56	236.05	303.22	323.92	352.94
20	165.32	224.96	302.85	323.64	356.12	386.45	385.92
30	218.16	304.77	368.71	432.26	494.12	511.40	571.54
40	318.72	342.57	401.87	419.24	479.51	538.93	579.17
50	267.07	377.64	471.62	521.06	596.08	592.36	642.89
60	331.92	369.96	448.79	546.19	714.67	729.99	732.57

Tab. 4.3: Peak forces acting on specimens for different drop heights, *H*, and pre-deformations, *D*

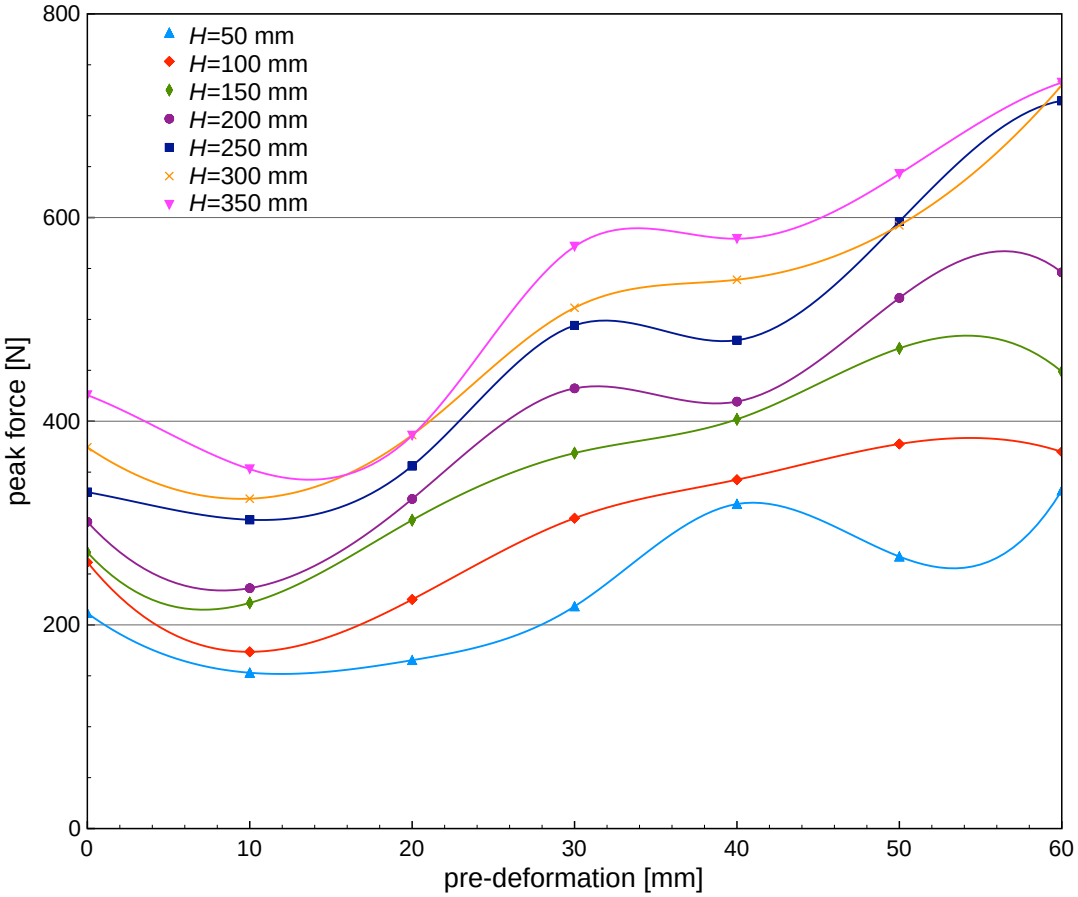

Fig. 4.12: Relation between the peak force, F_{peak}, acting on the top of column and its pre-deformation for different drop heights, H

The larger affecting impact force leads also to larger amplitudes in horizontal vibrations of the column (compare Figure 4.8 with Figure 4.11). The relation between the peak horizontal displacement of the column at its mid-height and its pre-deformation for different drop heights is shown in Figure 4.13. An evident trend of larger peak amplitude for greater drop height and greater pre-deformation is visible. The gain of horizontal vibrations are believed to be responsible for the higher damping ratio of vibrations, as can be seen in Figure 4.11.

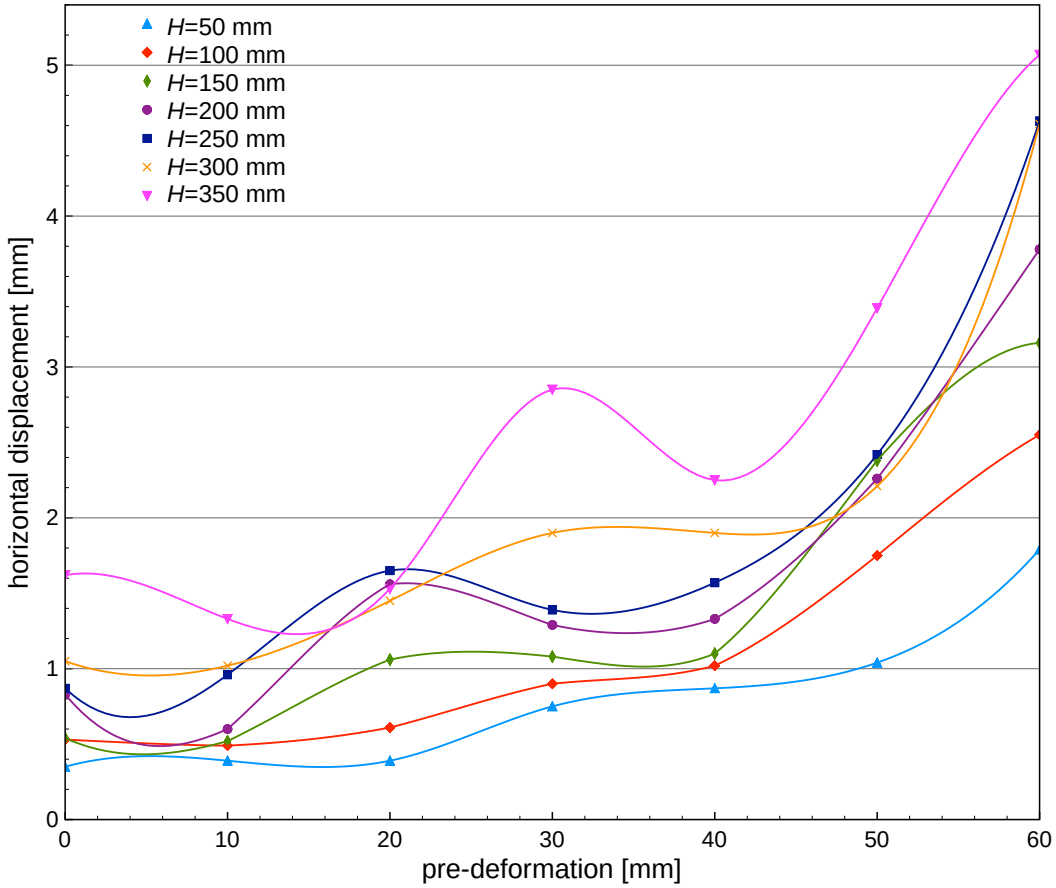

Fig. 4.13: Relation between the peak horizontal displacement of the column and its pre-deformation for different drop heights, *H*

4.4 Conclusions

The results of the experimental study focused on dynamic behaviour of deformed steel columns, that are additionally subjected to vertical impact load as the result of soft-storey collapse during earthquake, have been presented in this chapter. The investigation has been conducted for different values of the initial relative horizontal displacement between the base and the top of the columns. In the experiment, impact load has been generated by a steel sphere dropped from different heights onto a pad of technical clay, so as to simulate nearly plastic impact observed in the reality during earthquakes.

The results of the experiment show that, with the increase in the pre-deformation of a column, the value of the peak force acting on its top initially decreases and then shows a considerable increase trend. Moreover, with the increase in the pre-deformation, the peak horizontal displacement of the middle part of column substantially increases for all height drop values considered. The above conclusions confirm the conclusion formulated in Chapter 3 that the deformation of columns introduced due to earthquake loading has a substantial negative influence. The experimental results indicate, however, that even the deformed column is still capable to carry considerable dynamic load before its failure due to stability loss.

Chapter 5.

NUMERICAL ANALYSIS OF A MODEL OF DEFORMED STEEL COLUMN

5.1 Introduction

The experimental investigation on the behaviour of horizontally deformed steel columns (the deformation as the result of horizontal ground motion) that are additionally subjected to vertical impact load has been conducted in Chapter 4. In that chapter, however, the introduced pre-deformation was a static one and the influence of the dynamic effects of the earthquake excitation was not considered (limitations of the experimental setup). Therefore, the aim of Chapter 5 is to extend the study and investigate numerically the dynamic response of a model of steel column under ground motion excitation that is additionally subjected to vertical impact load. The numerical model of the specimen has been created and its accuracy has been confirmed by comparing the results of the numerical analysis with the experimental results. In the first stage of the numerical study, a number of cases, concerning different pre-deformations of the column as well as various impact load time histories (related to different drop heights) have been considered. Then, the detailed nonlinear analysis has been conducted by exciting horizontally the base of the specimen using the harmonic ground motion excitation as well as by applying impact vertical load at different times of the excitation. The geometric nonlinearity

(large strain analysis) as well as the elasto-plastic material behaviour with the strain rate effect have been considered in the numerical analysis.

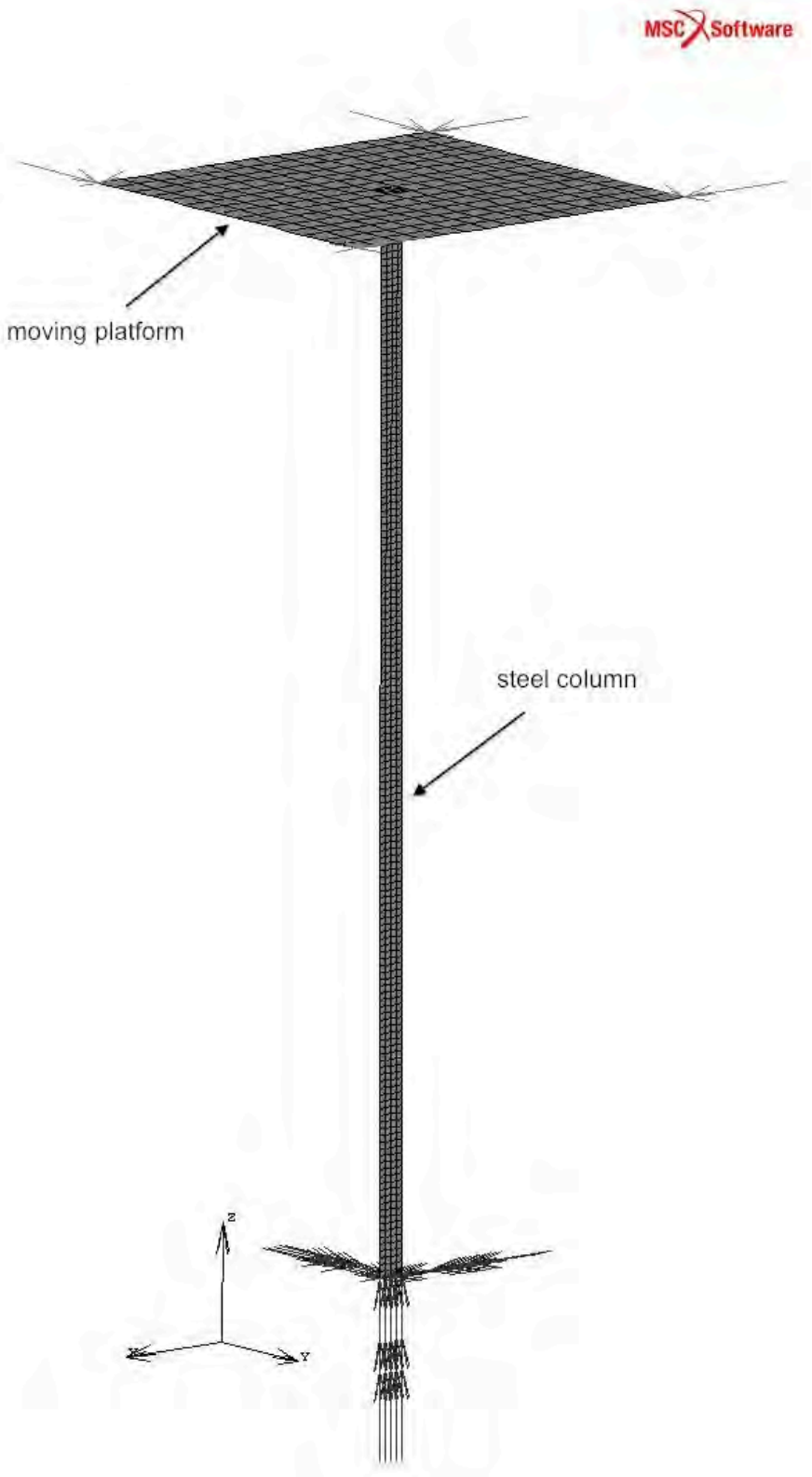

Fig. 5.1: Numerical model of the steel column with moving platform

5.2 Model and its validation

For the purposes of numerical analysis, a Finite Element (FE) model of steel columns, which have been tested experimentally in Chapter 4, has been created using the commercial software MSC Marc (see Figure 5.1). The numerical model of the specimen, with the length of 800 mm and cross section of 3×20 mm, has been constructed out of 640 four-node shell elements (see Hartmann and Katz 2004, Hughes 1987). The moving platform, which was mounted at the top of the column and used during the experiments to drop a steel sphere onto it, has been considered to be important element to be also included in the numerical analysis. Its model has been constructed out of 240 four-node shell elements. All material properties as well as original dimensions have been assured to be the same as in the experimental study. Taking into account the boundary conditions valid during the experiment, the numerical model of the specimen has been fixed at the bottom of the column and only vertical movement at four corners of the platform (locations of linear bearings) has been allowed.

The accuracy of the numerical model has been first verified by comparing the results of the numerical analysis with the results obtained from the experimental tests described in Chapter 4. For this purpose, similarly as in the case of the experimental study, a static horizontal pre-deformation has been introduced at the bottom of the numerical model of the column and the specimen has been subjected to vertical impact load acting on its top (see Figure 5.2). The same impact load time histories as measured during the experiment, by dropping a steel sphere onto the platform, have been used. The geometric nonlinearity, by conducting the large strain numerical analysis, has been taken into account.

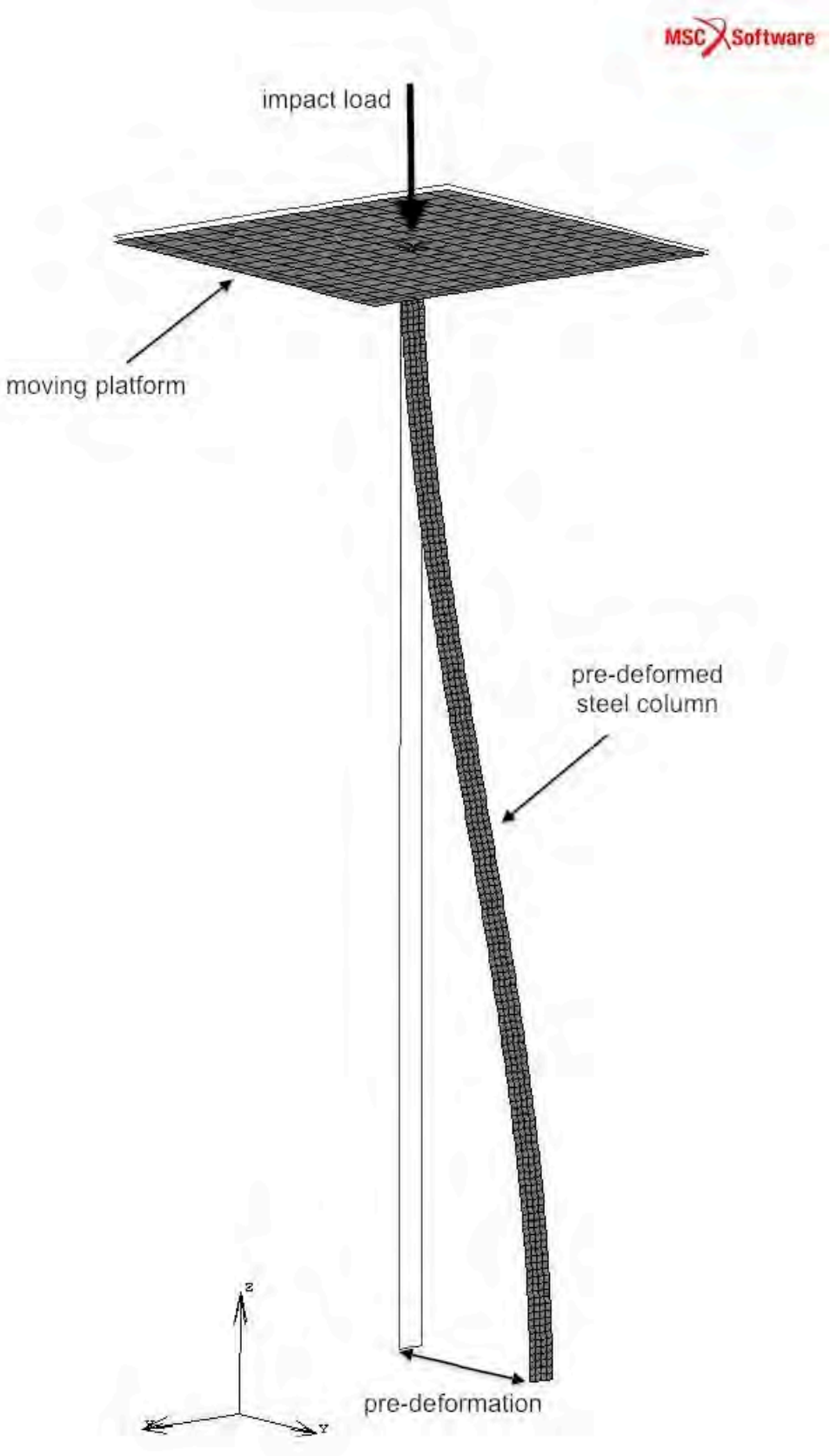

Fig. 5.2: Numerical model of the pre-deformed steel column subjected to vertical impact load

A number of cases, concerning different pre-deformations (relative horizontal displacement between the top and the bottom of the column) as well as various impact load time histories (related to different drop heights) have been considered in the study. The difference between the results of the experiment and the results of the numerical analysis has been assessed by calculating the normalized root mean square (RMS) error (see Bendat and Piersol 1971):

$$\mathrm{RMS} = \frac{\sqrt{\sum_{i=1}^{NV}(V_i - \bar{V}_i)^2}}{\sqrt{\sum_{i=1}^{NV} {V_i}^2}} \cdot 100\% \qquad (5.1)$$

where V_i, $\bar{V}_i$ are the values from the time history record obtained from the experiment and from the numerical analysis, respectively; and *NV* denotes a number of values in these history records.

The example of the comparison between the results of the numerical analysis and the results obtained from the experimental tests, in the form of the horizontal displacement time histories at the middle of the column (pre-deformation of 20 mm, drop height of 200 mm), is presented in Figure 5.3. For this case, the natural frequency of vibrations of a specimen as well as the damping ratio is equal to 24.91 Hz and 0.68%, respectively. Using equation (5.1), the RMS error for the time histories shown in Figure 5.3 has been calculated as equal to 7.90%. The average RMS error for all cases considered has been found to be as small as 6.43% confirming the accuracy of the numerical model created.

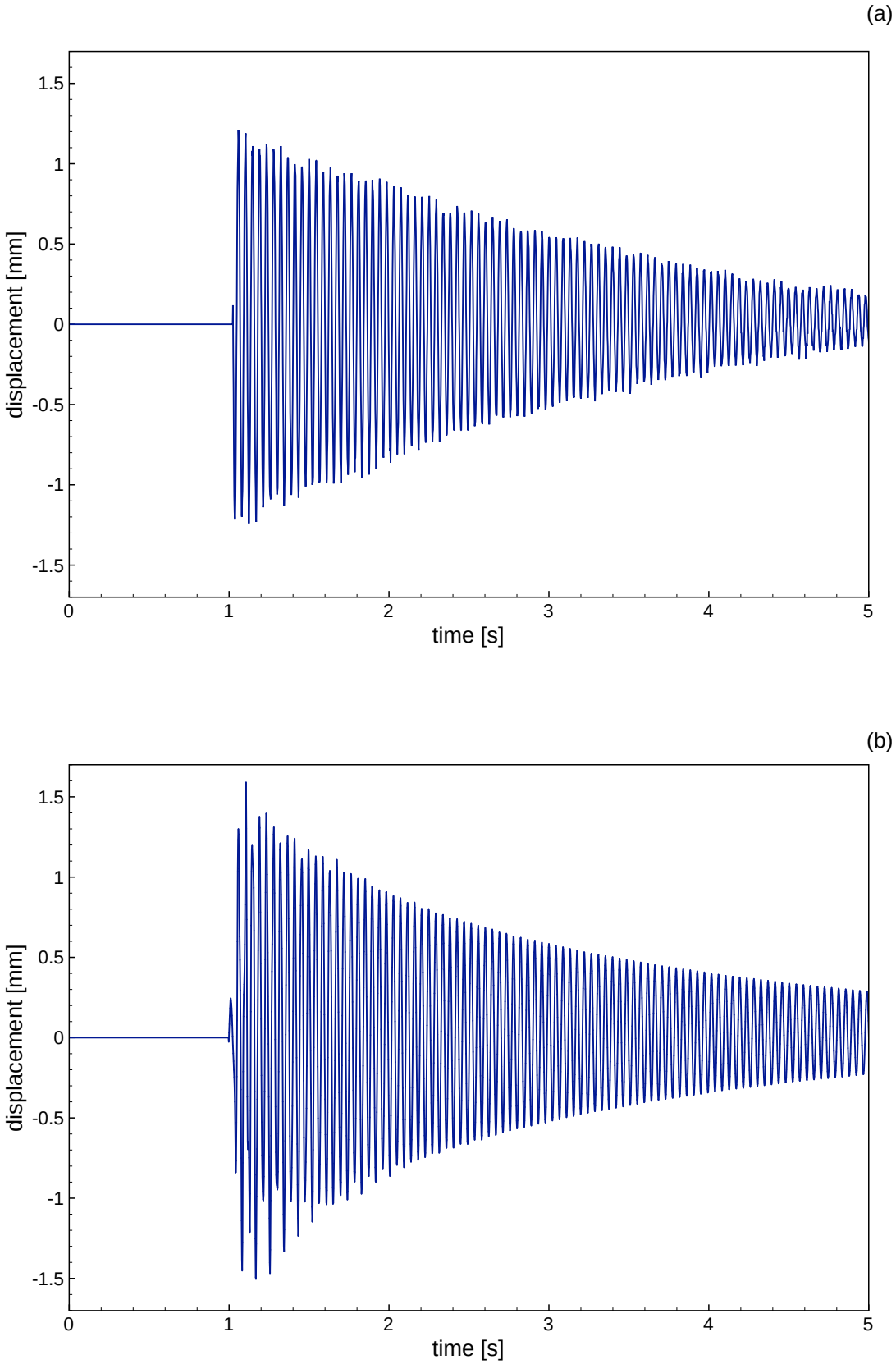

Fig. 5.3: Horizontal displacement time histories at the middle of the column (pre-deformation of 20 mm, drop height of 200 mm): (a) experiment; (b) numerical analysis

5.3 Numerical analysis

In the first stage of the numerical analysis, the parametric investigation has been conducted in order to assess the influence of the pre-deformation of the column as well as the influence of the impact load on the response of the steel column (see also Migda and Jankowski 2012b, 2012d). The analysis has been conducted for the statically pre-deformed columns (see Figure 5.2) subjected to different impact load time histories. The horizontal pre-deformation was increased from 0 mm by 10 mm up to 60 mm. It should be underlined, that in the case of pre-deformation equal to zero, the initial imperfection has been introduced in the specimen (observed always in the reality) so as to induce its bending in the particular direction. The impact load time histories, as measured during the experiment for different drop heights (see Chapter 4), have been applied onto the platform. The above conditions have allowed the numerical models of the steel column to remain in the elastic range as well as to prevent from dynamic stability loss.

5.3.1 Parametric study on statically pre-deformed columns

The examples of the preliminary results in the form of the maps of mean normal stress distributions at the bottom part of the pre-deformed specimen, for the case of 60 mm pre-deformation, are presented in Figure 5.4 and Figure 5.5. In particular, Figure 5.4 shows the mean normal stresses before impact, while Figure 5.5 presents the mean normal stresses at the stage of the peak impact force acting at the top of the pre-deformed column. By comparing Figure 5.4 with Figure 5.5, it can been observed that the increase in the stress values at the bottom part of the specimen due to impact load can be as large as 235.9%.

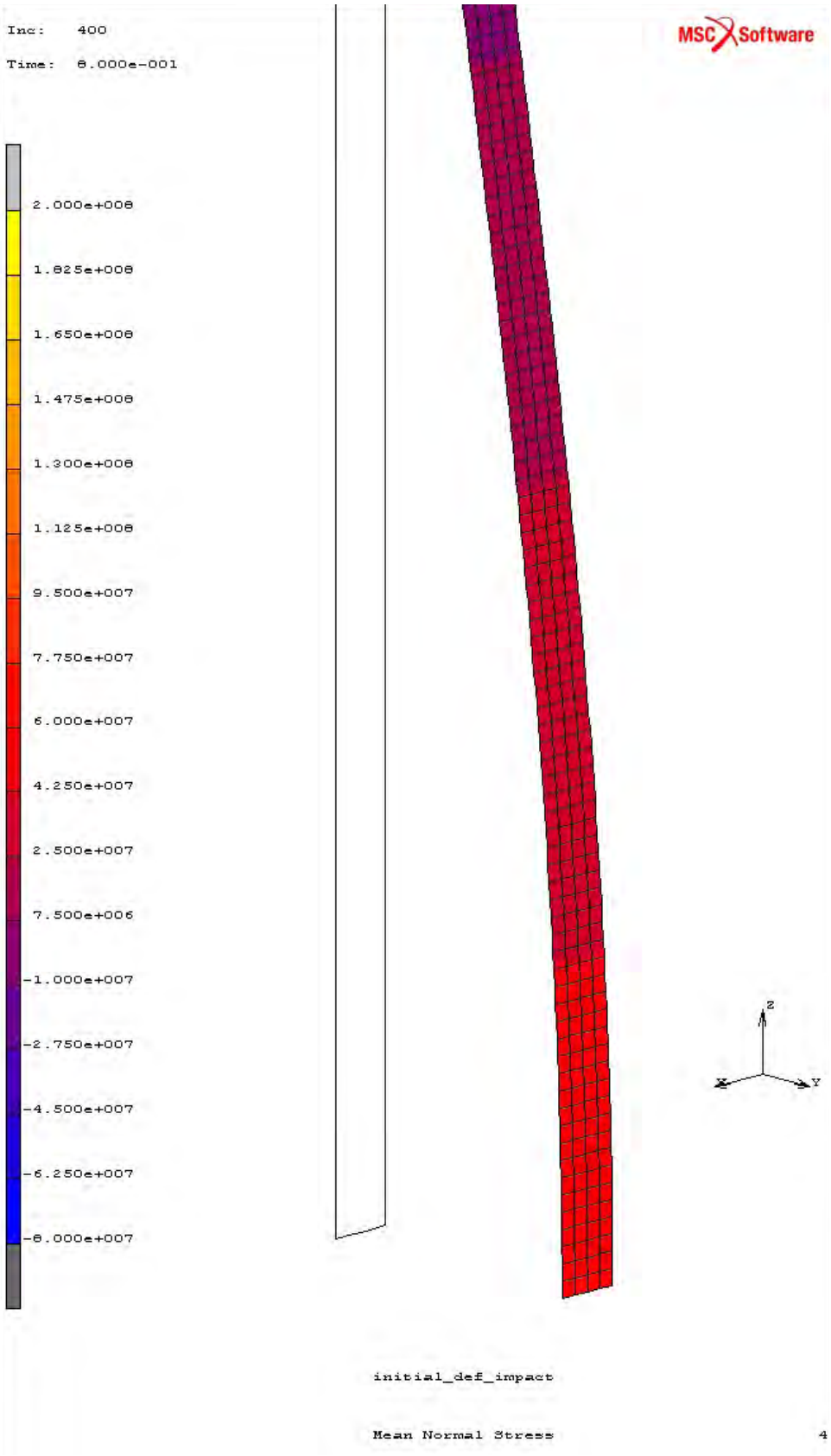

Fig. 5.4: Map of mean normal stresses at the bottom part of the deformed specimen (pre-deformation of 60 mm) before impact

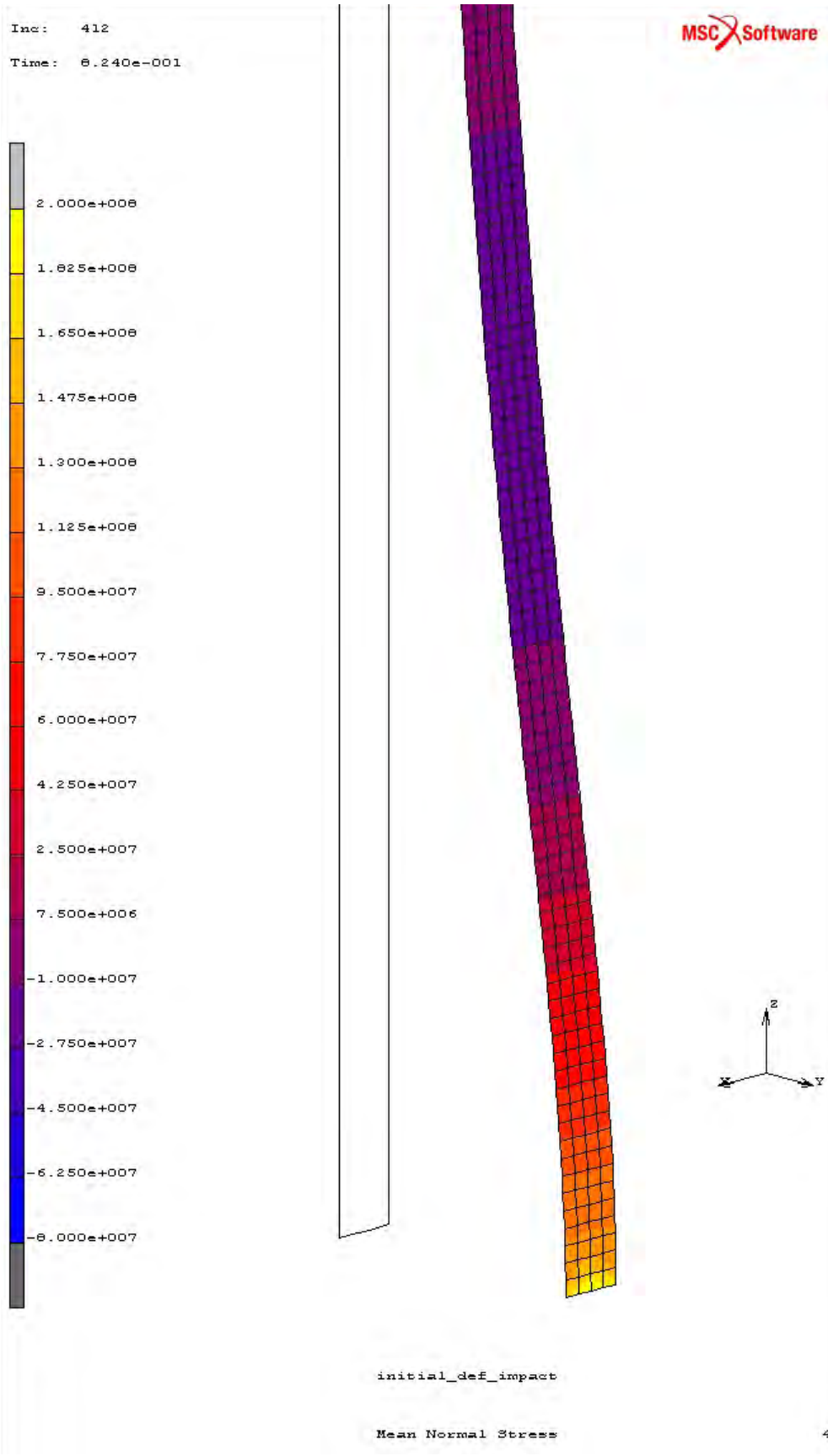

Fig. 5.5: Map of mean normal stresses at the bottom part of the deformed specimen (pre-deformation of 60 mm) at the time of the peak impact force acting at the top of the column

The results from the parametric analysis are presented in Figure 5.6 and Figure 5.7. Figure 5.6 shows the peak values of the mean normal stress at the bottom of the specimen with respect to its pre-deformation (for different drop heights). It can be observed from the figure that the value of the peak mean normal stress uniformly and substantially increases with the increase in the pre-deformation. In the case of the drop height of 350 mm, for example, the increase in the mean normal stress value for the deformed column (pre-deformation of 60 mm) with relation to the undeformed specimen is as large as 1321.4%.

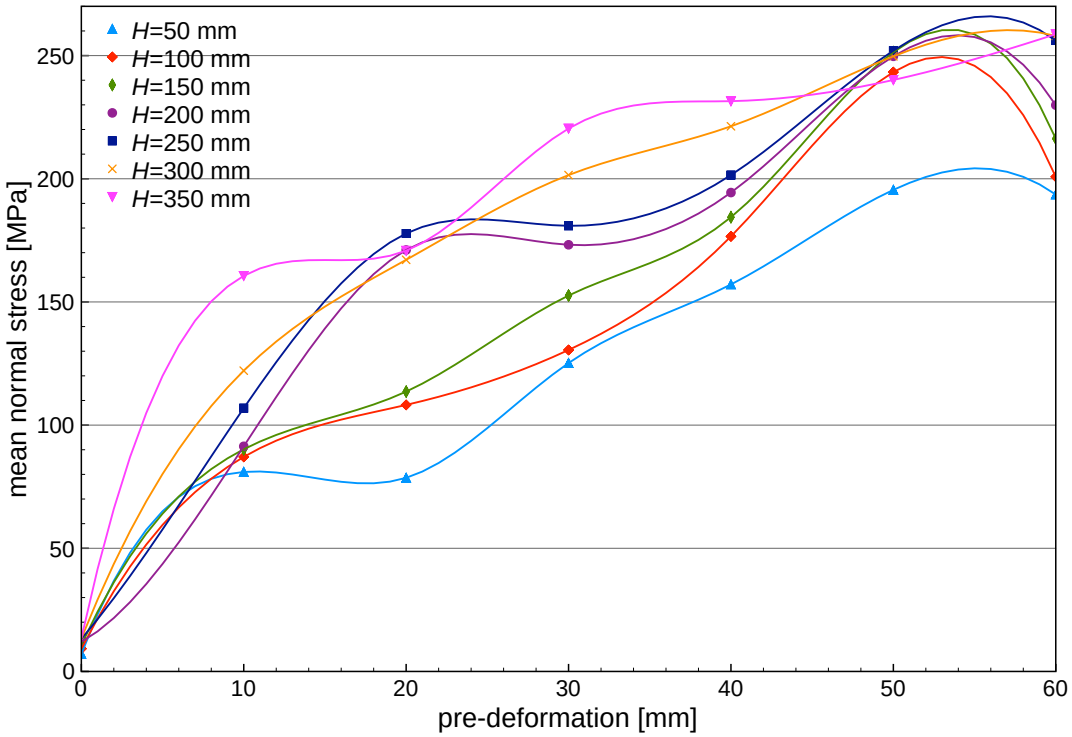

Fig. 5.6: Peak mean normal stress vs. pre-deformation of the column for different drop heights, *H*

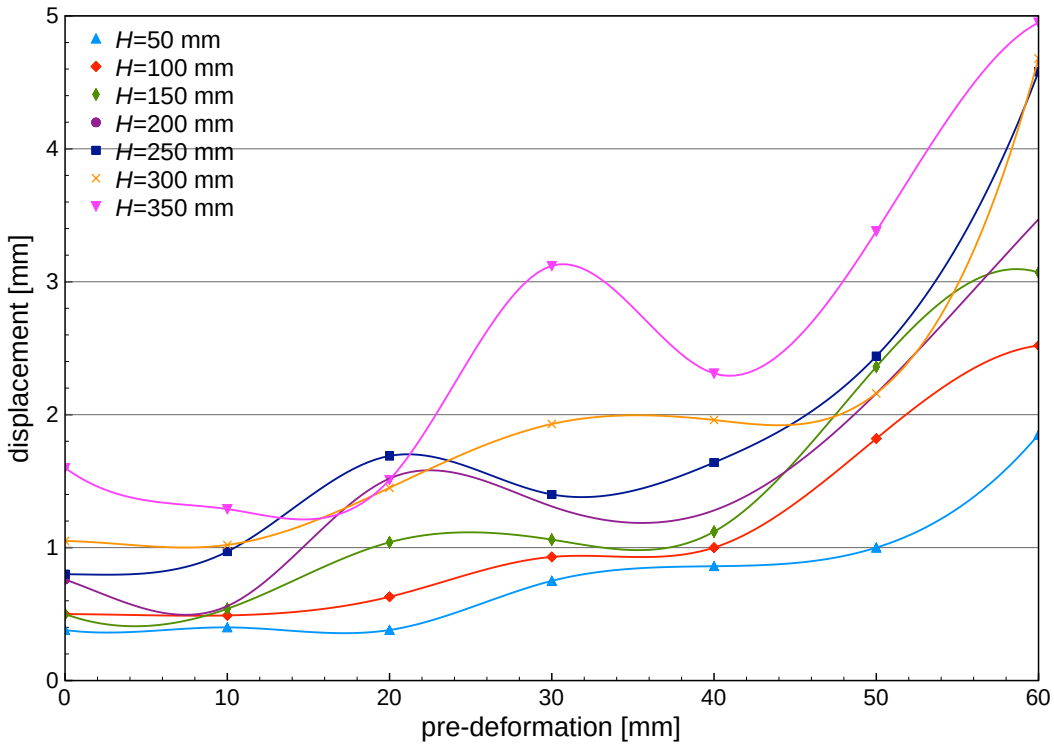

Fig. 5.7: Peak horizontal displacement of the column at its mid-height vs. its pre-deformation for different drop heights, *H*

The peak values of the horizontal displacement of the column at its mid-height with respect to pre-deformation (for different drop heights) is presented in Figure 5.7. It can be seen from the figure that larger pre-deformation results in larger amplitudes in horizontal vibrations of the column. An evident trend of larger peak horizontal displacement for greater drop heights is also visible. In the case of the drop height of 350 mm, for example, the increase in the peak horizontal displacement of the column at its mid-height for the pre-deformed column (pre-deformation of 60 mm) with relation to the undeformed specimen is as large as 469.0%.

5.3.2 Nonlinear study under dynamic excitation

In the second stage of the numerical analysis, the nonlinear analysis has been conducted by exciting horizontally the base of the column (see Figure 5.1) using the harmonic ground motion excitation. The sine wave having the excitation frequency tuned with the natural frequency of the specimen has been used in the analysis. Together with the geometric nonlinearity (large strain analysis), the nonlinear, elasto-plastic material behaviour has also been considered (Jirásek and Bažant 2002, Stein *et al.* 2004). Additionally, the strain rate effect has been taken into account in the numerical analysis by relating the yield strength of steel with the strain rate following the relation obtained from the experimental study, as shown in Figure 2.14 for mild steel 7 (Ansell 2006).

It has been assumed in the analysis that vertical impact takes place at different times of the excitation. Figure 5.8 shows the horizontal displacement time history of the column at its mid-height (response at time range 0.82 - 0.92 s) with dots indicating moments of impact for five different cases considered in the study. The peak values of impact force has been applied at the following times:

case 1: $t_1 = 0.859$ s,

case 2: $t_2 = 0.862$ s,

case 3: $t_3 = 0.869$ s,

case 4: $t_4 = 0.877$ s,

case 5: $t_5 = 0.880$ s,

related to different stages of horizontal deformation of the specimen. Similarly as in the parametric investigation, the impact load time histories measured during the experiment (see Chapter 4) have been used in the study. This time, however, those

time histories have been scaled so as to allow the specimen to enter into the inelastic range, which was not possible in the case of experimental study (limitations of the experimental setup). This approach has allowed us to extend the analysis and investigate the response of the column involving nonlinear material behaviour. The examples of the results, in the form of the horizontal displacement time histories of the column at its mid-height for five different cases of impact, as compared to the time history when impact is not applied, are shown in Figure 5.9. Additionally, the comparison between the displacement time histories for impact with peak value of impact force at $t_3 = 0.869$ s (case 3 related to the peak horizontal deformation of the column) with and without considering the strain rate effect is also presented in Figure 5.10.

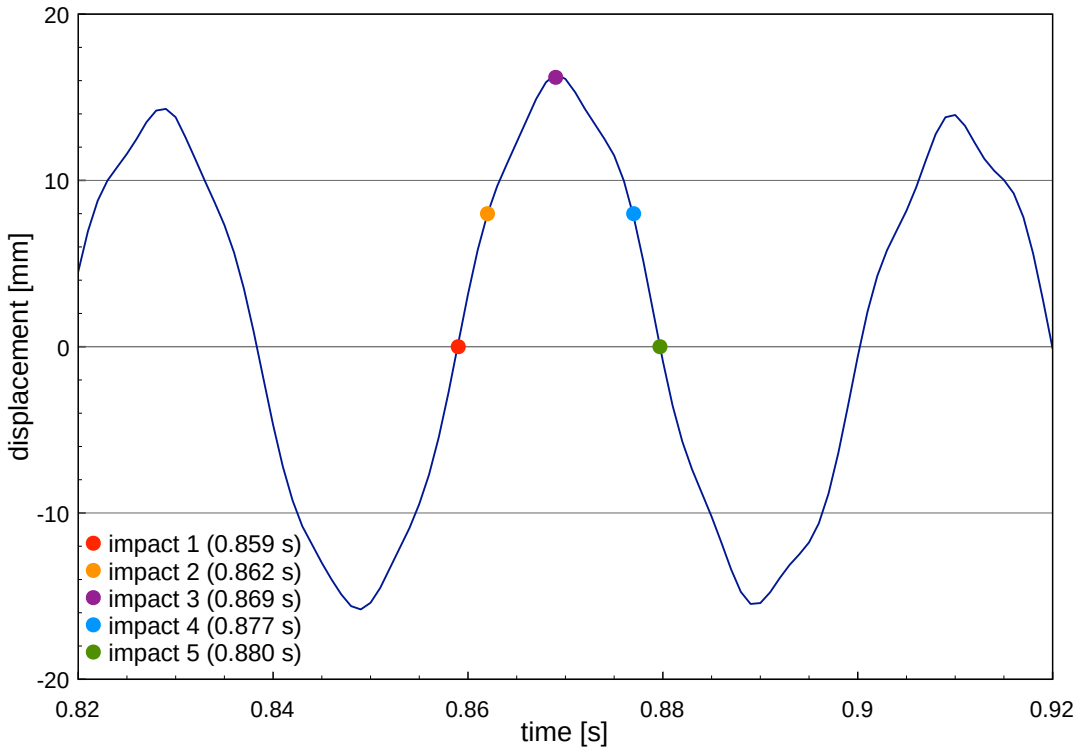

Fig. 5.8: Horizontal displacement time history of the column at its mid-height under harmonic ground motion (time range 0.82 - 0.92 s) with dots indicating different moments of peak values of impact force

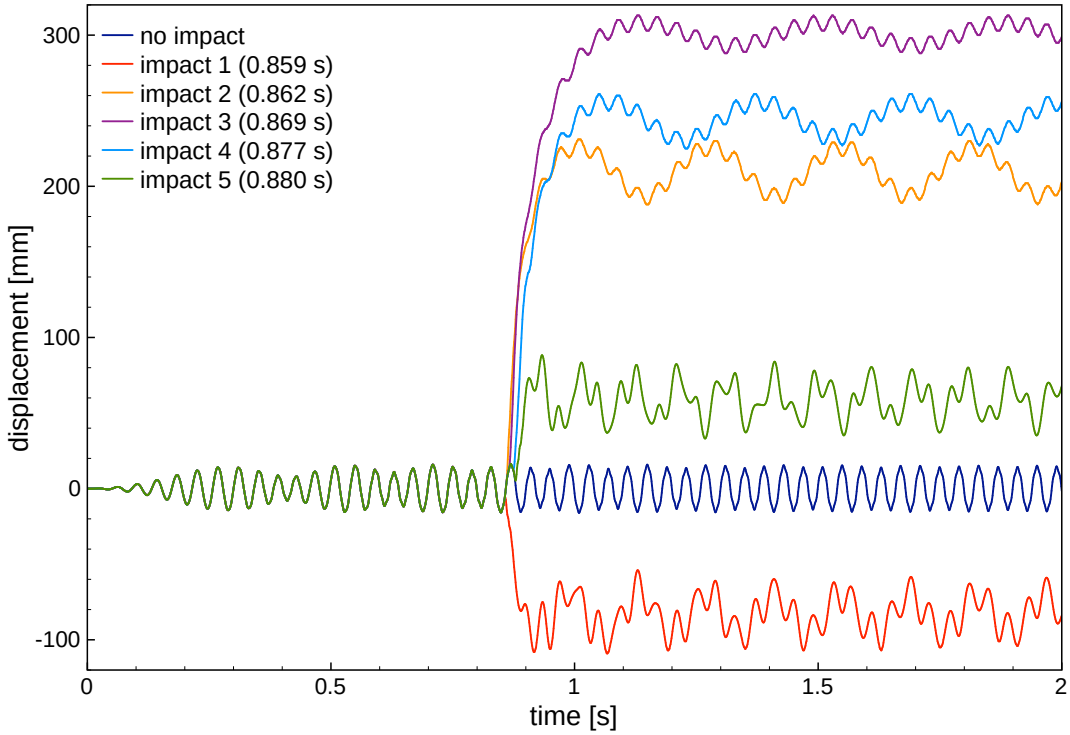

Fig. 5.9: Horizontal displacement time histories of the column at its mid-height under harmonic ground motion for five different cases of impact as compared to the time history when impact is not applied

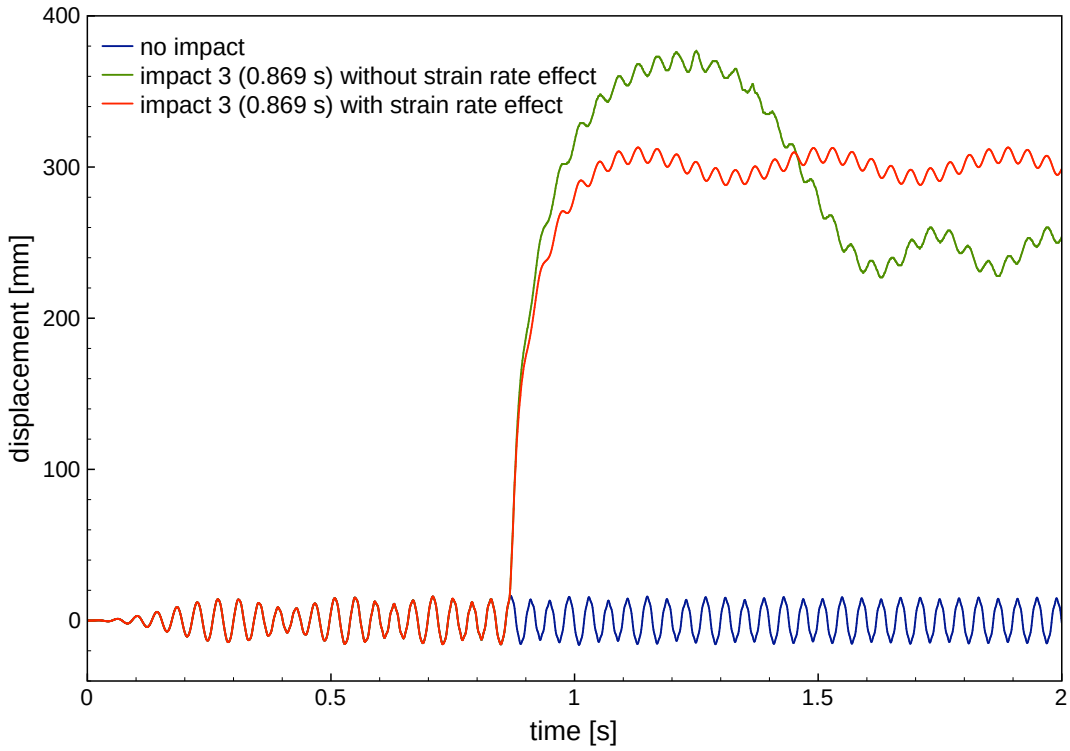

Fig. 5.10: Comparison between the displacement time histories under harmonic ground motion for impact case 3 with and without considering the strain rate effect

It can be seen from Figure 5.9 that vertical impact has a significant influence on the behaviour of the steel column under dynamic ground motion excitation leading to the increase in its response. It can be seen that incorporation of the nonlinearity of material behaviour has resulted in entering into the plastic range in all the cases considered (see permanent displacement of the column at Figure 5.9). Moreover, the obtained results clearly indicate that the time of impact plays a substantial role in the overall behaviour. It can be seen from Figure 5.9 that, for the case when impact takes place at the time of peak horizontal deformation of the column (impact case 3), the increase in the peak structural response is as large as 1808,4% with relation to the peak response without impact. On the other hand, when impact takes place when the actual displacement of the horizontally excited column is relatively small (impact cases 1 and 5), the influence of vertical impact on the response is less significant. Figure 5.9 shows that, in such situations, the increase in the peak horizontal displacement of the column at its mid-height is equal to 438.4%, as compared to the peak response without impact.

It can also be seen from Figure 5.10 that incorporation of the strain rate effect in the numerical analysis is really important and the difference between the responses with and without considering this effect can be substantial. In the case when the strain rate effect is taken into account and vertical impact takes place at the time of the peak horizontal deformation of the column (impact case 3), the decrease in the peak structural response is equal to 20.32%, as compared to case when the effect in not considered.

5.4 Conclusions

The numerical investigation concerning the behaviour of a model of deformed steel column, that is additionally subjected to vertical impact load (the result of soft-storey failure during earthquake), has been described in this chapter. In the first stage of the study, the analysis has been conducted for different values of the static horizontal pre-deformation of the column. Then, the base of the column has been dynamically excited by harmonic ground motion and vertical impact load has been applied at different times of the excitation. The geometric nonlinearity (large strain analysis) as well as the elasto-plastic material behaviour with the strain rate effect have been taken into account.

The results of the first stage of the numerical study show that, with the increase in the static pre-deformation of the column, the peak mean normal stress values induced at the bottom of the specimen as well as the peak horizontal displacement at the middle of the column show a substantial increase trend for all height drop values considered. The above conclusions indicate that the initial pre-deformation of columns has a substantial negative influence, what is fully consistent with the results of the experimental study described in Chapter 4.

The results of the second stage of the numerical study show that vertical impact may substantially influence the response of the column, which is dynamically excited in its horizontal direction. The results confirm the main conclusion of Chapter 3 that the time of impact plays a substantial role in the overall behaviour under ground motion excitation. It has been shown that the response may be increased significantly if impact is initiated when the specimen is in the range of its peak horizontal deformation. On the other hand, when impact takes place when the actual displacement of the horizontally excited column is relatively small, the

influence of vertical impact on the response is less significant. Moreover, the results indicate that the incorporation of the strain rate effect in the numerical analysis is really important in order to increase its accuracy.

Chapter 6.

NUMERICAL ANALYSIS OF A STEEL FRAME BULIDING DURING EARTHQUAKE

6.1 Introduction

The numerical analysis described in Chapter 5 has been focused on the response of the selected structural member of the building. The investigation has concerned the dynamic response of the steel column under harmonic ground motion excitation that is additionally subjected to vertical impact load. The aim of Chapter 6 is to show the results of a detailed, nonlinear, three-dimensional numerical analysis using FEM (see Bathe 1982, Zienkiewicz and Taylor 2002) concerning the behaviour of the whole multi-storey steel frame building that suffers from a soft-storey failure under real earthquake excitation. A model of the structure has been exposed to an impact due to falling of the upper floors onto the slab of the first storey. During the analysis, different moments have been chosen for the impact so as to estimate the most critical moment for the building (see also Migda and Jankowski 2013a). The geometric nonlinearity due to impact and the second order effects as well as the elasto-plastic material behaviour with the strain rate effect have been considered in the numerical analysis.

The main advantage of the analysis described in Chapter 6 is related to the fact that it allow us to verify the conclusions obtained from previous chapters in

which simplifies numerical models have been used. By considering the FE model of a real building, the scale-effect problem can be overcome without the need of putting up some assumptions based on comparison between real structures and scaled models.

6.2 Numerical model

A four-storey steel frame building, with the plan dimensions of 31.68 m by 19.44 m and a storey height of 3.6 m, has been considered in the analysis (compare Liu *et al.* 2003). The grid of the columns of the structure is 8.0 m by 6.5 m with a cantilever type slab overhanging. The steel columns with a cross section of I270HEB are used as the major load-carrying members. The horizontal structural members consist of the concrete slabs with the thickness of 0.2 m. A number of additional steel bracings, with the cross section of 0.002 m^2, are also used to increase the structural stability.

The detailed numerical model of the structure has been created using the FEM software MSC Marc. The steel columns have been modelled by the use of four-node quadrilateral shell elements with the detailed reflection of their geometry. Shell elements (four-node as well three-node ones) have also been used in the case of concrete slabs. Steel bracings have been modelled by two-node truss elements. The structural supports of the model have been considered to be fixed and the soil-structure interaction has not been taken into account in the study. Figures 6.1-6.4 show, respectively, the general view, the front view, the side view and the top view of the model consisting in total of 15016 elements and 16092 nodes. The detailed view of the mesh refinement in the area of the column-slab connections is also presented in Figure 6.5, whereas the details of the model of columns (with indicated

reference node at the mid-height of the element) are shown in Figure 6.6. Moreover, Table 6.1 summarizes the geometric parameters as well as material properties that have been used in the FE model of the building.

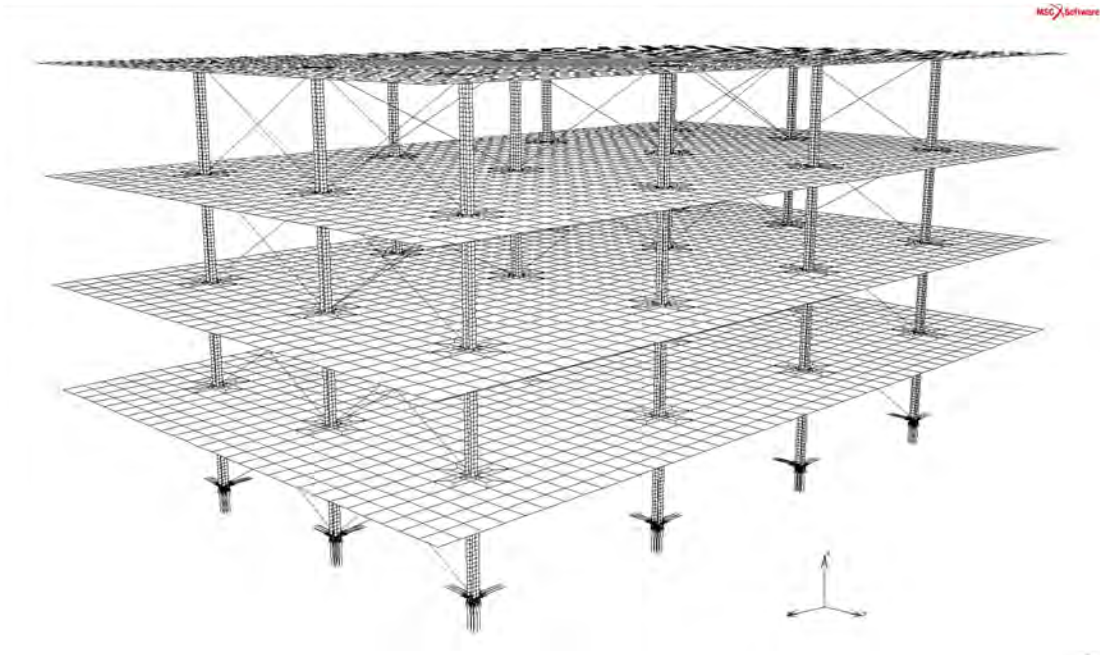

Fig. 6.1: General view of the numerical model of the building

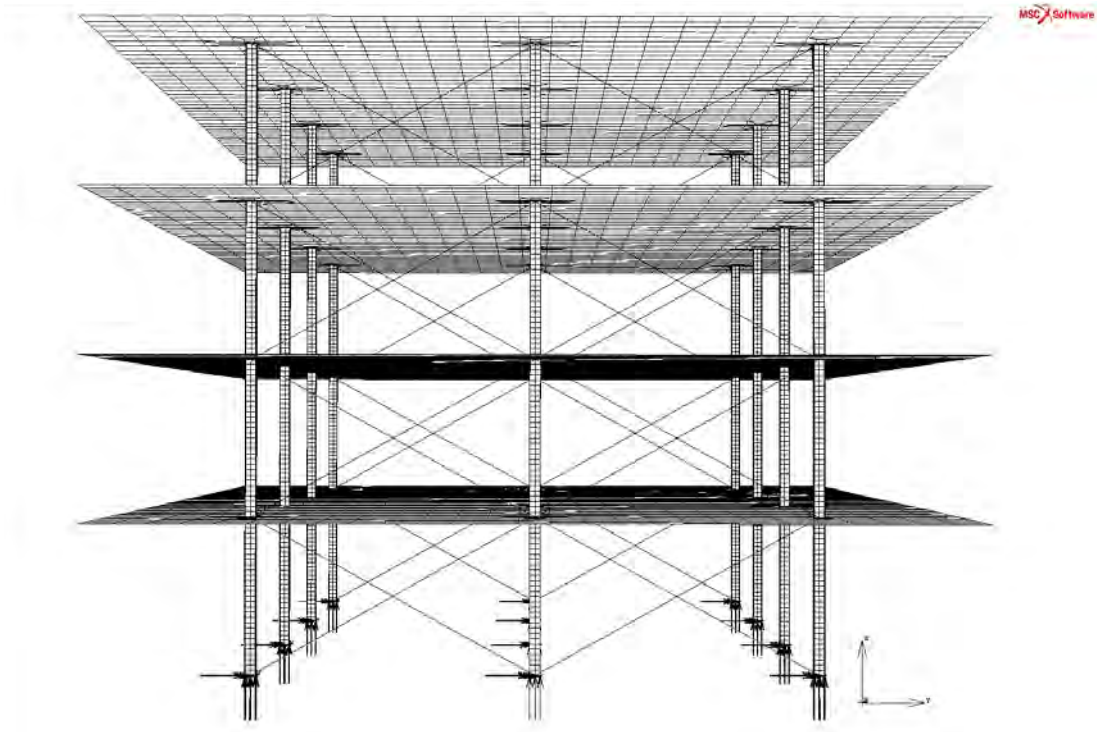

Fig. 6.2: Front view of the numerical model of the building

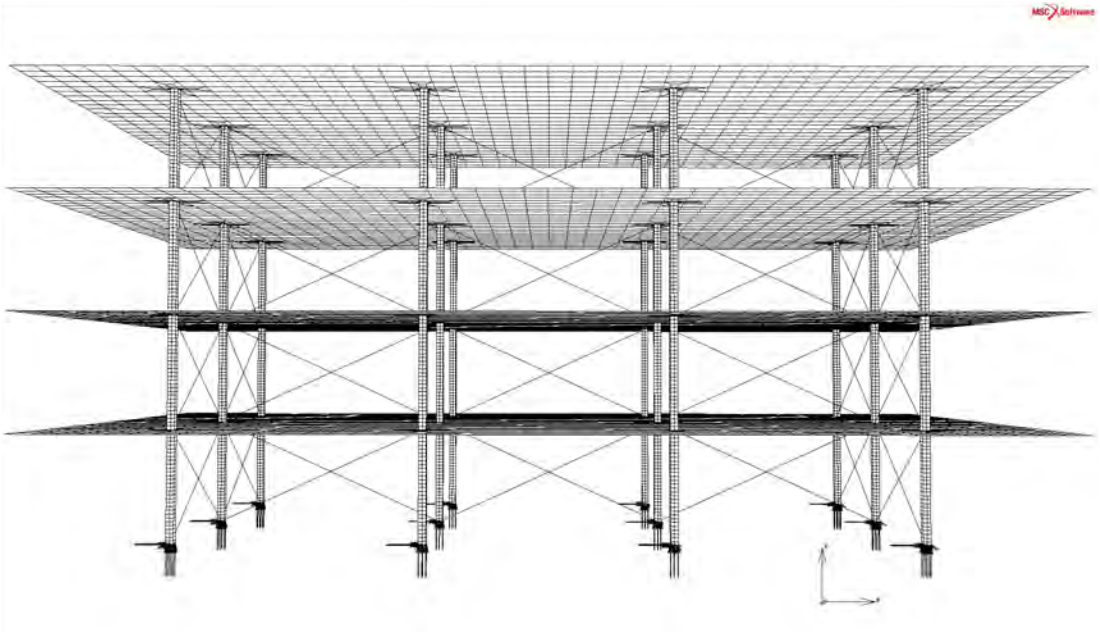

Fig. 6.3: Side view of the numerical model of the building

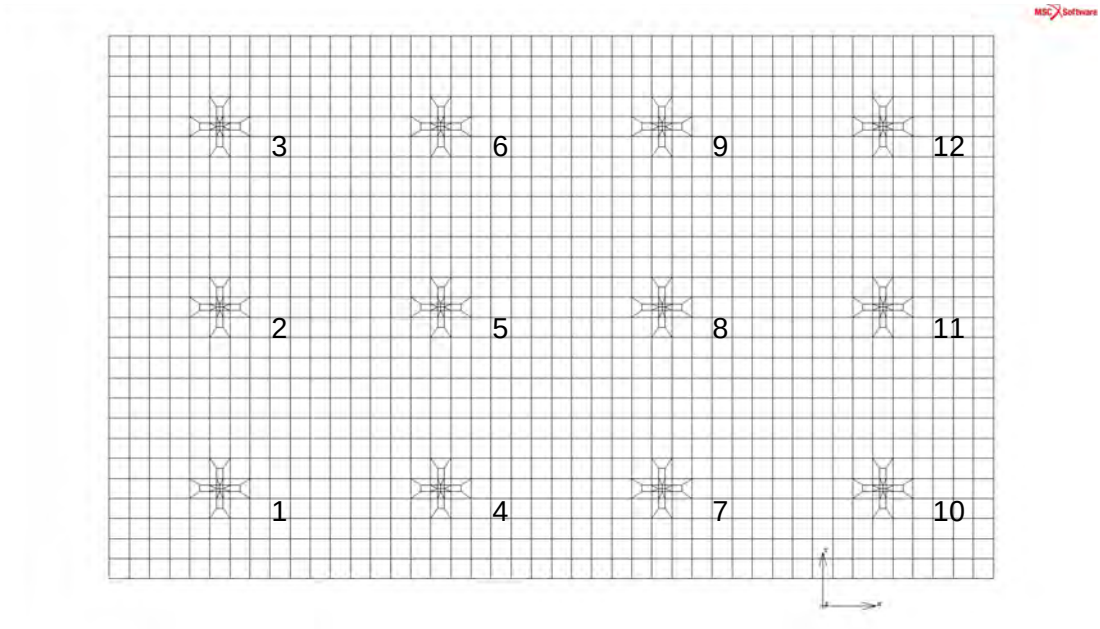

Fig. 6.4: Top view of the numerical model of the building with indicated numbers of columns

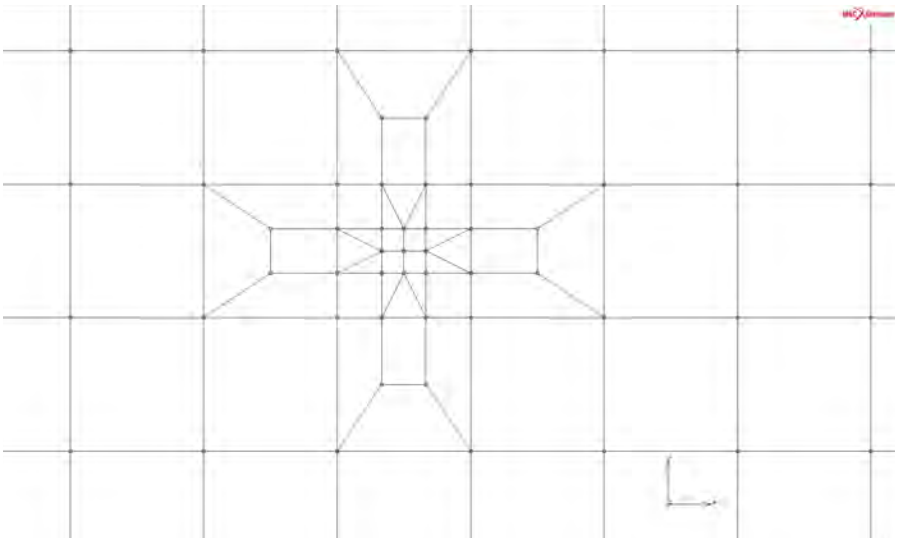

Fig. 6.5: Detailed view of mesh refinement in the area of the column-slab connections

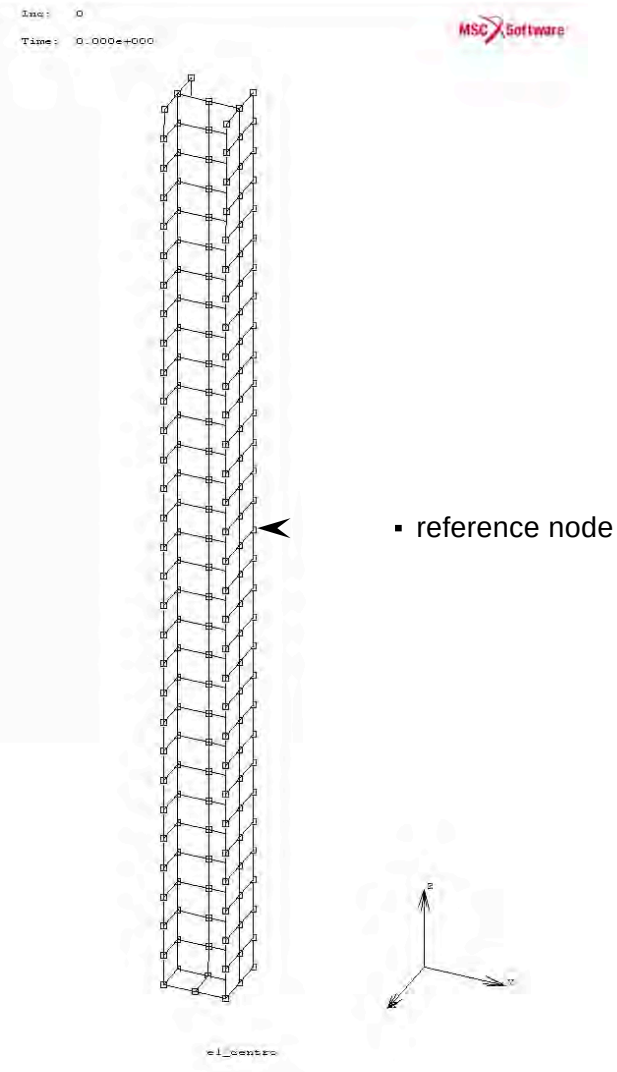

Fig. 6.6: Details of the model of columns with indicated reference node

member		slab	column		bracing
			flange	web	
element properties	type	shell	shell	shell	truss
	no. of nodes	3/4	4	4	2
geometric properties	thickness, h [m]	0.2	0.017	0.01	-
	area, A [m^2]	-	-	-	0.002
material properties	mass density, ρ [kg/m^3]	2400	7850	7850	7850
	Young's modulus, E [GPa]	31	215	215	215
	Poisson's ratio, ν [-]	0.2	0.3	0.3	0.3

Tab. 6.1: Properties used for the building model

6.3 Modal analysis

In order to verify the dynamic properties of the numerical model created, a modal analysis has been first carried out. The results of the analysis showing the first three natural vibration modes of the building are presented in Figures 6.7-6.9. As it can be seen from Figure 6.7, the first natural vibration mode is a longitudinal one (X direction) with the natural frequency of 1.238 Hz. The second vibration mode of the structure (see Figure 6.8), obtained for the natural frequency of 1.648 Hz, is a torsional one. Finally, Figure 6.9 indicates that the third natural vibration mode is a transverse one (Y direction). The natural frequency for this mode has been calculated as equal to 1.960 Hz. It should be underlined that the determined values of the natural frequencies of the FE model of the building are within the range of typical values concerning four-storey steel frame buildings (see Chopra 1995, Liu *et al.* 2003).

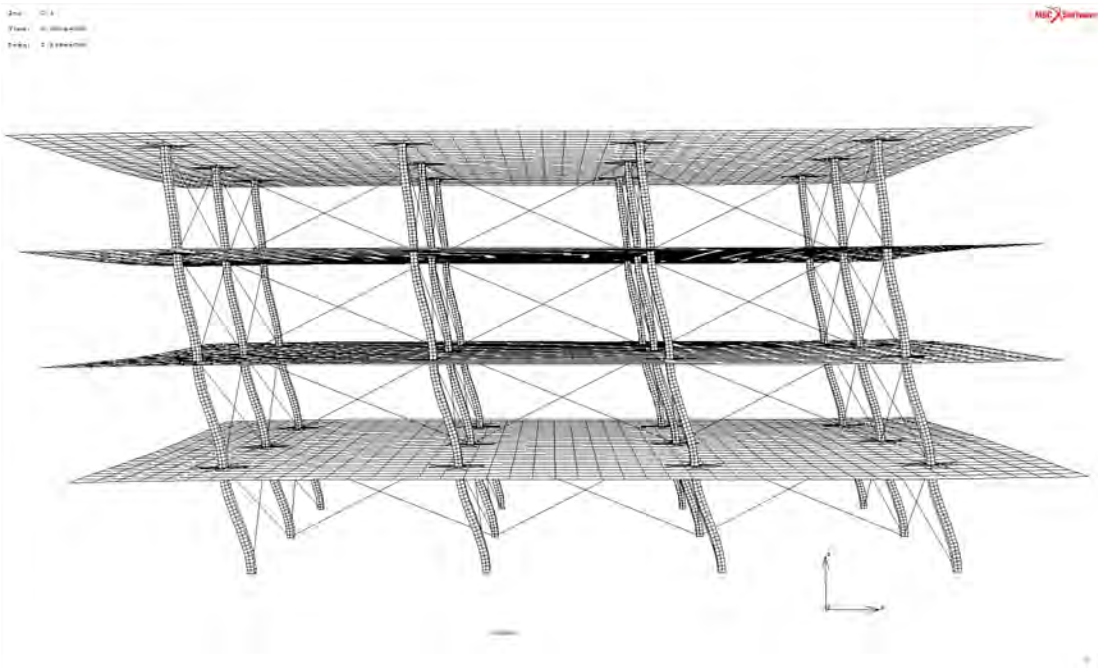

Fig. 6.7: First vibration mode (longitudinal) related to the natural frequency f_1=1.238 Hz

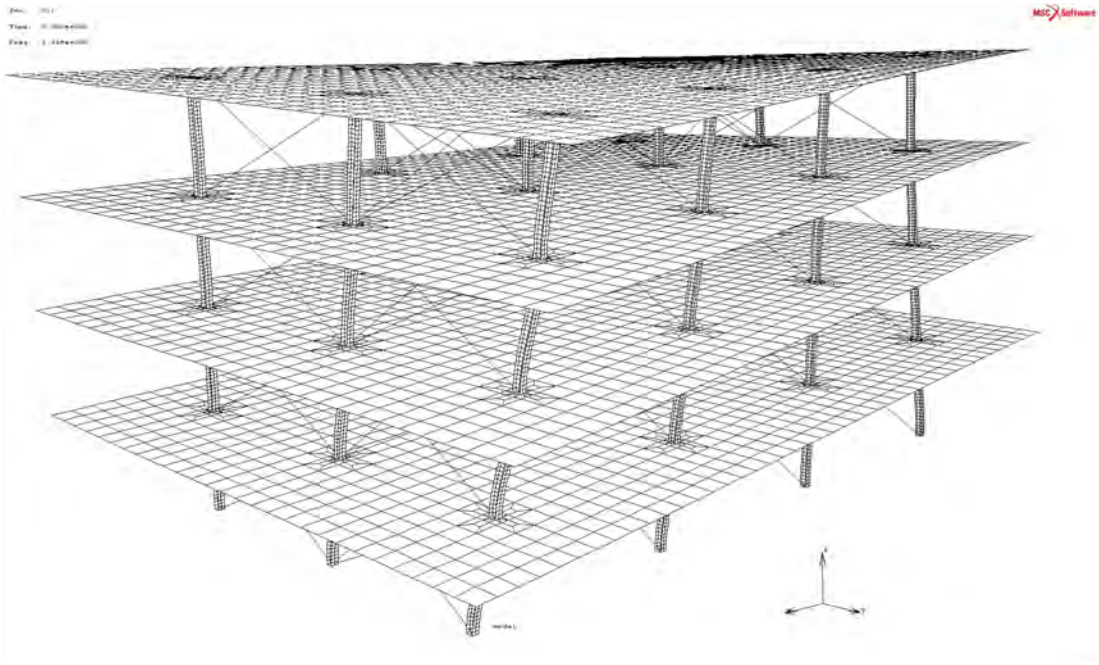

Fig. 6.8: Second vibration mode (torsional) related to the natural frequency f_2=1.648 Hz

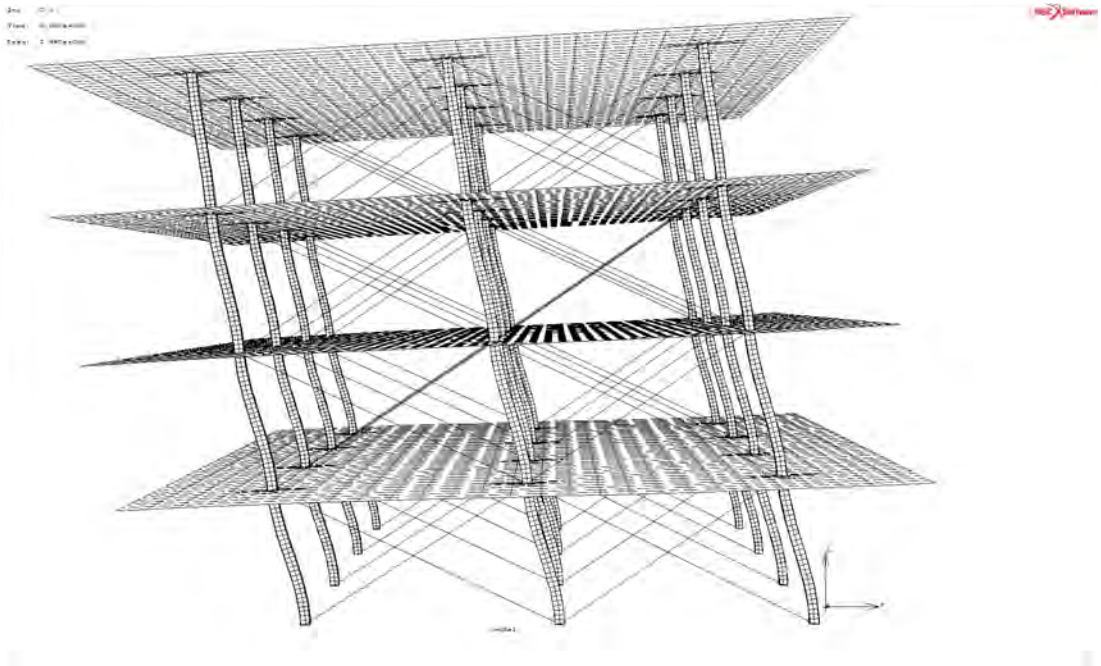

Fig. 6.9: Third vibration mode (transverse) related to the natural frequency f_3=1.960 Hz

6.4 Dynamic analysis

6.4.1 Parameters of the analysis

A detailed nonlinear numerical analysis has been carried out using the model of the structure shown in Figures 6.1-6.6. The dynamic analysis under ground motion excitation has been conducted in three directions (two horizontal and one vertical) simultaneously. The NS, EW and UD components of the El Centro earthquake (see Figure 3.5, Figure 6.10 and Figure 6.11) have been applied along the longitudinal (X), transverse (Y) and vertical (Z) direction, respectively. The structural response has been determined by the use of the time-stepping Newmark method (Newmark 1959), with the standard parameters: $\gamma_N = 0.5$, $\beta_N = 0.25$ assuring the stability and accuracy of the results (Chopra 1995).

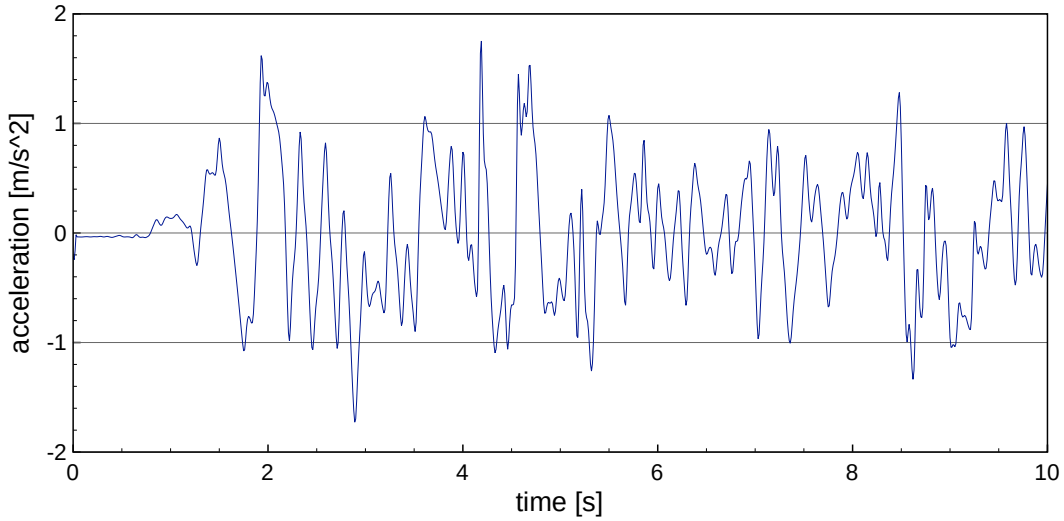

Fig. 6.10: Acceleration time history of the EW component of the El Centro earthquake (18.05.1940)

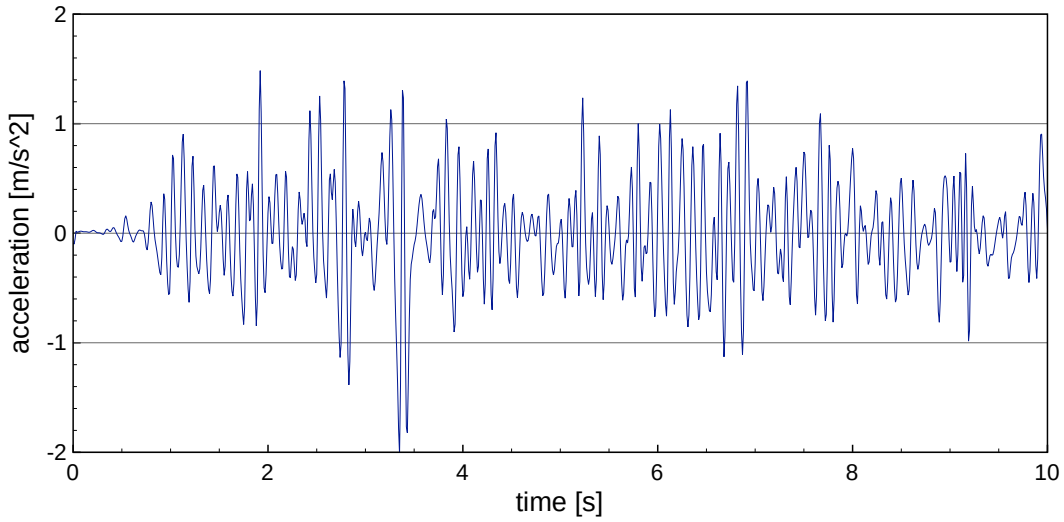

Fig. 6.11: Acceleration time history of the UD component of the El Centro earthquake (18.05.1940)

Viscous damping of the Rayleigh type has been employed in the model so as to simulate the dissipation of energy during structural vibrations as the result of earthquake excitation. The Rayleigh damping multipliers have been calculated using the following formulas (Chopra 1995, Clough and Penzien 1993):

$$a_0 = \xi \frac{2\omega_1\omega_2}{\omega_1+\omega_2} \tag{6.1}$$

$$a_1 = \xi \frac{2}{\omega_1 + \omega_2} \tag{6.2}$$

$$\omega_i = 2\pi f_i \tag{6.3}$$

where a_0 and a_1 is the mass matrix and the stiffness matrix multiplier, respectively; and f_i is the frequency for *i*-th vibration mode. In order to cover the frequency range including the basic natural frequencies for both horizontal directions: X and Y (see Chopra 1995), the calculations have been carried out for the first and the third natural frequency related to the longitudinal and transverse vibration modes (see Figure 6.7 and Figure 6.9). The calculated Rayleigh damping multipliers are summarized in Table 6.2.

damping ratio, ξ [%]	first natural frequency, f_1 [Hz]	third natural frequency, f_3 [Hz]	mass matrix multiplier, a_0 [-]	stiffness matrix multiplier, a_1 [-]
2%	1.238	1.960	0.19069	0.00199

Tab. 6.2: Rayleigh damping multipliers

The nonlinear, elasto-plastic material behaviour (see Jirásek and Bažant 2002, Kłosowski and Woźnica 2004) has been considered in the analysis. Additionally, the strain rate effect has been taken into account in the numerical analysis by relating the yield strength of steel with the strain rate following the relation obtained from the experimental study, as shown in Figure 2.14 (Ansell 2006). In the case of columns, the relation for mild steel 7 has been employed. On the other hand, the relation for high strength steel 8 has been used in the case of bracings.

Together with the material nonlinearity, the geometric nonlinearities due to impact as well as due to the second-order effects have also been incorporated in the analysis. In order to investigate the behaviour of the building subjected to the soft-storey failure, the collapse of the arbitrary chosen second storey has been initiated

assuming its damage at different moments during the response of the structure. Then, it has been assumed in the numerical model, that the remains of the second storey do not offer the resistance allowing for the free fall of the third and the fourth storey onto the slab of the first storey of the building. Impact between the falling upper storeys and the first storey slab has been modelled by the way of defining different contact bodies (Stronge 2000, Wriggers 2002). This approach allows us to prevent structural members in contact from their penetration and impose friction forces due to relative movement along the contact surface. In the analysis, the coefficient of friction equal to 0.5 has been applied (see Wriggers 2002).

In order to investigate the importance of different moments of impact on the behaviour of the first storey columns, the response of the building under the El Centro earthquake without the soft-storey failure has been first determined. The results of this analysis in the form of displacement time histories for the slab of the first storey in X, Y and Z direction are shown in Figures 6.12-6.14. The resultant horizontal displacement for the slab of the first storey, $W_H(t)$, is also presented in Figure 6.15. It has been calculated according to the formula:

$$W_H(t) = \sqrt{W_X^2(t) + W_Y^2(t)} \tag{6.4}$$

where $W_X(t)$, $W_Y(t)$ is the horizontal displacement of the first storey slab in X and Y direction, respectively. Four different moments of impact between the upper storeys and the slab of the first storey have been considered in the analysis:

case 1: $t_1 = 4.060$ s,

case 2: $t_2 = 3.750$ s,

case 3: $t_3 = 3.470$ s,

case 4: $t_4 = 3.920$ s,

The above times, related to different stages of horizontal deformations, have been marked by dots in Figure 6.15.

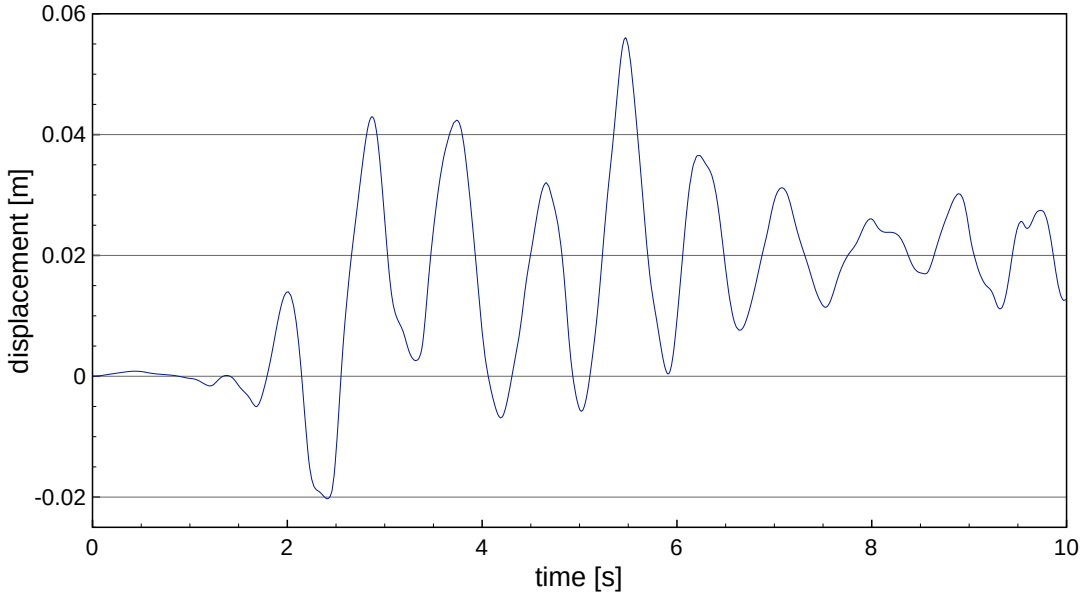

Fig. 6.12: Horizontal displacement time history of the first storey slab (X direction) under the El Centro earthquake

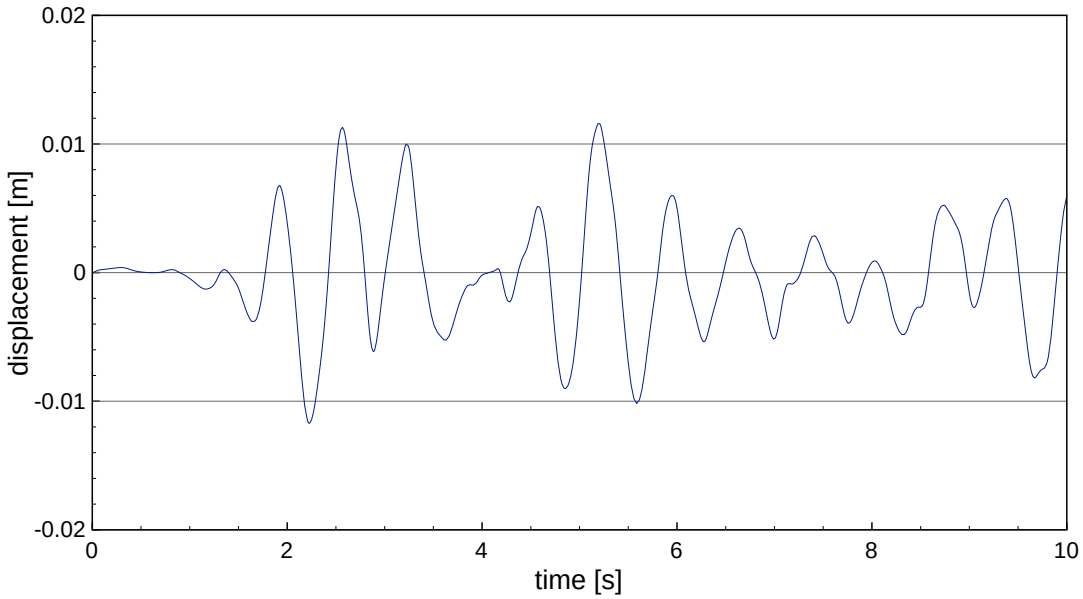

Fig. 6.13: Horizontal displacement time history of the first storey slab (Y direction) under the El Centro earthquake

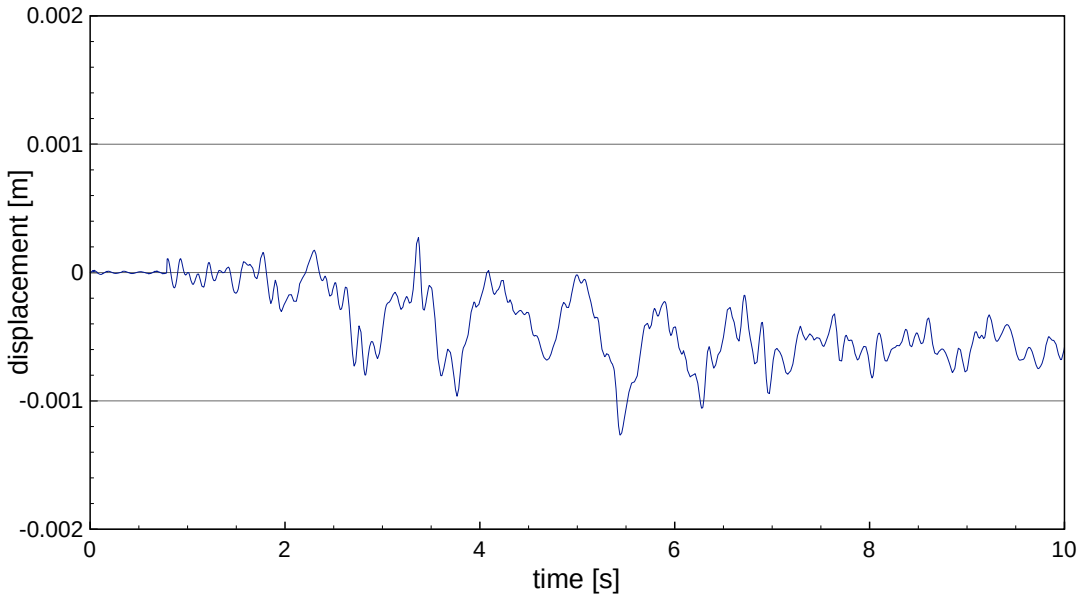

Fig. 6.14: Vertical displacement time history of the first storey slab (Z direction) under the El Centro earthquake

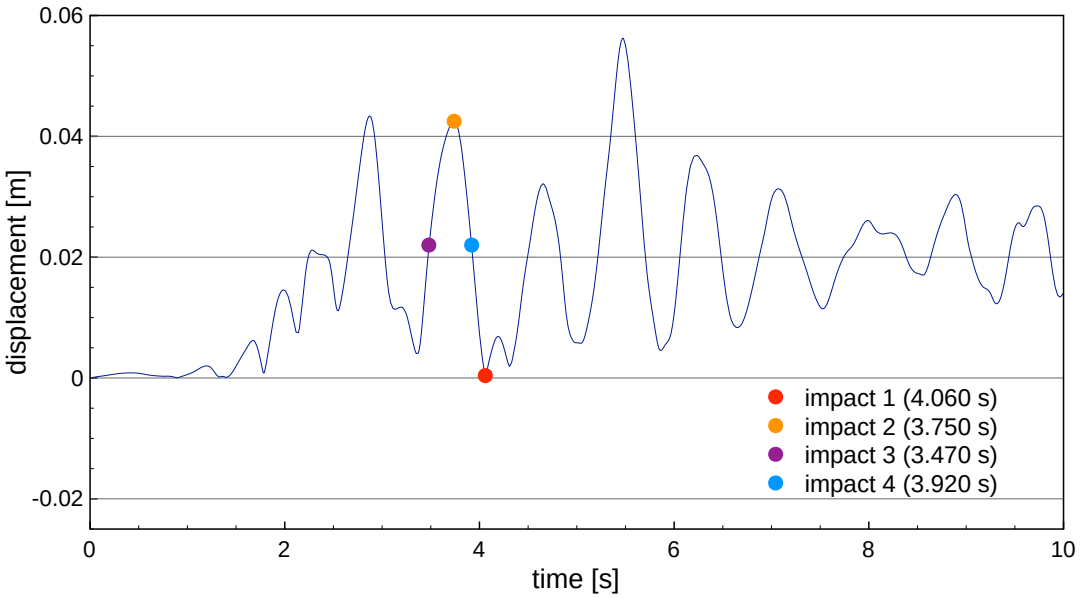

Fig. 6.15: Resultant horizontal displacement time history of the first storey slab under the El Centro earthquake with dots indicating different moments of impact

6.4.2 Structural response

The nonlinear, three-dimensional, numerical analysis has been conducted for four different impact times within two cases. First, the response of the four-storey steel frame building (see its model in Figures 6.1-6.6) under the El Centro earthquake excitation has been determined without considering the strain rate effect in steel. Then, a similar analysis has been carried out taking into account the effect of the strain rate. The examples of the results are shown in Figures 6.16-6.31. In particular, Figures 6.16-6.27 present the resultant displacement time histories of the reference point at the mid-height of the first storey columns (see its location in Figure 6.6) for four different moments of impact, as compared to the time history when impact does not take place (no soft-storey failure). The views of the deformed model of the building after the ground motion, showing the equivalent von Mises stress distribution, are also shown in Figures 6.28-6.31.

It can be seen from Figures 6.16-6.31 that vertical impact, the due to the fall of upper storeys after the soft-storey failure of the second storey, has a substantial influence on the behaviour of the first storey columns of the steel frame building under earthquake excitation. Their response due to impact has increased significantly after entering into the inelastic range as the result of yielding. Moreover, the results clearly indicate that the moment of the impact plays a significant role. It has been observed that the most critical moment for the first storey columns for being subjected to a vertical impact is when the resultant horizontal displacement of the first storey slab is close to its peak (impact time $t_2 = 3.750$ s). For this case, most of the columns of the first storey have collapsed (see Figure 6.29) and their resultant displacements at their mid-height have increased substantially (see Figures 6.16-6.27).

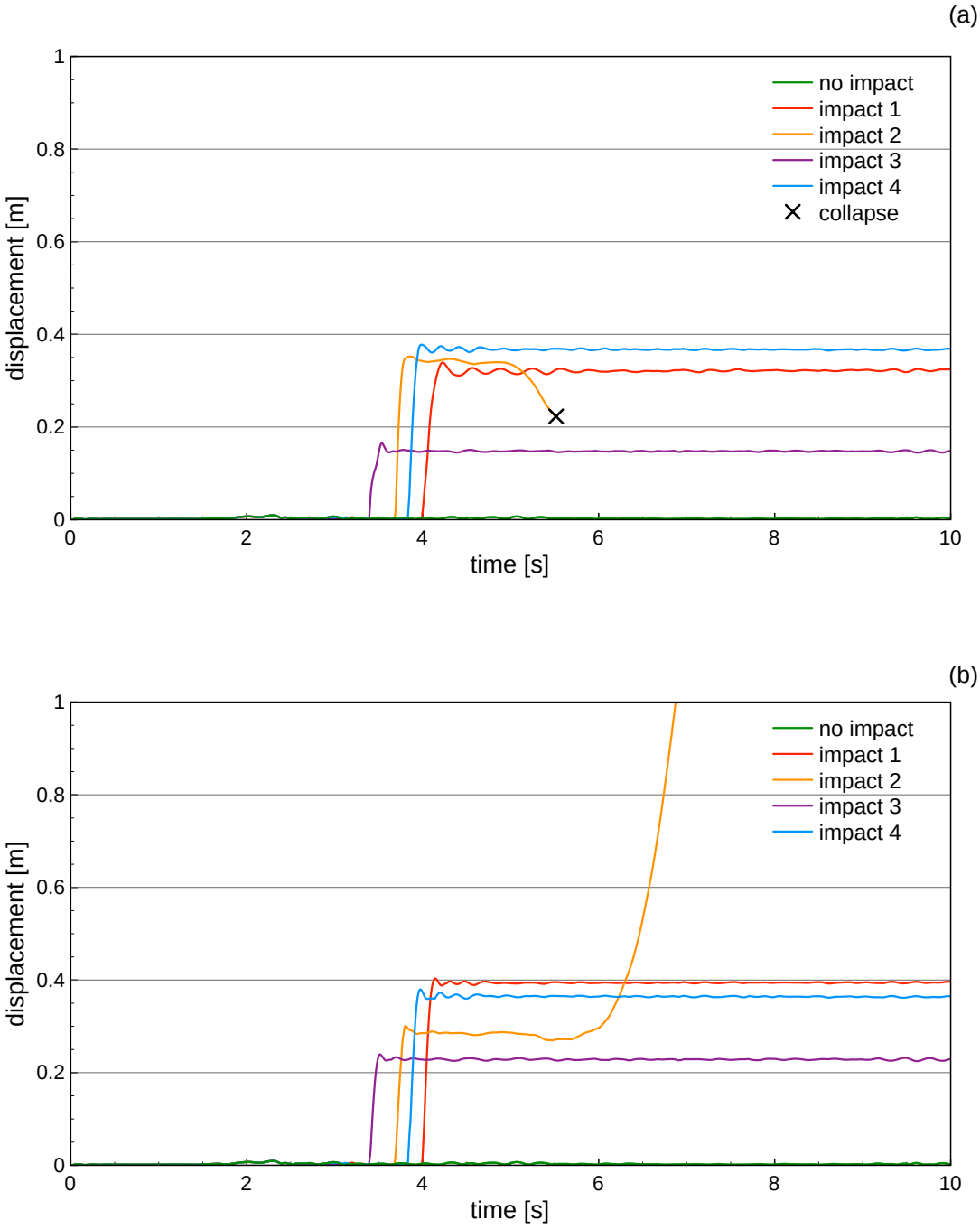

Fig. 6.16: Resultant displacement time histories at the mid-height of column no. 1 for four different moments of impact and for the case when impact does not take place: a) without strain rate effect; b) with strain rate effect

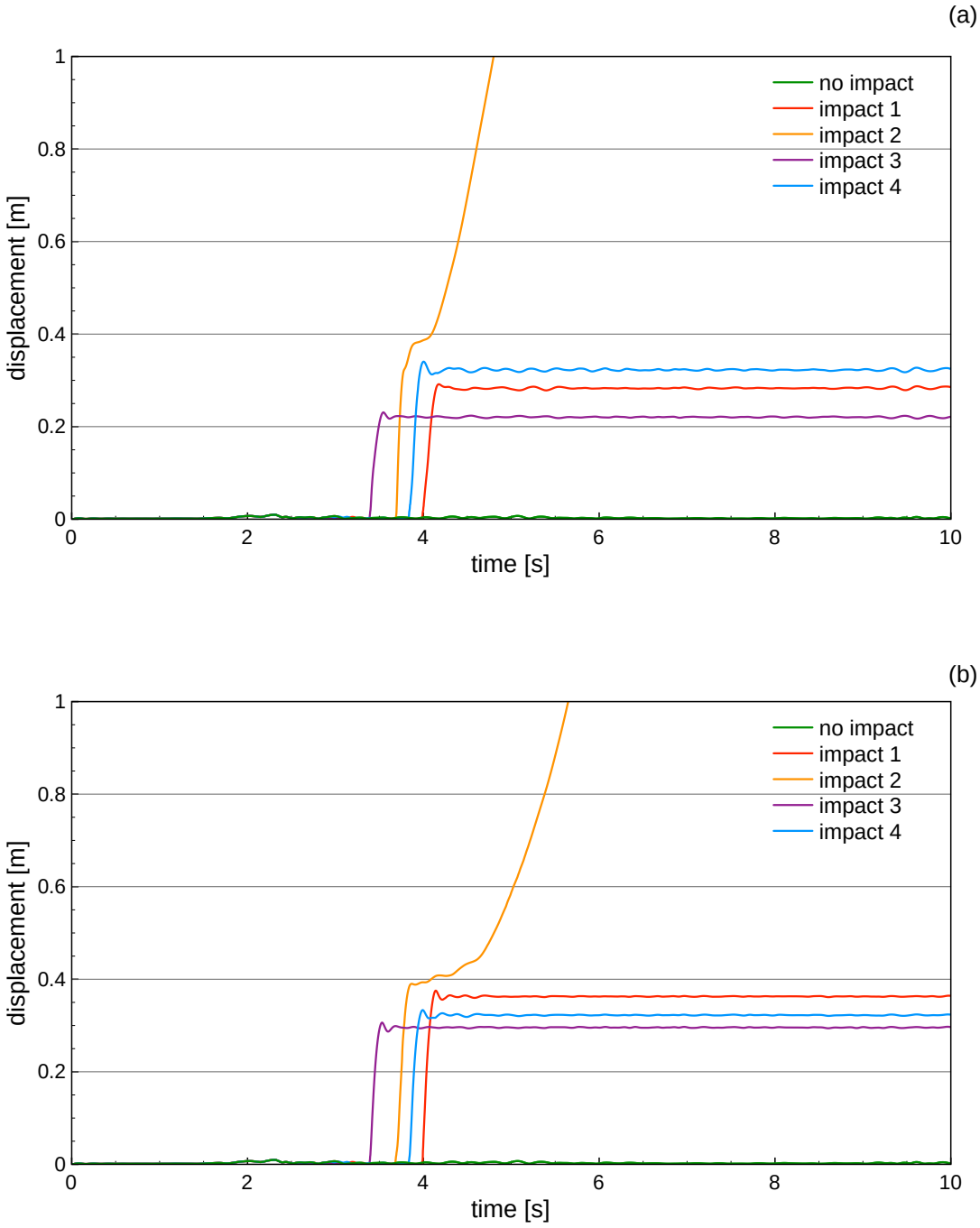

Fig. 6.17: Resultant displacement time histories at the mid-height of column no. 2 for four different moments of impact and for the case when impact does not take place: a) without strain rate effect; b) with strain rate effect

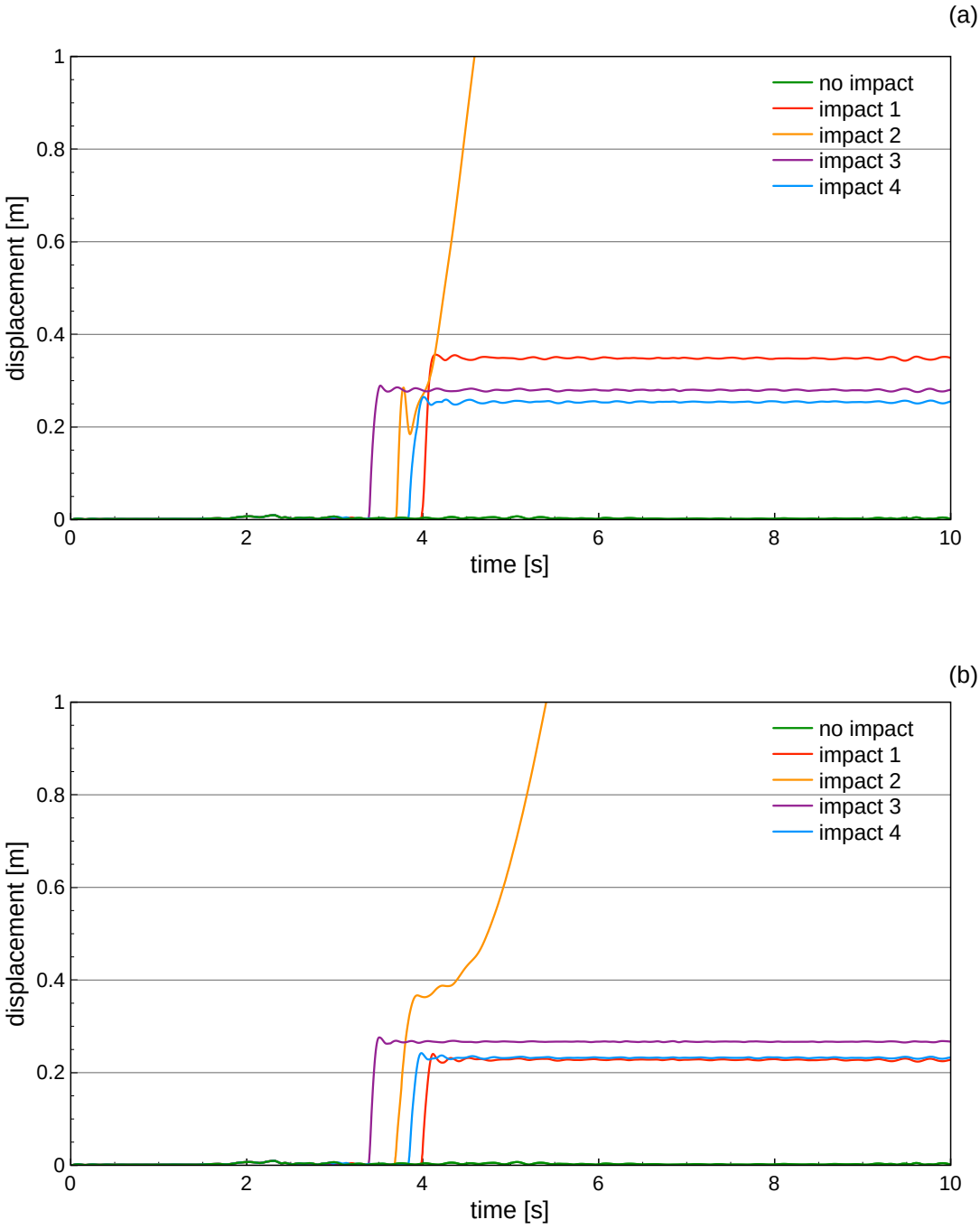

Fig. 6.18: Resultant displacement time histories at the mid-height of column no. 3 for four different moments of impact and for the case when impact does not take place: a) without strain rate effect; b) with strain rate effect

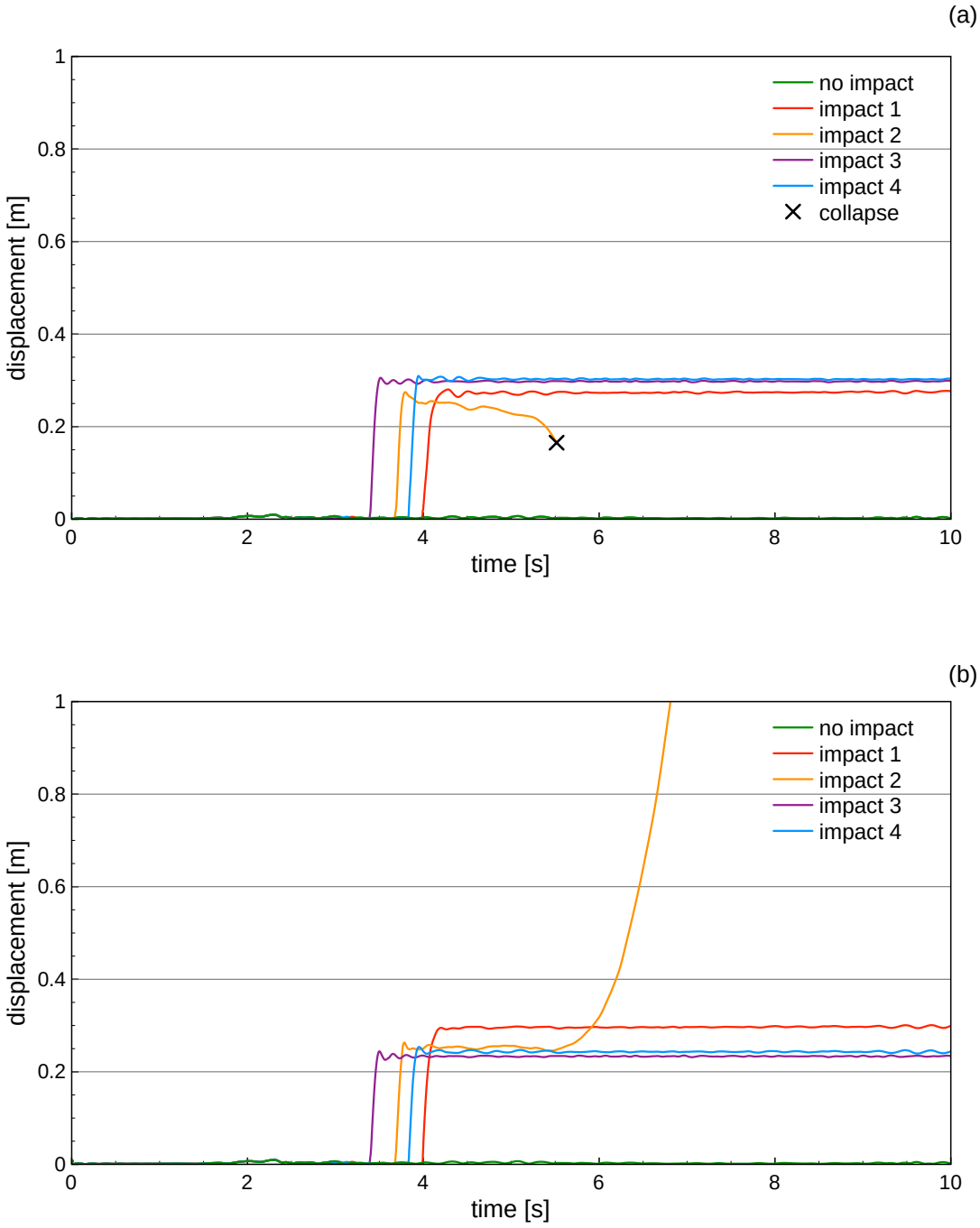

Fig. 6.19: Resultant displacement time histories at the mid-height of column no. 4 for four different moments of impact and for the case when impact does not take place: a) without strain rate effect; b) with strain rate effect

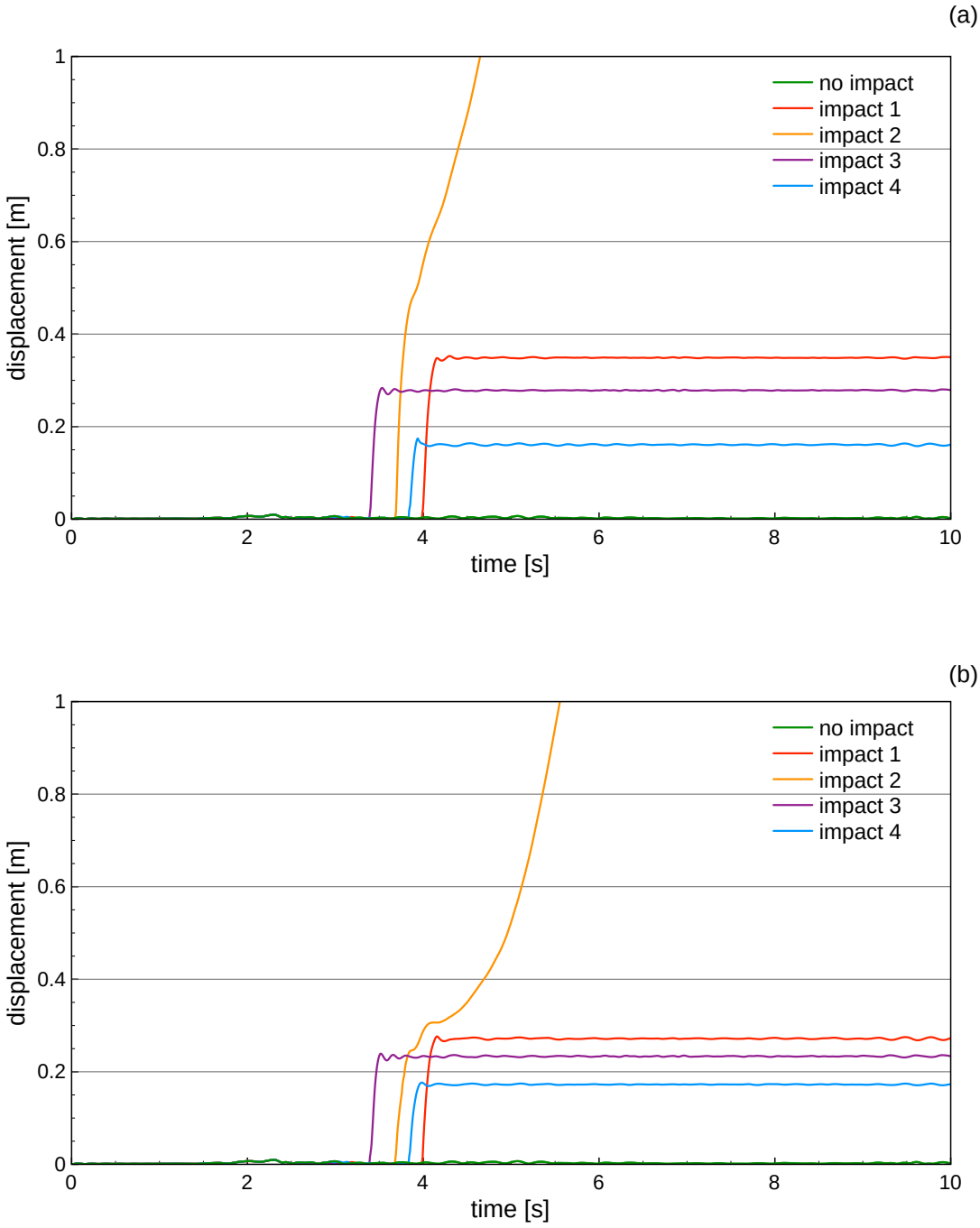

Fig. 6.20: Resultant displacement time histories at the mid-height of column no. 5 for four different moments of impact and for the case when impact does not take place: a) without strain rate effect; b) with strain rate effect

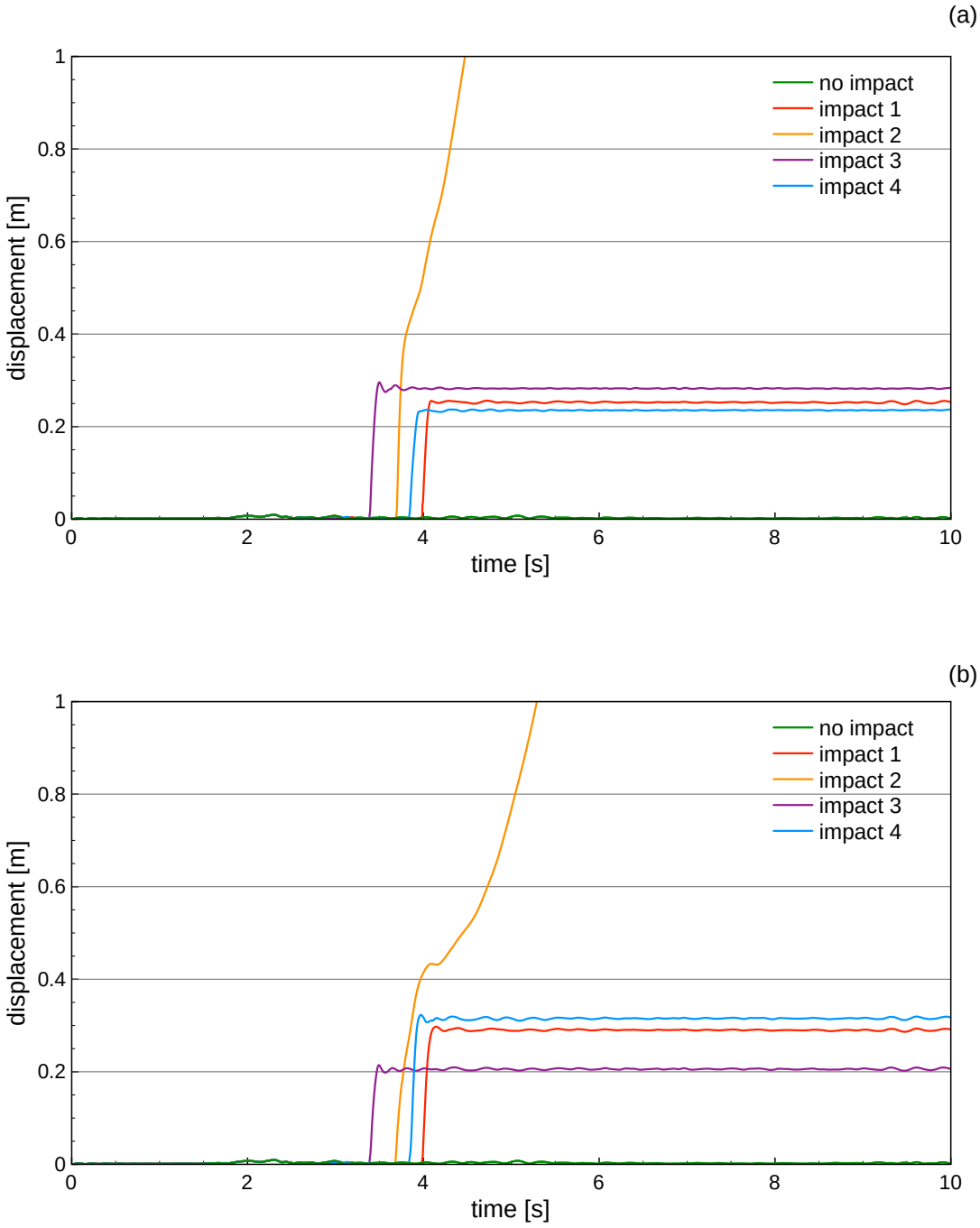

Fig. 6.21: Resultant displacement time histories at the mid-height of column no. 6 for four different moments of impact and for the case when impact does not take place: a) without strain rate effect; b) with strain rate effect

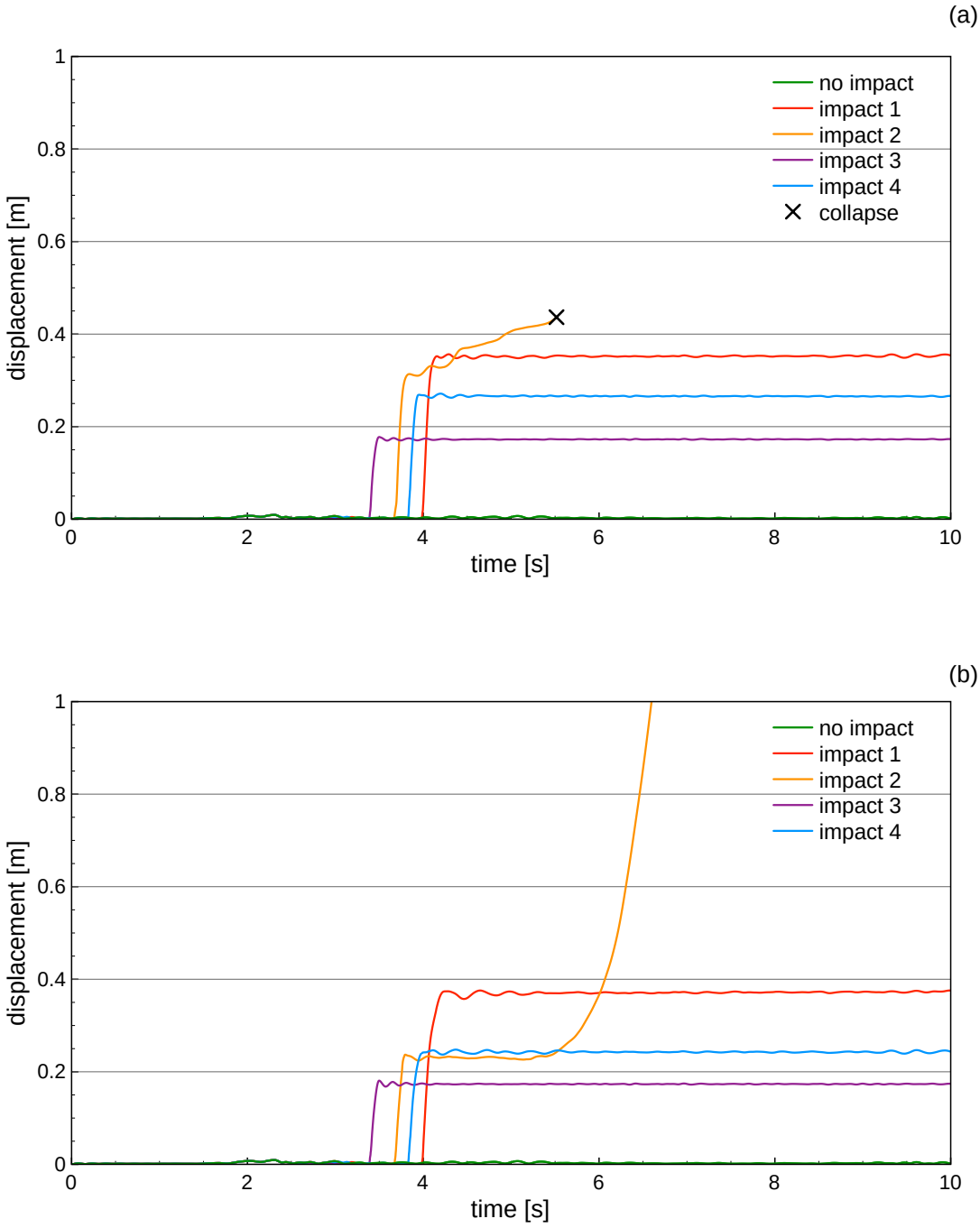

Fig. 6.22: Resultant displacement time histories at the mid-height of column no. 7 for four different moments of impact and for the case when impact does not take place: a) without strain rate effect; b) with strain rate effect

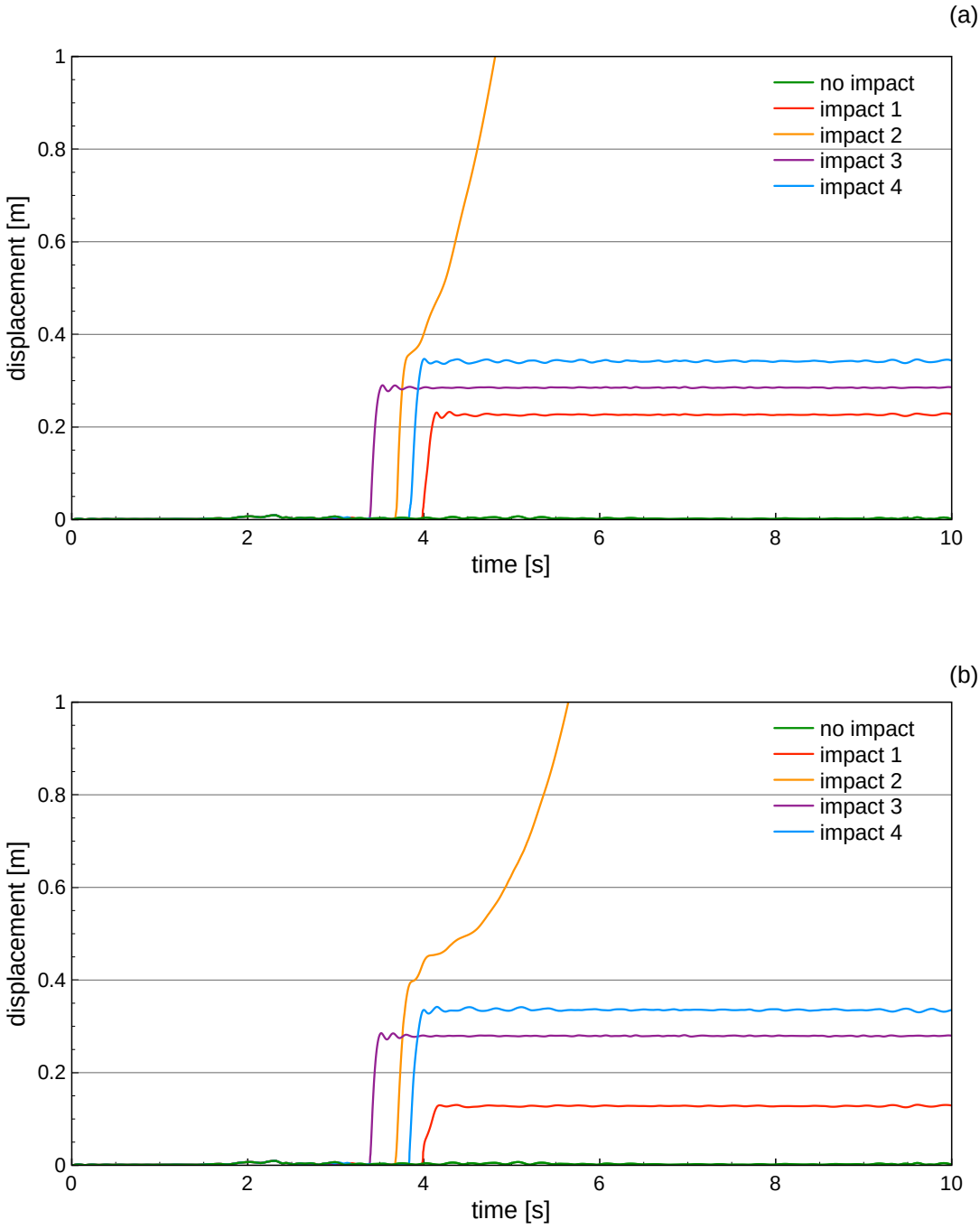

Fig. 6.23: Resultant displacement time histories at the mid-height of column no. 8 for four different moments of impact and for the case when impact does not take place: a) without strain rate effect; b) with strain rate effect

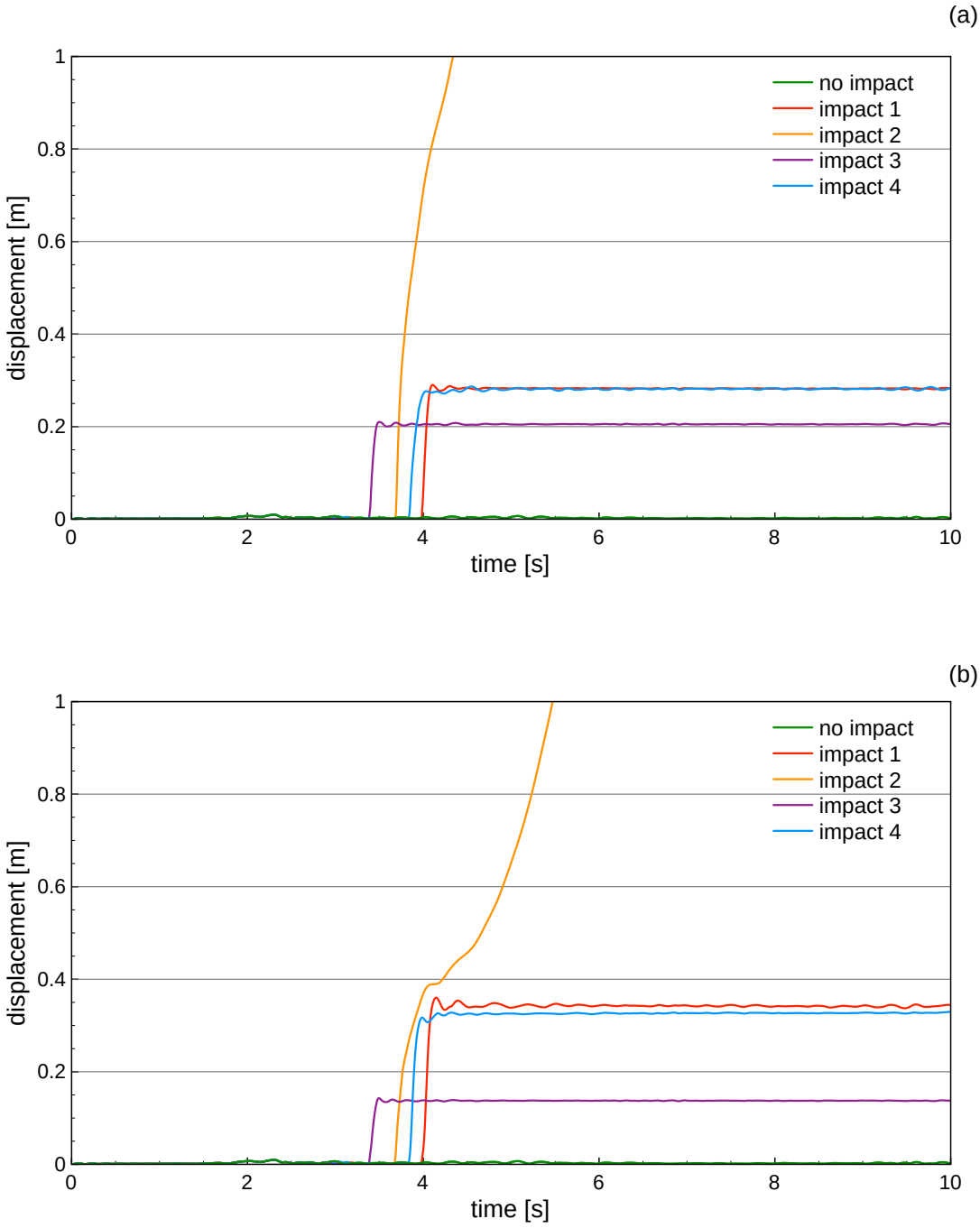

Fig. 6.24: Resultant displacement time histories at the mid-height of column no. 9 for four different moments of impact and for the case when impact does not take place: a) without strain rate effect; b) with strain rate effect

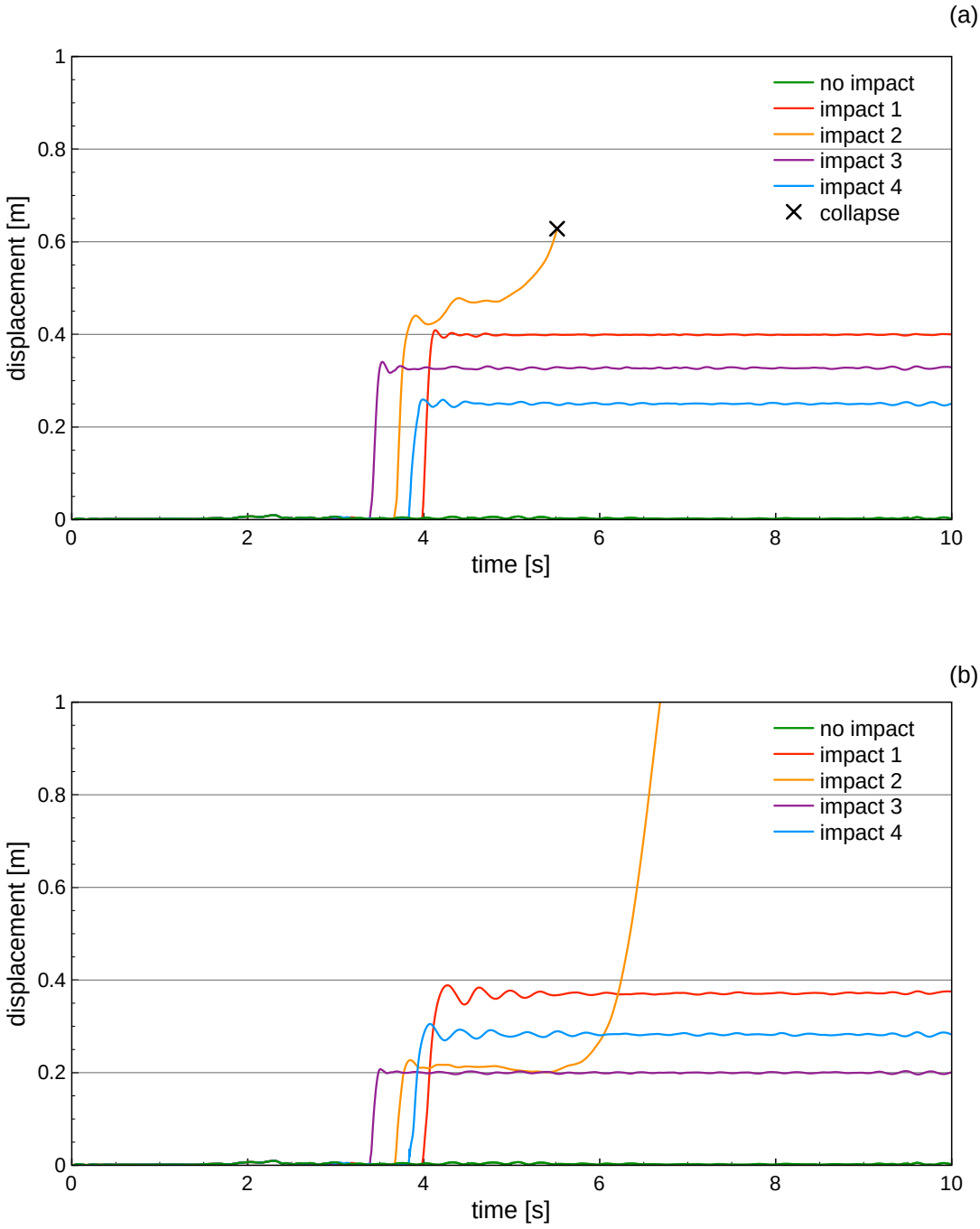

Fig. 6.25: Resultant displacement time histories at the mid-height of column no. 10 for four different moments of impact and for the case when impact does not take place: a) without strain rate effect; b) with strain rate effect

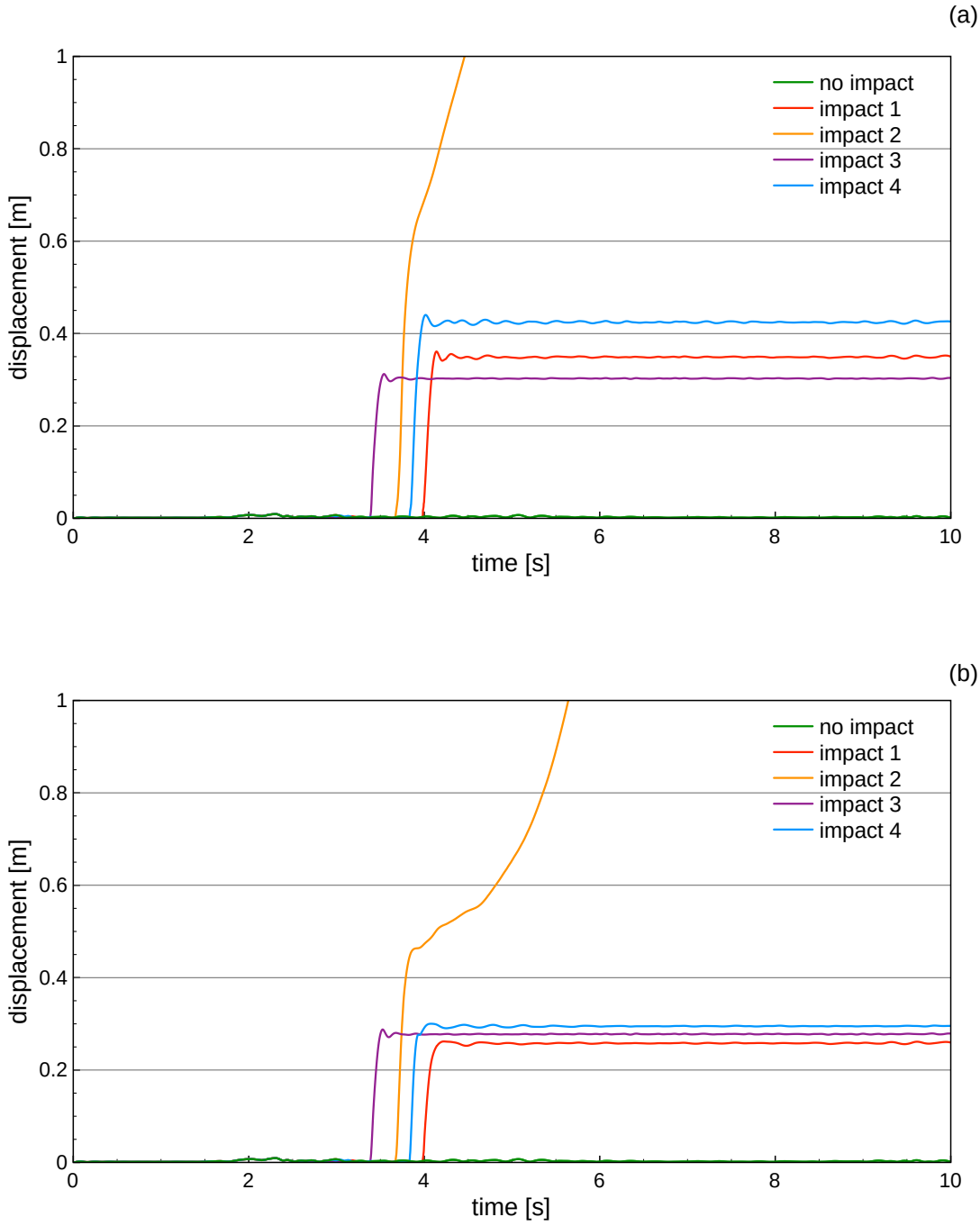

Fig. 6.26: Resultant displacement time histories at the mid-height of column no. 11 for four different moments of impact and for the case when impact does not take place: a) without strain rate effect; b) with strain rate effect

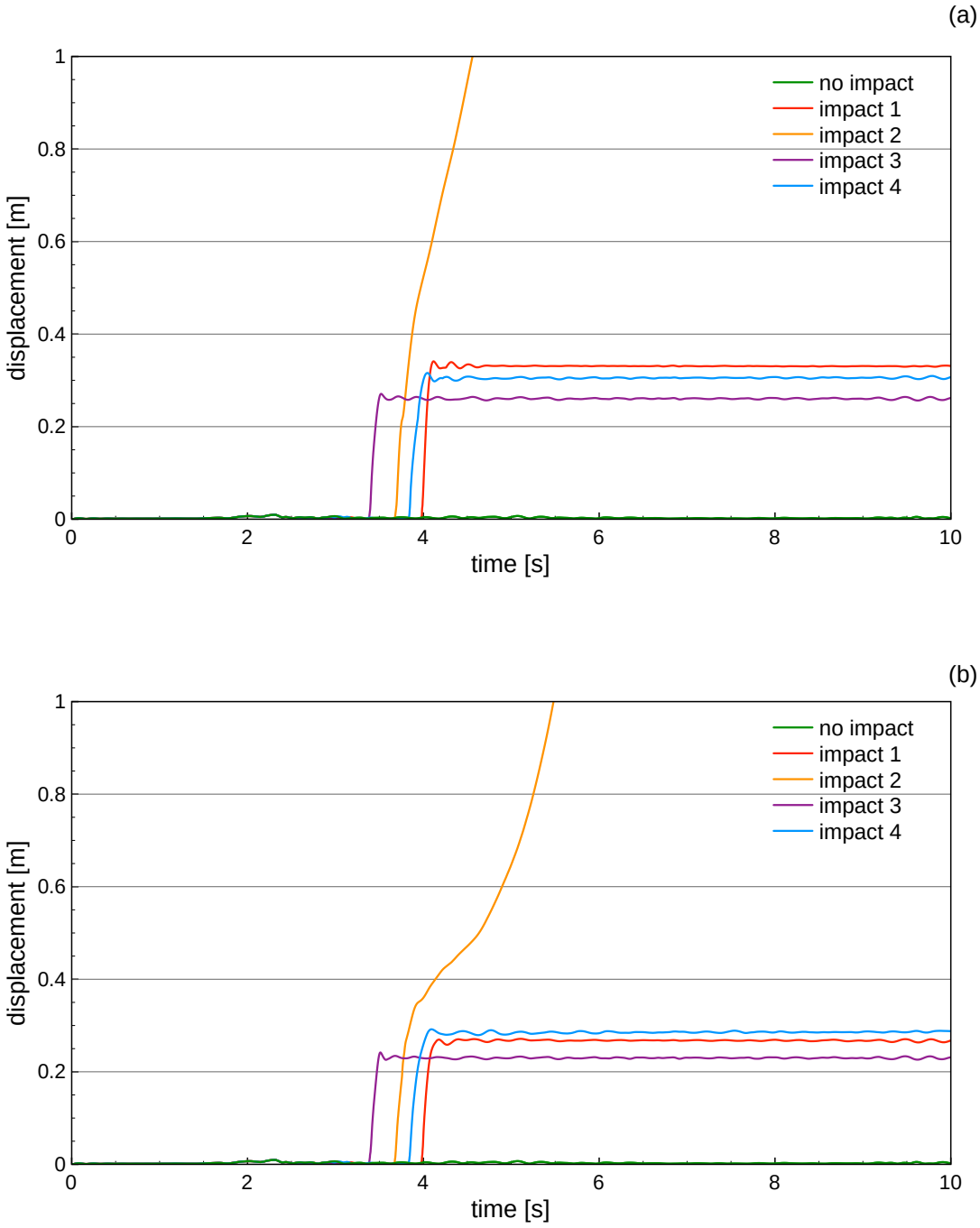

Fig. 6.27: Resultant displacement time histories at the mid-height of column no. 12 for four different moments of impact and for the case when impact does not take place: a) without strain rate effect; b) with strain rate effect

(a)

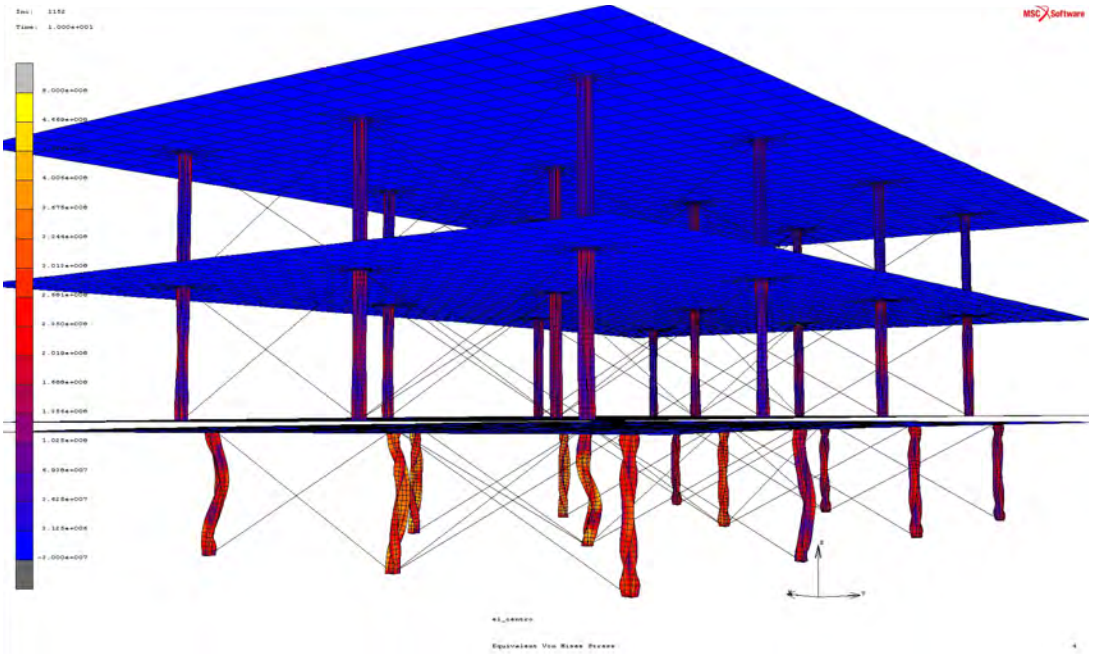

(b)

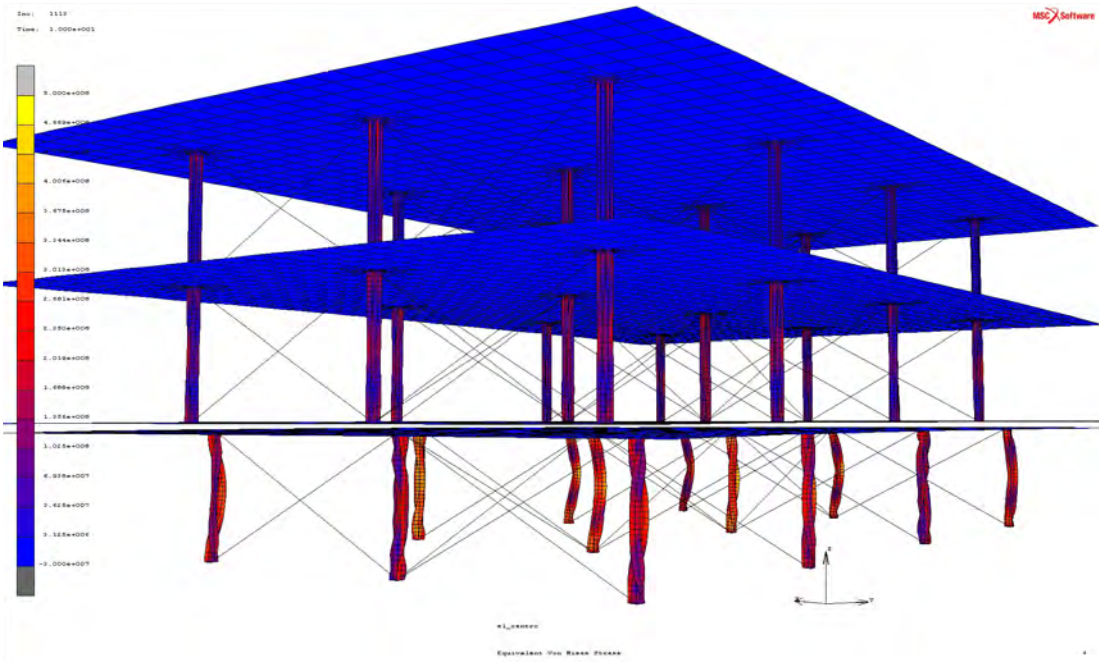

Fig. 6.28: General view of the deformed building model for the case of impact 1 showing the distribution of equivalent von Mises stress: a) without strain rate effect;
b) with strain rate effect

(a)

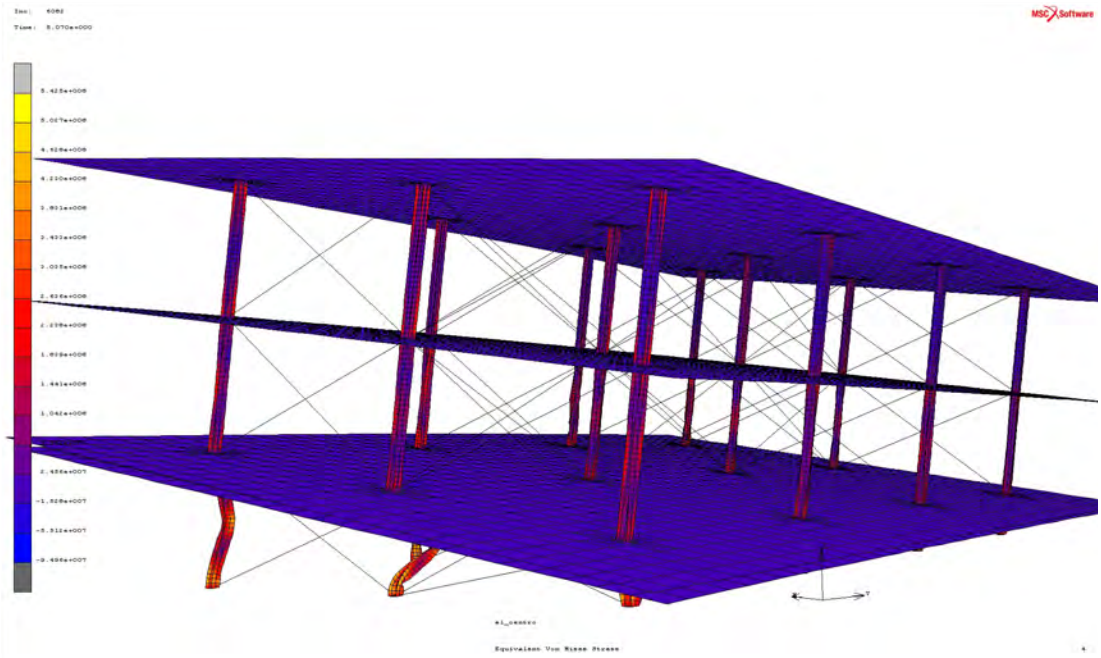

(b)

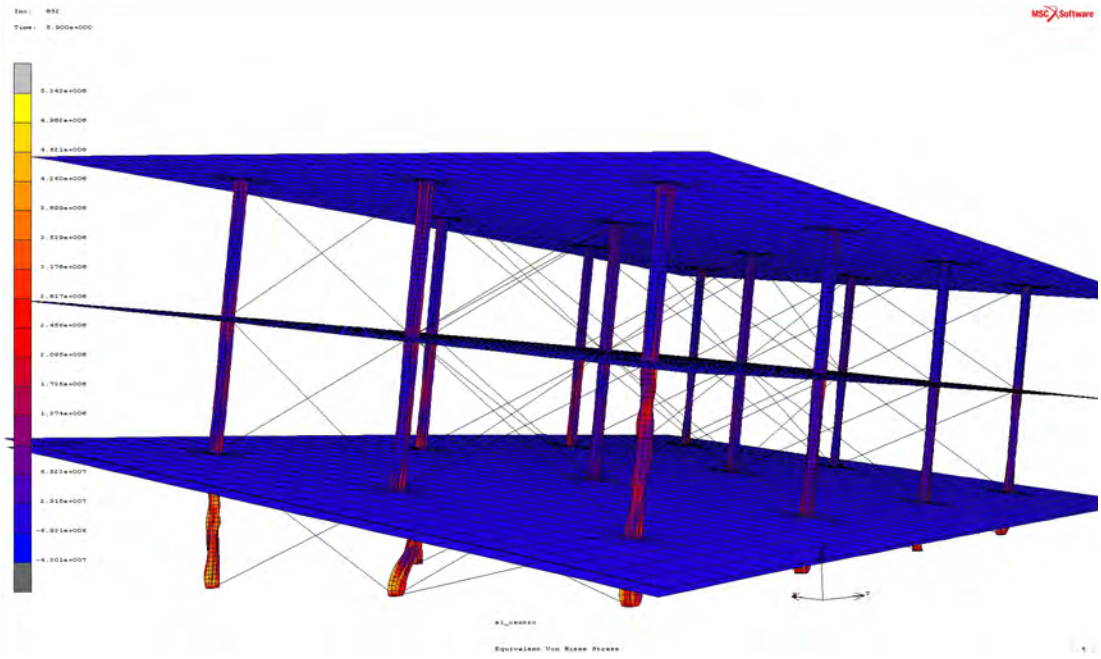

Fig. 6.29: General view of the deformed building model for the case of impact 2 showing the distribution of equivalent von Mises stress: a) without strain rate effect; b) with strain rate effect

(a)

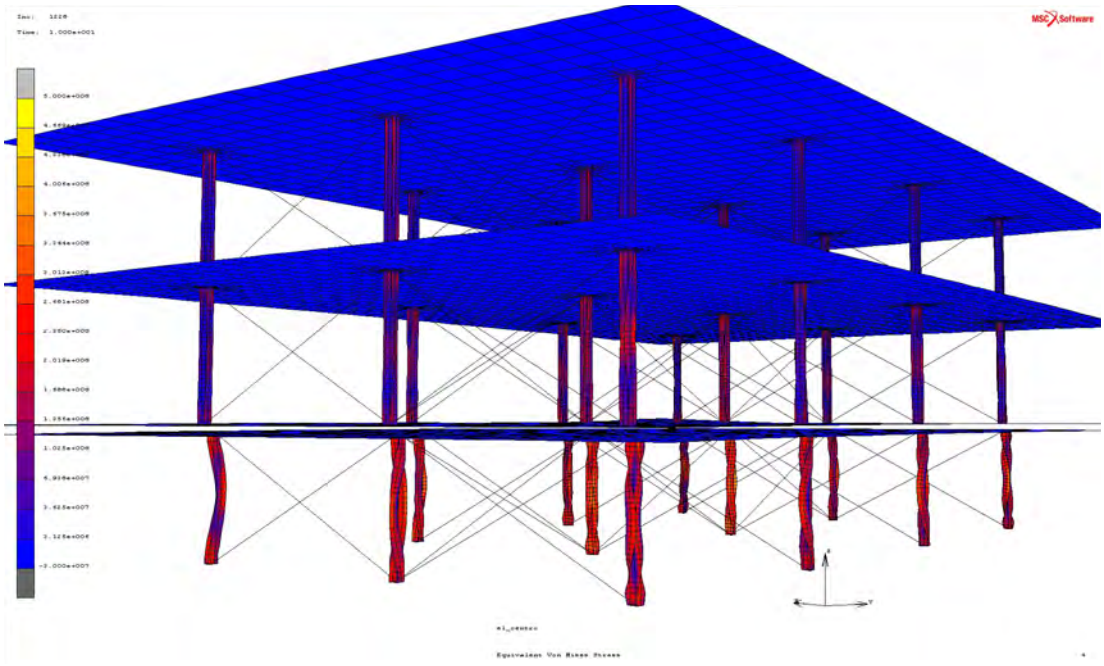

(b)

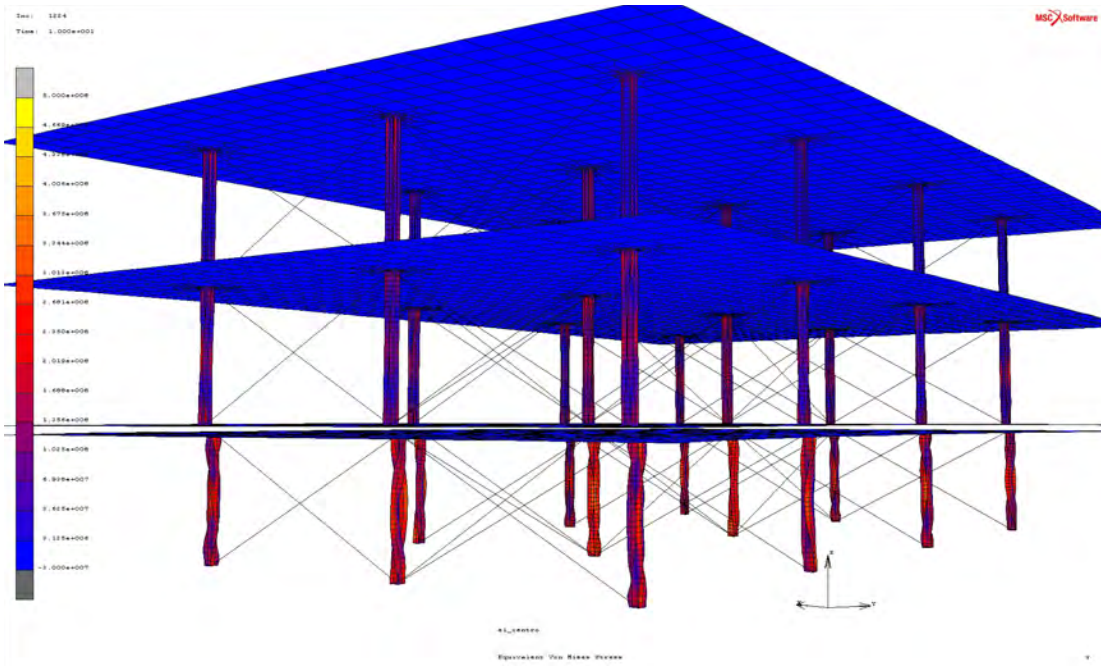

Fig. 6.30: General view of the deformed building model for the case of impact 3 showing the distribution of equivalent von Mises stress: a) without strain rate effect;
b) with strain rate effect

(a)

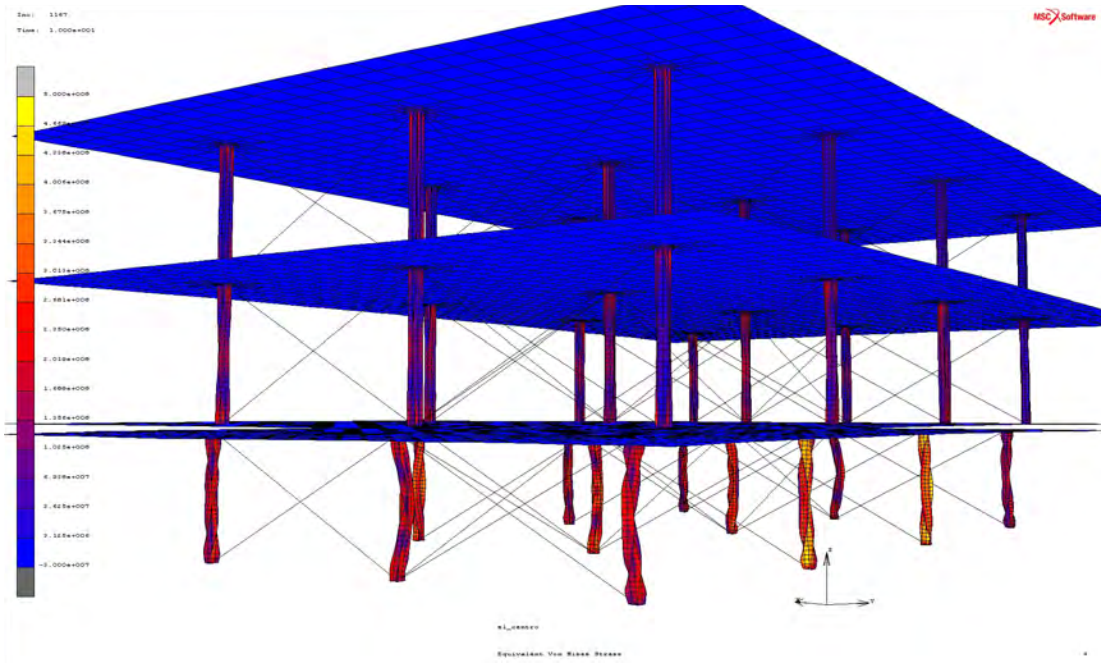

(b)

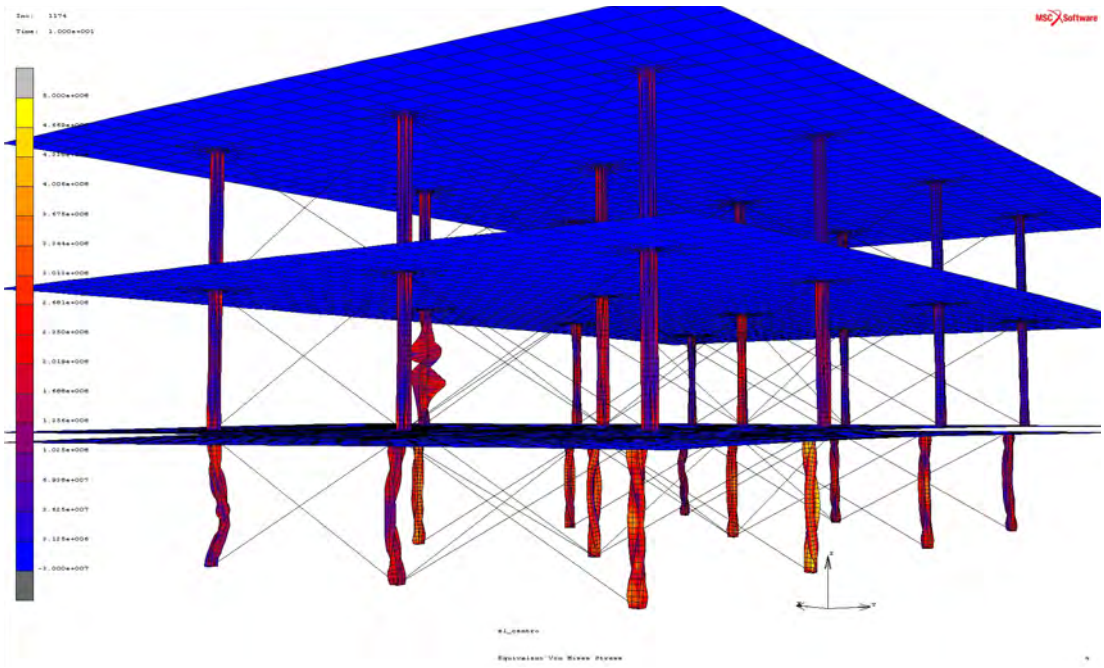

Fig. 6.31: General view of the deformed building model for the case of impact 4 showing the distribution of equivalent von Mises stress: a) without strain rate effect; b) with strain rate effect

On the other hand, when impact takes place at the time when the resultant horizontal displacement of the first storey slab is close to zero (impact time $t_1 = 4.060$ s), the influence of vertical impact on columns of the first storey is less significant. It can be seen form Figure 6.28 that, for this case, the columns of the first storey are able to withstand the additional force generated by impact without leading to the collapse, even though the plastic deformations took place.

The results of the study also indicate that a substantial difference in the response of the building under earthquake excitation concern the two other cases of impact time ($t_3 = 3.470$ s and $t_4 = 3.920$ s). The difference between the peak responses for the above cases, as compared to the peak response when impact takes place when the resultant deformation of the first storey slab is equal to zero ($t_1 = 4.060$ s) can be as large as 161,7% (see, for example, Figure 6.23b). It should be mentioned, however, that the moment of impact taking place at the half-way to the peak horizontal resultant displacement of the first storey slab may lead to the substantial increase (see, for example, Figure 6.23) as well as to the decrease (see, for example, Figure 6.25) in the structural response, as compared to the response for impact case 1.

It can also be seen comparing Figures 6.16a-6.31a with Figures 6.16b-6.31b that the incorporation of the strain rate effect in the numerical analysis is really important and the difference between the responses with and without considering this effect is substantial. In the case of impact at the time when the resultant horizontal displacement of the first storey slab is close to zero (impact 1), for example, the difference between the peak structural responses of the first storey columns at their mid-height is within the range of 5.0-43.8%.

6.5 Conclusions

The results of a detailed, nonlinear, three-dimensional numerical analysis, focused on the behaviour of a multi-storey steel frame building that suffers from a soft-storey failure under ground motion excitation, have been presented in this chapter. A numerical model of the structure has been created in FEM computer software and has been exposed to an impact that would have been generated after a soft-storey failure due to falling of the upper floors onto the slab of the first storey. The geometric nonlinearity due to impact and the second order effects as well as the elasto-plastic material behaviour with the strain rate effect have been considered in the analysis.

The results of the detailed nonlinear numerical analysis, concerning the behaviour of model of the steel frame building under real earthquake excitation, confirm conclusions obtained in the previous chapters in which simplified numerical models have been used. They show that not only the value of the impact force is crucial but also the moment when impact occurs. It has been confirmed that the most critical moment for the structure for being subjected to a vertical impact (due to the soft-storey failure of the second storey) is when the horizontal deformation of the first storey slab is close to its peak. Moreover, the results clearly indicate that the incorporation of the strain rate effect in the numerical analysis is really important in order to increase its accuracy.

Chapter 7.

FINAL CONCLUSIONS AND REMARKS

The present PhD dissertation has been devoted to the study concerning the behaviour of steel columns that experience horizontal deformations and are additionally subjected to vertical impact load, as the effect of the soft-storey failure during earthquakes. The response of a multi-storey steel frame building that suffers from a soft-storey failure under earthquake excitation has also been investigated in details.

7.1 Final conclusions

The horizontal stiffness degradation of building steel columns subjected to impact, caused by the fall of the upper storeys after soft-storey failure, has been first investigated in this dissertation. The results of that study have indicated that the degradation of horizontal stiffness of the columns may have a considerable influence on the structural response under earthquake excitation. Moreover, the results have shown that the time of impact plays a substantial role in the overall behaviour of a building under earthquake excitation. It has been found out that the structural response may be increased significantly if impact takes place when the structure is in the range of its peak deformations during the ground motion, especially when the structure is just approaching its extreme position. It has also been shown that the derived formula for the degradation of the column's stiffness, as the result of

dynamic vertical load, can be successfully used in numerical analysis when lumped mass models of buildings are used.

Further study has concerned the experimental investigation focused on the behaviour of models of deformed steel columns that are additionally subjected to vertical impact load. The results of the experiments have shown, that with the increase in the pre-deformation of a column (relative displacement between the top and the bottom) the value of the peak force acting on its top initially decreases and then shows a considerable increase trend. Moreover, the experimental results have indicated that, with the increase in the pre-deformation, the peak horizontal displacement of the middle part of column substantially increases for all height drop values considered.

The detailed numerical investigation concerning the behaviour of a model of deformed steel column, that is additionally subjected to vertical impact load (the result of soft-storey failure during earthquake), has been studied in the next part of this dissertation. The results of the first stage of the study have shown, that with the increase in the static pre-deformation of the column the peak mean normal stress values induced at the bottom of the specimen as well as the peak horizontal displacement at the middle of the column show a substantial increase trend for all height drop values considered. On the other hand, the results of the second stage of the numerical study have indicated that vertical impact may substantially influence the response of the column, which is dynamically excited in its horizontal direction. It has been shown that the response may be increased significantly if impact is initiated when the specimen is in the range of its peak horizontal deformation. Moreover, the results have indicated that the incorporation of the strain rate effect in the numerical analysis is really important in order to increase its accuracy.

The last part of this work has been devoted to the detailed, nonlinear, three-dimensional analysis focused on the behaviour of multi-storey steel frame building, that suffers from a soft-storey failure under ground motion excitation. The results of that study have confirmed conclusions obtained in the previous chapters of this dissertation in which simplified numerical models have been used. They have shown that not only the value of the impact force is crucial but also the moment when impact occurs. It has been confirmed, based on the results obtained, that the most critical moment for the structure for being subjected to a vertical impact (due to the soft-storey failure) is when the horizontal deformation is close to its peak. The results have also shown that the incorporation of the strain rate effect in the impact-involved numerical analysis is really important in order to increase its accuracy.

7.2 General remarks

Nowadays, civil engineers have an extensive set of rules and codes, e.g. Eurocodes, which help them in designing safe and economic structures. These rules and codes apply for all different kind of load conditions and for most cases can be assumed to be appropriate. This includes also the seismic loads specified in Eurocode 8 (ECS 1998). So, one could assume that codes should be sufficient for the design of new structures even those which are exposed to earthquake loading preventing the soft-storey failure. Unfortunately, seismic loads are of a random kind and do not always meet the assumed boundary conditions on which codes have been based. There are also buildings that have been designed before the present regulations of Eurocode 8, or other guidelines for earthquake resistant design, have been formulated. In such structures, the soft-storey failure may take place as the results of earthquake loading.

This work can be considered as the first comprehensive study dealing with the effects of the soft-storey failure on the response of building under earthquake excitation. The results obtained have provided us valuable information concerning the behaviour of steel columns of the lower storeys exposed to extreme load conditions after falling the upper floors. They have clearly indicated that not only the value of the impact force is crucial but also the stage of deformation of columns when impact takes place. It is believed that this fact is important in understanding the fact that in some cases the soft-storey failure does initiate the progressive collapse, while in other cases does not.

Besides the fact that the study has led us to variable conclusions, further research is needed in order to extend our knowledge on the behaviour of buildings after soft-storey failure during earthquakes. This should include further experimental studies on larger structural models, including full scale models of buildings on shaking tables. Moreover, the study described in this dissertation has been focused on the numerical analyses concerning multi-storey steel building neglecting the soil-structure interaction. Further numerical investigations on more detailed structural models of different types of buildings under three-dimensional ground motion excitations incorporating the influence of supporting soil are therefore required.

ACKNOWLEDGMENTS

I would like to express my gratitude to my doctoral supervisor prof. Robert Jankowski for his enormous patience, clemency and devotion as well as for his guidance in my scientific research and sharing with me his experience and knowledge in the field of experimental and numerical methods in earthquake engineering.

I would also like to thank my family for their understanding and tolerance due to the immense time spent at home working in front of my computer and not being available for their inquiries. Especially, I would like to express my gratitude to my wife for supporting me and for her help with some of my experiments, because without it I would not be able to conduct them. And speaking of family I would like to thank Markus Horschig for being a brother to me for the last 27 years and for those to come.

For constructive criticism and some important remarks as well as for some explanations regarding FEM and also for conducting some crucial calculations for me (due to her much faster computer) I would like to thank my very dear friend dr. Izabela Lubowiecka.

I would also like to thank my very close friends Beata and Łukasz Antoniewicz as well as Wojciech Sylka for putting my academic struggles (and not only the scientific ones) into the right perspective and helping me to keep in touch with reality.

Last, but not least, I would like to thank Michael Wesemann and Barend J. Thijsse, the authors of Plot. The numerical calculations have been executed with the support of the Academic Computer Centre (TASK) in Gdansk.

BIBLIOGRAPHY

[1] Adachi T., T. Tanaka, A. Sastranegara, A. Yamaji, S-K. Kim and I-Y. Yang (2004), Effect of transverse impact on buckling behaviour of a column under static axial compressive force, *International Journal of Impact Engineering*, **30**: 465-475.

[2] Amiri J.V., Q.Y. Ahmadi and B. Ganjavi (2008), Assessment of reinforced concrete buildings with shear wall based on Iranian seismic code (third edition), *Journal of Applied Sciences*, **8**: 4274-4283.

[3] Anagnostopoulos S.A. (1988), Pounding of buildings in series during earthquakes *Earthquake Engineering and Structural Dynamics*, **16**: 443-456.

[4] Anagnostopoulos S.A. and K.V. Spiliopoulos (1992), An investigation of earthquake induced pounding between adjacent buildings, *Earthquake Engineering and Structural Dynamics*, **21**: 289-302.

[5] Ansell A. (2006), Dynamic testing of steel for a new type of energy absorbing rock bolt, *Journal of Constructional Steel Research*, **62**: 501-512.

[6] Arslan M.H. and H.H. Korkmaz (2007), What is to be learned from damage and failure of reinforced concrete structures during recent earthquakes in Turkey? *Engineering Failure Analysis*, **14**: 1-22.

[7] ASCE (2006), *Minimum Design Loads for Buildings and other Structures, ASCE Standard, ASCE/SEI 7-05*, Reston, USA: American Society of Civil Engineers.

[8] Bathe K.J (1982), *Finite Element Procedures in Engineering Analysis*, Englewood Cliffs, USA: Prentice-Hall.

[9] Bendat J.S. and A.G. Piersol (1971), *Random Data: Analysis and Measurement Procedures*, New Jersey, USA: Wiley Interscience.

[10] Chau K.T. and X.X. Wei (2001), Pounding of structures modelled as non-linear impacts of two oscillators, *Earthquake Engineering and Structural Dynamics*, **30**: 633-651.

[11] Chen W.F. and C. Scawthorn (2003), *Earthquake Engineering Handbook*, Boca Raton, USA: CRC Press.

[12] Chmielewski T. and Z. Zembaty (1998), *Podstawy dynamiki budowli (Fundamentals of structural dynamics)*, Warszawa: Arkady (in Polish).

[13] Chopra A.K. (1995), *Dynamics of Structures: Theory and Applications to Earthquake Engineering*, Englewood Cliffs, USA: Prentice-Hall.

[14] Ciesielski R. and J. Kawecki (ed.) (1978-2012), *Materiały sympozjum "Wpływy sejsmiczne i parasejsmiczne na budowle" (Proceedings of Workshop: "Seismic and paraseismic effects on structures)*, Kraków (in Polish).

[15] Clough R.W. and J. Penzien (1993), *Dynamics of Structures*, International Edition: McGraw-Hill.

[16] Cui S., H. Hao and H.K. Cheong (2001), Dynamic buckling and post-buckling of imperfect columns under fluid-solid interaction, *International Journal of Solids and Structures*, **38**: 8879-8897.

[17] Cui S., H. Hao and H.K. Cheong (2002), Theoretical study of dynamic elastic buckling of columns subjected to intermediate velocity impact loads, *International Journal of Mechanical Sciences*, **44**: 687-702.

[18] Cui S., H.K. Cheong and H. Hao (1999), Experimental study of dynamic buckling of plates under fluid-solid slamming, *International Journal of Impact Engineering*, **22**: 675-691.

[19] Davies R.G. and C.L. Magee (1976), The effect of strain rate upon the tensile deformation of materials, *Journal of Engineering Materials and Technology*, Paper No. 76-Mat-FF.

[20] Davis R.O. (1992), Pounding of buildings modelled by an impact oscillator, *Earthquake Engineering and Structural Dynamics*, **21**: 253-274.

[21] Davoodi M., M.A. Sakhi and M.K. Jafari (2009), Comparing classical and modern signal processing techniques in evaluating modal frequencies of Masjed Soleiman Embankment Dam during earthquakes, *Asian Journal of Applied Sciences*, **2**: 36-49.

[22] Dorf R.C. (2005), *The Engineering Handbook*, Boca Raton, USA: CRC Press.

[23] ECS (1998), *Eurocode 8: Design Provisions for Earthquake Resistance of Structures*, Brussels, Belgium: European Committee for Standardization.

[24] El Ganainy H. and M.H. El Naggar (2009), Seismic performance of three-dimensional frame structures with underground stories, *Soil Dynamics and Earthquake Engineering*, **29**: 1249-1261.

[25] El Kafrawy O. and A. Bagchi (2007), Computer aided design and analysis of reinforced concrete frame buildings for seismic forces, *Information Technology Journal*, **6**: 798-808.

[26] Elkholy S. and K. Meguro (2004), Numerical simulation of high-rise steel buildings using improved applied element method, *13th World Conference on*

Earthquake Engineering, Vancouver, Canada, 1-6 August 2004, Paper No. 930.

[27] Elnashai A.S. and L. Di Sarno (2008), *Fundamentals of Earthquake Engineering*. New York, USA: John Wiley & Sons.

[28] Ghobarah A., M. Saatcioglu and I. Nistor (2006), The impact of the 26 December 2004 earthquake and tsunami on structures and infrastructure, *Engineering Structures*, **28**: 312-326.

[29] Goldsmith W. (1960), *Impact: The Theory and Physical Behaviour of Colliding Solids*, London, UK: Edward Arnold.

[30] Green N.B. (1981), *Earthquake Resistant Building Design and Construction*, New York, USA: Van Nostrand Reinhold Company.

[31] Gur J.A. and I. Elishakoff (1997), Dynamic instability of a transversely isotropic column subjected to a compression pulse, *Computers and Structures*, **62**: 811-815.

[32] Hao H., H.K. Cheong and S. Cui (2000), Analysis of imperfect column buckling under intermediate velocity impact, *International Journal of Solids and Structures*, **37**: 5297-5313.

[33] Hartmann F. and C. Katz, (2004), *Structural Analysis with Finite Elements*, Berlin, Germany: Springer-Verlag.

[34] Hilpert J.H. and K. Willnow (1999), Simulation of the dynamic behavior of steel structures under impact loading, *Transactions of the 15th International Conference on Structural Mechanics in Reactor Technology*, Seoul, Korea, 15-20 August, 1999.

[35] Hughes T.J.R. (1987), *The Finite Element Method*. Englewood Cliffs, USA: Prentice-Hall.

[36] Inel M., H.B. Ozmen and H. Bilgin (2008), Re-evaluation of building damage during recent earthquakes in Turkey, *Engineering Structures*, **30**: 412-427.

[37] Jankowski R. (2005), Non-linear viscoelastic modelling of earthquake-induced structural pounding, *Earthquake Engineering and Structural Dynamics*, **34**: 595-611.

[38] Jankowski R. (2006), Analytical expression between the impact damping ratio and the coefficient of restitution in the non-linear viscoelastic model of structural pounding, *Earthquake Engineering and Structural Dynamics*, **35**: 517-524.

[39] Jankowski R. (2008), Earthquake-induced pounding between equal height buildings with substantially different dynamic properties, *Engineering Structures*, **30**: 2818-2829.

[40] Jankowski R. (2009), Non-linear FEM analysis of earthquake-induced pounding between the main building and the stairway tower of the Olive View Hospital, *Engineering Structures*, **31**: 1851-1864.

[41] Jankowski R. (2010), Experimental study on earthquake-induced pounding between structural elements made of different building materials, *Earthquake Engineering and Structural Dynamics*, **39**: 343-353.

[42] Jankowski R. (2012), Non-linear FEM analysis of pounding-involved response of buildings under non-uniform earthquake excitation, *Engineering Structures*, **37**: 99-105.

[43] Jirásek M. and Z.P. Bažant (2002), *Inelastic Analysis of Structures*, Chichester, UK: John Wiley & Sons.

[44] Ju R-S., H-J. Lee, C-C. Chen and C-C. Tao (2012), Experimental study on separating reinforced concrete infill walls from steel moment frames, *Journal of Constructional Steel Research*, **71**: 119-128.

[45] Juhasova E. (1991), *Seismic Effects on Structures,* International edition: Elsevier.

[46] Karagiozova D. and N. Jones (1996), Dynamic elastic-plastic buckling phenomena in a rod due to axial impact, *International Journal of Impact Engineering*, **18**: 919-947.

[47] Karayannis C.G. and M.J. Favvata (2005), Earthquake-induced interaction between adjacent reinforced concrete structures with non-equal heights, *Earthquake Engineering and Structural Dynamics*, **34**: 1-20.

[48] Kenny S., N. Pegg and F. Taheri (2000), Dynamic elastic buckling of a slender beam with geometric imperfections subject to an axial impulse, *Finite Elements in Analysis and Design*, **35**: 227-246.

[49] Kłosowski P. and K. Woźnica (2004), Numerical treatment of elasto viscoplastic shells in the range of moderate and large rotations, *Computational Mechanics*, **34**: 194-212.

[50] Krabiell A. and W. Dahl (1981), Influence of temperature and strain rate on yield strength of structural steels of different strength. *Archiv für das Eisenhüttenvesen* **52**: 429-436 (in German).

[51] Krawinkler H. and G. Seneviratna (1998), Pros and cons of a pushover analysis of seismic performance evaluation, *Engineering Structures*, **20**: 452-464.

[52] Langer J. (1980): *Dynamika budowli (Structural dynamics)*, Wrocław: Wydawnictwo Politechniki Wrocławskiej (in Polish).

[53] Leyko J. (1997), *Mechanika ogólna, Dynamika (Theoretical mechanics, Dynamics)*, Warszawa: Wydawnictwo Naukowe PWN (in Polish).

[54] Liu M., S.A. Burns and Y.K. Wen (2003), Optimal seismic design of steel frame buildings based on life cycle cost considerations, *Earthquake Engineering and Structural Dynamics*, **32**: 1313-1332.

[55] Mahmoud S. and R. Jankowski (2009), Elastic and inelastic multi-storey buildings under earthquake excitation with the effect of pounding, *Journal of Applied Sciences*, **9**: 3250-3262.

[56] Mahmoud S., X. Chen and R. Jankowski (2008), Structural pounding models with Hertz spring and nonlinear damper, *Journal of Applied Sciences*, **8**: 1850-1858.

[57] Maison B., D. Bonowitz, L. Kornfield and D. McCormick (2011), Adjacency issues in soft-story wood-frame buildings, *Report to Structural Engineers Association of Northern California*, California, USA.

[58] Maison B.F. and K. Kasai (1992), Dynamics of pounding when two buildings collide, *Earthquake Engineering and Structural Dynamics*, **21**: 771-786.

[59] Malinowski J.Z., Z.L. Kowalewski and L. Kruszka (2007), *Doświadczalna metoda oraz badania plastycznego płynięcia metali w bardzo wysokich prędkościach odkształceń (Experimental method and study on plastic yielding*

of metals under very high strain rates), Warszawa: Wydawnictwo Instytutu Podstawowych Problemów Techniki Polskiej Akademii Nauk (in Polish).

[60] Mania R.J. (2010), *Wyboczenie dynamiczne cienkościennych słupów z materiałów lepkoplastycznych (Dynamic buckling of thin-walled columns made of viscoplastic materials)*, Zeszyty Naukowe Politechniki Łódzkiej nr 1059, Łódź: Wydawnictwo Politechniki Łódzkiej (in Polish).

[61] Manjoine M.J. (1944), Influence of rate of strain and temperature on yield stresses of mild steel, *Journal of Applied Mechanics* **11**: 211-218.

[62] Migda W. (2007), Uderzeniowe obciążenia prętów (Impact loads on bars), *Zeszyty Naukowe Politechniki Śląskiej: Budownictwo*, **112**: 153-160 (in Polish).

[63] Migda W. and R. Jankowski (2009), Experimental study on the behaviour of steel columns under seismic-induced axial impact load, *PAMM – Proceedings in Applied Mathematics and Mechanics*, **9**: 253-254.

[64] Migda W. and R. Jankowski (2010), Doświadczalne badania smukłych słupów poddanych deformacji i obciążeniom uderzeniowym podczas trzęsień ziemi (Experimental study on slender deformed columns under impact load due to earthquake excitation), *Czasopismo Techniczne*, **107**: 135-142 (in Polish).

[65] Migda W. and R. Jankowski (2011), Experimental study on steel columns subjected to impact load under earthquake conditions, *Current Scientific Challenges in Concrete and Steel Structures and Concrete Technology – III Gdansk-Kaiserslautern International PhD Symposium*, Gdańsk, 11-12 July 2011, pp.105-112.

[66] Migda W. and R. Jankowski (2012a), Behaviour of deformed steel columns exposed to impact load during earthquakes: experimental study, *Journal of Applied Sciences*, **12**: 466-472.

[67] Migda W. and R. Jankowski (2012b), Behaviour of deformed steel columns exposed to impact load during earthquakes: numerical analysis, *Journal of Applied Sciences*, **12**: 2304-2311.

[68] Migda W. and R. Jankowski (2012c), Degradacja sztywności słupów budynku na skutek działania pionowego obciążenia uderzeniowego w czasie wstrząsów sejsmicznych (Degradation of stiffness of building columns due to vertical impact loading during seismic excitations), *XIII Sympozjum „Wpływy Sejsmiczne i Parasejsmiczne na Budowle”* [CD-ROM], Kraków, 22-23 November 2012, pp.1-10 (in Polish).

[69] Migda W. and R. Jankowski (2012d), Experimental and numerical study on deformed steel columns subjected to impact load during earthquakes, *Proc. of XVIIIth International Symposium “Vibrations, Shocks and Noise 2012”*, [Flesh-memory], Paris-Clamart, France, 3-5 July 2012, Paper no.27.

[70] Migda W. and R. Jankowski (2013a), Numerical analysis of a steel frame building with soft-storey failure under ground motion excitation, *Key Engineering Materials*, **525-526**: 481-484.

[71] Migda W. and R. Jankowski (2013b), An approach for the response of buildings subjected to impact load after soft-story failure due to earthquake excitation, *Shock and Vibration* (accepted for publication).

[72] Mo Y.L. and Y.F. Chang (1995), Application of base isolation concept to soft first story buildings, *Computers and Structures*, **55**: 883-896.

[73] Naeim F. (2001), *The Seismic Design Handbook*, New York, USA: Kluwer Academic Publisher.

[74] Naeim F. and J.M. Kelly (1999), *Design of Seismic Isolated Structures: From Theory to Practice*, New York, USA: John Wiley & Sons.

[75] Naeini S.A. and A. Zarincheh (2010), Site effect microzonation and seismic hazard analysis of Kermanshah region in Iran, *Journal of Applied Sciences*, **10**: 2231-2240.

[76] Newmark N. (1959), A method of computation for structural dynamics, *Journal of Engineering Mechanics Division ASCE*, **85**: 67-94.

[77] Papadrakakis M., C. Apostolopoulou, A. Zacharopoulos and S. Bitzarakis (1996), Three-dimensional simulation of structural pounding during earthquakes, *Journal of Engineering Mechanics*, **122**: 423-431.

[78] Paulay T. and M.J.N. Priestley (1992), *Seismic Design of Reinforced Concrete and Masonry Buildings*, New York, USA: John Wiley & Sons.

[79] Plumier A., C. Doneux, L. Stoychev and T. Demarco (2005), Mitigation of soft storey failures of R.C. structures under earthquake by encased steel profiles, *Proceedings of the Fourth International Conference on Advances in Steel Structures (ICASS'05)*, Shanghai, China, 1-6 August 2004.

[80] Ruangrassamee A. and K. Kawashima (2001), Relative displacement response spectra with pounding effect, *Earthquake Engineering and Structural Dynamics*, **30**: 1511-1538.

[81] Rutenberg A. (1981), A direct P-delta analysis with using standard plane frame computer programs, *Computers and Structures*, **14**: 97-102.

[82] Rutenberg A. (1982), Simplified P-delta analysis for asymmetric structures, *ASCE Journal of the Structural Division*, **108**: 1995-2013.

[83] Sasan M. and S. Mohammadsadegh (2011), Seismic evaluation of middle span steel I-girder bridges, *Journal of Applied Sciences*, **11**: 104-110.

[84] Sastranegara A., T. Adachi and A. Yamaji (2005), Improving energy absorption of impacted column due to transverse impact: A finite element analysis, *International Journal of Impact Engineering*: **32**: 444-460.

[85] Sastranegara A., T. Adachi and A. Yamaji (2006), Effect of transverse impact on buckling behavior of compressed column, *Thin-Walled Structures*, **44**: 701-707.

[86] Sezen H., A.S. Whittaker, K.J. Elwood and K.M. Mosalam (2003), Performance of reinforced concrete buildings during the August 17, 1999 Kocaeli, Turkey earthquake, and seismic design and construction practise in Turkey, *Engineering Structures*, **25**: 103-114.

[87] Shah Q.M. (2006), Strain rate effect on the failure strain and hardness of metallic armor plates subjected to high velocity projectile impact, *Journal of Engineering Science and Technology*, **2**: 166-175.

[88] Stein E., R. de Borst and T.J.R. Hughes (2004), *Encyclopedia of Computational Mechanics*, Chichester, UK: John Wiley & Sons.

[89] Stronge W.J. (2000), *Impact mechanics*, Cambridge, UK: Cambridge University Press.

[90] Talaat M. and K.M. Mosalam (2009), Modeling progressive collapse in reinforced concrete buildings using direct element removal, *Earthquake Engineering and Structural Dynamics*, **38**: 609-634.

[91] Timoshenko S. and J. Gere (1961), *Theory of Elastic Stability*, New York, USA: McGraw-Hill.

[92] Tsang H.-H. and N.T.K. Lam (2008), Collapse of reinforced concrete column by vehicle impact, *Computer-Aided Civil and Infrastructure Engineering*, **23**: 427-436.

[93] Vaynman S., M.E. Fine, S. Lee and H.D. Espinosa (2006), Effect of strain rate and temperature on mechanical properties and fracture mode of high strength precipitation hardened ferritic steels, *Scripta Materialia*, **55**: 351-354.

[94] Watanabe F. (1997), Behavior of reinforced concrete buildings during the Hyougoken-Nanbu earthquake, *Cement Concrete Comp.*, **19**: 203-211.

[95] Wibowo A., J.L. Wilson, N.T.K. Lam and E.F. Gad (2010), Collapse modeling of a precast soft storey building in Australia, *Engineering Structures*, **32**: 1925-1936.

[96] Więch B. and R. Jankowski (2012): Behaviour of steel columns under impact, *Technology and Art*, **2012/3**: 90-93.

[97] Wiegel R. L. (1970), *Earthquake Engineering*, Englewood Cliffs, USA: Prentice-Hall.

[98] Wilson E.L. (2002), *Three-Dimensional Static and Dynamic Analysis of Structures. A Physical Approach with Emphasis on Earthquake Engineering*, Berkeley, USA: Computers and Structures Inc.

[99] Wriggers P. (2002), *Computational Contact Mechanics*, Chichester, UK: John Wiley & Sons.

[100] Wu B. and H. Zhong (2000), Efficient computation for lower bound dynamic buckling loads of imperfect systems under impact loading, *International Journal of Non-Linear Mechanics,* **35**: 735-743.

[101] Yoshimura M. (1997), Nonlinear analysis of a reinforced concrete building with a soft first storey collapsed by the 1995 Hyogoken-Nanbu earthquake, *Cement and Concrete Composites,* **19**: 213-221.

[102] Zembaty Z. (1987), On the reliability of tower-shaped structures under seismic excitations, *Earthquake Engineering and Structural Dynamics,* **15**: 76l-775.

[103] Zembaty Z. (2007), Non-stationary random vibrations of a shear beam under high frequency seismic effects, *Soil Dynamics and Earthquake Engineering*, **27**: 1000-1011.

[104] Zhang Y. and I. Scharf (2009), Validation of nonlinear viscoelastic contact force models for low speed impact, *Journal of Applied Mechanics*, **76**: 051002(1-12).

[105] Zhang Y. and I. Scharf (2011), Force reconstruction for low velocity impacts using force and acceleration measurements, *Journal of Vibration and Control*, **17**: 407-420.

[106] Zhang Z. and F. Taheri (2002), Numerical studies on dynamic pulse buckling of FRP composite laminated beams subjected to an axial impact, *Composite Structures*, **56**: 269-277.

[107] Zhoudao L., S. Lei and Y. Jiangtao (2011), Experimental study on the seismic behaviour of strengthened concrete column-beam joints by simulated earthquake, *Procedia Engineering*, **14**: 1871-1878.

[108] Zienkiewicz O.C. and R.L. Taylor (2002), *The Finite Element Method*, Oxford, UK: Butterworth-Heinemann.